Approches d'apprentissage automatique basées sur l'analyse du cycle de marche pour l'aide au diagnostic de la maladie de Parkinson

Nicolas Khoury

UNIVERSITÉ PARIS-EST

École doctorale MSTIC

THÈSE

présentée en vue de l'obtention du grade de

DOCTEUR DE L'UNIVERSITÉ PARIS-EST

Par

Nicolas KHOURY

Approches d'apprentissage automatique basées sur l'analyse du cycle de marche pour l'aide au diagnostic de la maladie de Parkinson

Machine learning approaches based on gait cycle analysis for diagnosis aid of Parkinson's disease

---

Spécialité: Image, Signal et Automatique

Soutenue publiquement le 12 Novembre 2019, devant le jury composé de:

Rapporteur	M. Mohamed CHETOUANI	Sorbonne Université
Rapporteur	M. Hichem MAAREF	Université d'Evry Val d'Essonne
Examinateur	M. Stéphane ESPIÉ	IFSTTAR
Examinateur	Mme. Samia NEFTI-MEZIANI	University of Salford
Examinateur	M. Amar RAMDANE CHERIF	Université de Versailles Saint-Quentin-en-Yvelines
Encadrant	M. Ferhat ATTAL	Université Paris Est Créteil
Co-directeur	M. Samer MOHAMMED	Université Paris Est Créteil
Directeur	M. Yacine AMIRAT	Université Paris Est Créteil

Thèse effectuée au sein du
Laboratoire Image, Signaux, et Systèmes Intellgents
de l'Univeristé Paris-Est Créteil

Domaine Chérioux
120-122, Rue Paul Armangot
94400 Vitry-sur-Seine
France

Contents

List of Figures

List of Tables

Abbreviations

AP	**A**ntero**P**osterior
BSS	**B**lind **S**ource **S**eparation
CART	**C**lassification **A**nd **R**egression **T**ree
CCD	**C**harge **C**oupled **D**evice
CDTW	**C**ontinuous **D**ynamic **T**ime **W**arping
CoP	**C**enter **o**f **P**ressure
CV	**C**oefficient of **V**ariation
DDTW	**D**erivative **D**ynamic **T**ime **W**arping
DFT	**D**iscrete **F**ourier **T**ransforms
DT	**D**ecision **T**ree
DTW	**D**ynamic **T**ime **W**arping
DSiVM	**D**ifferential **S**ignal **V**ector **M**agnitude
EDR	**E**dit **D**istance on **R**eal sequences
EGG	**E**lectroglottographic
ELGAM	**E**xtra-**L**aboratory **G**ait **A**ssessment **M**ethod
EM	**E**xpectation-**M**aximization
EMG	**E**lectro**m**yo**g**raphy
FA	**F**actors **A**nalysis
FC	**F**ourier **C**oefficients
FSR	**F**orce **S**ensitive **R**esistors
FT	**F**unctional **T**ree
GA	**G**ait **A**symmetry
GARS	**G**ait **A**bnormality **R**ating **S**cale
GC	**G**ait **C**ycle
GMM	**G**aussian **M**ixture **M**odel

GRF	**G**round **R**eaction **F**orces
HMM	**H**idden **M**arkov **M**odel
H & Y	**H**oehn & **Y**ahr
ICA	**I**ndependent **C**omponent **A**nalysis
IDDTW	**I**terative **D**eepening **D**ynamic **T**ime **W**arping
ID3	**I**terative **D**ichotomiser
IMU	**I**nertial **M**easurement **U**nits
IRT	**I**nfrared **T**hermography
k-nn	**k**-**n**earest **n**eighbors
LDA	**L**inear **D**iscriminant **A**nalysis
LFo	**L**eft **Fo**ot
LR	**L**ogistic **R**egression
LRF	**L**aser **R**ange **F**inders
LS-SVM	**L**east **S**quares-**S**upport **V**ector **M**achine
MCDTW	**M**ultidimensional **C**ontinuous **D**ynamic **T**ime **W**arping
MDC	**M**inimum **D**istance **C**lassifier
ML	**M**edio**L**ateral
MLP	**M**ulti-**L**ayer-**P**erception
MSWS-12	**M**ultiple **S**clerosis **W**alking **S**cale
NEWFM	**NE**ural network with **W**eighted **F**uzzy **M**embership functions
OMC	**O**ptical **M**otion **C**apture
PART	**P**artial C4.5 decision tree
PD	**P**arkinson's **D**isease
PDTW	**P**iecewise **D**ynamic **T**ime **W**arping
PCA	**P**rincipal **C**omponent **A**nalysis
PIGD	**P**ostural **I**nstability and **G**ait **D**ifficulty
PNN	**P**robabilistic **N**eural **N**etwork
POMA	Tinetti **P**erformance-**O**riented **M**obility **A**ssessment
Q-BTDNN	**Q**-**B**ackpropagated **T**ime **D**elay **N**eural **N**etwork
RAS	**R**hythmic **A**uditory **S**timulation
RBFNN	**R**adial **B**asis **F**unction **N**eural **N**etwork
RF	**R**andom **F**orest
RFo	**R**ight **Fo**ot

RMS	**R**oot **M**ean **S**quare
SiVM	**S**ignal **V**ector **M**agnitude
SMA	**S**ignal **M**agnitude **A**rea
STD	**ST**andard **D**eviation
STIP	**S**patial-**T**emporal **I**mage of **P**lantar pressure
SVM	**S**upport **V**ector **M**achine
ToF	**T**ime-**o**f-**F**light
TUG	**T**imed **U**p and **G**o
TWED	**T**ime-**W**arped **E**dit **D**istance
T25-FW	**T**imed **25**-**F**oot **W**alk
UPDRS	**U**nified **P**arkinson's **D**isease **R**ating **S**cale
UPDRSM	**U**nified **P**arkinson's **D**isease **R**ating **S**cale-**M**otor Section
WDTW	**W**eighted **D**ynamic **T**ime **W**arping

Abstract

Parkinson's disease (PD) is a slow, progressive, and chronic neurodegenerative disorder. It is the second most common neurological disease (after Alzheimer's disease) and affects considerably the elderly population worldwide. This thesis exploits gait cycle analysis to diagnose PD. Gait disturbances are often observed with the PD evolution. Therefore, the main objective of this thesis is to develop a clinical tool to aid the diagnosis of Parkinson's disease using clinical-based features extracted from vertical Ground Reaction Forces (vGRFs). This tool is mainly devoted to being used in a clinical environment as a support tool to physiotherapists in their PD diagnosis process. To achieve an accurate classification, on the one hand, between healthy and PD subjects, and on the other hand, between subjects with different levels of disease severity, clinical-based features are exploited and more specifically the repeatability of gait cycle in PD subjects by measuring the similarity of stance phases. A similarity measure between gait cycles carried out using the Continuous Dynamic Time Warping (CDTW) technique is proposed. The obtained results showed that the use of CDTW-based features improves significantly the classification accuracy rates for discriminating healthy subjects from PD subjects. Finally, we propose an extension of the CDTW for feature computation by analysing the similarity between time-series during the stance phases in the multidimensional domain. The obtained results showed clearly significant improvements when using multidimensional CDTW based features with respect to the case when using unidimensional ones.

Keywords: Parkinson's disease, Gait cycle analysis, Wearable Sensors, Supervied/unsupervised classification algorithms, Continuous Dynamic Time Warping (CDTW).

Chapter 1

Introduction

Parkinson's disease (PD) is a slow, progressive, and chronic neurodegenerative disorder. It affects the human central nervous system by destroying dopaminergic neurons which produce dopamine, a neurotransmitter that sends messages to the brain to control the human movement. PD is the second most common neurological disease (after Alzheimer's disease) and affects an enormous portion of the elderly population worldwide. Globally, nearly 5 million people [1] are affected by this disease; this number could double by 2030. In France, 200 000 people [2] suffer from PD and about 25 000 new cases [3] are diagnosed each year. The disease begins 5 to 10 years before any clinical symptoms appear. Four main characteristics or motor symptoms of PD, referred by the acronym TRAP (Tremor, Rigidity, Akinesia, Postural instability), characterise the PD disease. In addition, there are other symptoms and motor signs that can appear with the progress of PD, including gait and posture disorders such as festination (rapid shuffling step and walking with a forward-flexed posture), freezing of gait, and short gait step.

The Parkinson's disease diagnosis is a difficult and subjective task, mainly in the early stages, and there is no available biomarker or specific test for such a diagnosis. Statistics show that the PD misdiagnosis rate is around 25 % and 40 % of the PD cases are finally found to be related to other pathologies. It should be noted that each

[1] Dorsey, E.R.; Constantinescu, R.; Thompson, J.P.; Biglan, K.M.; Holloway, R.G.; Kieburtz, K.; Marshall, F.J. et al. Projected number of people with Parkinson disease in the most populous nations, 2005 through 2030, Neurology **2007**, Volume 68, No. 5, pp. 384-386.

[2] https://solidarites-sante.gouv.fr/fichiers/bo/2015/15-09/ste_20150009_0000_0056.pdf (accessed on 15 October 2015)

[3] https://www.franceparkinson.fr/wp-content/uploads/2016/10/CP-FRANCE-PARKINSON-et-CGE-DISTRIBUTION.pdf) (accessed on 28 June 2018)

PD patient shows specific signs; the evolution of the disease and the progression of the symptoms are subject to each patient. For example, some symptoms such as speaking difficulty may appear after several years or may remain insignificant. In addition, 70 % of PD patients have resting tremors at the beginning of the disease while other patients have gait disorders or action tremor. According to clinicians, PD is diagnosed after the occurrence of one or more of the main motor symptoms (TRAP). For a better treatment and a more efficient control of the symptoms effects of the disease, it is necessary to carry out an accurate and early diagnosis.

This thesis exploits gait cycle analysis to diagnose PD. Gait disturbances are often observed with the PD evolution. Therefore, the main objective of this thesis is to provide an efficient machine learning tool that aims at supporting physiotherapists in the diagnosis process by exploiting the most relevant features extracted from gait cycles. The challenge is to achieve an accurate classification between healthy and PD subjects, and also, between subjects with different levels of severity of the disease. For this purpose, two possible improvements of the diagnosis accuracy are explored. The first one consists of considering only the most relevant spatio-temporal features from the clinical point of view among those extracted from vGRFs signals during walking. The second possible improvement is to exploit the repeatability of gait cycle in PD subjects and more precisely the similarity of stance phases time-series in unidimensional and multidimensional cases.

This manuscript is organized as follows:

Chapter 2 describes the general context of the thesis, which is related to the diagnosis of the Parkinson's disease. PD and its symptoms are first described and analysed. The second part of the chapter presents the different approaches used for the diagnosis of this neurodegenerative disease. Before analysing the diagnosis approach based on the analysis of human gait, a description of the gait cycle phases is presented. A review of the sensors commonly used for gait phases recognition is then shown. The positioning and objectives of the thesis are discussed in the last part of the chapter.

Chapter 3 proposes a data-driven approach for Parkinson's disease diagnosis. The first part of the chapter presents the general background including data pre-processing (features computation, feature extraction and feature selection) followed by a presentation of the main supervised and unsupervised classification approaches used in this

chapter. An online dataset of vertical Ground Reaction Forces (vGRFs) data collected from gait cycles of healthy subjects and PD patients is used. The next part of the chapter presents the methodological background in particular, (1) the feature extraction and feature selection processes, (2) the supervised and unsupervised classification approaches, as well as (3) the performance evaluation metrics. The remaining parts of the chapter are dedicated to the related works and the implementation of the above-mentioned methodology for the PD diagnosis.

Chapter 4 presents the Continuous Dynamic Time Warping (CDTW) technique for Parkinson's Disease (PD) diagnosis classification using gait cycle similarities. The first part of the chapter presents a brief synthesis on the time-series similarity evaluation techniques and focuses then on the Dynamic Time Warping technique and its extension to the Continuous Dynamic Time Warping (CDTW). The next part of the chapter is dedicated to the state of the art related to the use of DTW to analyse the gait cycle. The last parts present and discuss the data pre-processing process as well as the obtained results in terms of PD classification.

Chapter 5 describes the extension of the CDTW technique, proposed in chapter 4, to calculate the similarity between time-series during the stance phases in the multidimensional domain. The formulation of the CDTW in multidimensional domain is presented firstly and then applied to the PD subjects classification. Several supervised/unsupervised classification methods have been implemented and evaluated. Different cases were considered with respect to the number of classes in each sub-dataset, which correspond to the severity degree of PD according to H & Y scale.

Chapter 6 provides a general synthesis of the contributions of the thesis along with a discussion on perspectives for future work.

Chapter 2

Diagnosis of Parkinson's Disease

2.1 Introduction

The chapter describes the general context of the thesis, which concerns the diagnosis of the Parkinson's disease (PD). PD and its symptoms are first described and analysed. The second part of the chapter presents the different approaches used for the diagnosis of this neurodegenerative disease. Before analysing the diagnosis approach based on the analysis of human gait, a description of the gait cycle phases is presented. Finally, a review of the sensors commonly used for gait phases recognition is presented.

2.2 Parkinson's Disease

Parkinson's disease (PD) is a slow, progressive, and chronic neurodegenerative disorder. It affects the human central nervous system by destroying dopaminergic neurons which produce dopamine. Dopamine is a neurotransmitter that sends messages to the brain in order to control the human movement [1–3]. PD is the second most common neurological disease (after Alzheimer's disease) and affects an enormous portion of the elderly population worldwide [4–6]. Globally, nearly 5 million people are affected by this disease [7]; this number could double by 2030. In France, 200 000 people [8] suffer from PD and about 25 000 new cases [9] are diagnosed each year (Fig. 2.1).

FIGURE 2.1: Projections of the number of Parkinsonian cases over 45 years in France between 2010 and 2030 (by sex) [10]

The average age of diagnosis is 58 years [11], but 20 % are under 50 years old at diagnosis. However, rare genetic forms (approximately 5 %) can lead to an early occurrence before the age of 40 [12–14]. The disease begins 5 to 10 years before any clinical symptoms appear; at this point, approximately half of the dopaminergic neurons have already disappeared. Four main characteristics or motor symptoms of PD can appear, referred by the acronym TRAP and described in the following:

1. **Tremor**: rest tremor is the most common symptom of PD and the easily recognized one; the tremor frequency ranges between 4 and 6 Hz. It can involve the chin, jaw, lips and legs, and rarely involves the neck (head) or voice [15].

2. **Rigidity**: it characterises the resistance to limb movement caused to an increment in muscle tone, and continuous and excessive muscles contraction [15]. In the disease early stages, rigidity is usually asymmetrical and typically affects proximal muscles first as the shoulders and neck muscles, and then, it progresses to affect muscles of the face and extremities [16]. As the disease progress, rigidity affects the entire body and decreases the ability to move easily.

3. **Akinesia**: or Bradykinesia, is the typical PD clinical symptom characterising the movement slowness. It is a hallmark of basal ganglia disorder, which results in planning difficulties, starting and performing movements, and achieving sequential and synchronized tasks [17]. The initial signs are the slowness in performing daily living activities, with relatively long reaction times [18, 19].

4. **Postural instability**: it appears in the late stages of the disease, leading to equilibrium disorders and increased falls [20] and bone fractures [15]. However, no instability is observed in the early stages of the disease, especially among young people [21]. Up to 40 % of PD subjects may be subject to falls and approximately 10 % of them may have falls weekly with a correlation between the number of falls and the severity of the disease [15].

In addition, there are other symptoms and motor signs that can be appear with the progress of PD, including gait and posture disorders such as festination (rapid shuffling step and walking with a forward-flexed posture) [15], freezing gait, and short gait step. Furthermore, other signs such as the appearance of disturbances in speech, swallowing and voice disorders are also recognized as symptoms of PD progression [22]. All these

typical symptoms can make diagnosis easier, while the existence of various non-typical signs such as depression, pain, fatigue, etc. can render the diagnosis more difficult.

2.3 Diagnosis of Parkinson's Disease

The Parkinson's disease (PD) diagnosis is difficult, mainly in the early stages, and there is no available biomarker or specific test for such a diagnosis. Usually, to confirm the presence of PD, neurologists perform many clinical evaluations and analyse the patient's entire medical history. Moreover, in order to exclude the affections causing the Parkinsonism [1] and that are not necessarily due to PD, several imaging techniques and lab tests are carried out. Furthermore, a routinely used diagnostic method is to assess the patient's response to levodopa therapy ; the levodopa is a synthetic dopamine medication used to treat the PD. If the patient's response is positive to this treatment, it means that the patient's symptoms are related to PD, and that the patient is probably suffering from PD. Nevertheless, neurologists sometimes consider that, during the early stages of the disease, taking medication may be unnecessary [2, 23]. Sometimes, the diagnosis may take up to a year after a careful analysis of the patient's neurological history and clinical assessments. Despite these careful assessments, there is a strong possibility of misdiagnosis of PD for other neurological affections responsible for Parkinsonism. Statistics given in [24] show that the PD misdiagnosis rate is around 25 % and 40 % cases of PD are confused with other neurological affections [2]. It should be noted that each PD patient has specific signs; the evolution of the disease and the progression of symptoms are specific to each patient. For example, some symptoms such as speaking difficulty may appear after several years or may remain insignificant. According to clinicians, PD is diagnosed after the occurrence of one or more of the main motor symptoms. For a better treatment and a more efficient control of the symptoms effects of the disease, it is necessary to carry out an accurate and early diagnosis [23].

PD diagnosis approaches

Currently, the diagnosis made by specialists (neurologist, movement disorder specialist, speech disorder specialist, etc.) to assess the severity level of PD is conducted using various methods from several fields including Cognitive deficit [25–31], speech disorder

[1] a group of neurological disorders causing movement problems similar to those observed in PD

[32–34], human stability [35, 36], gait cycle [37–39] and others [40, 41] (Fig. 2.2). The approaches commonly used for diagnosing PD are briefly described below.

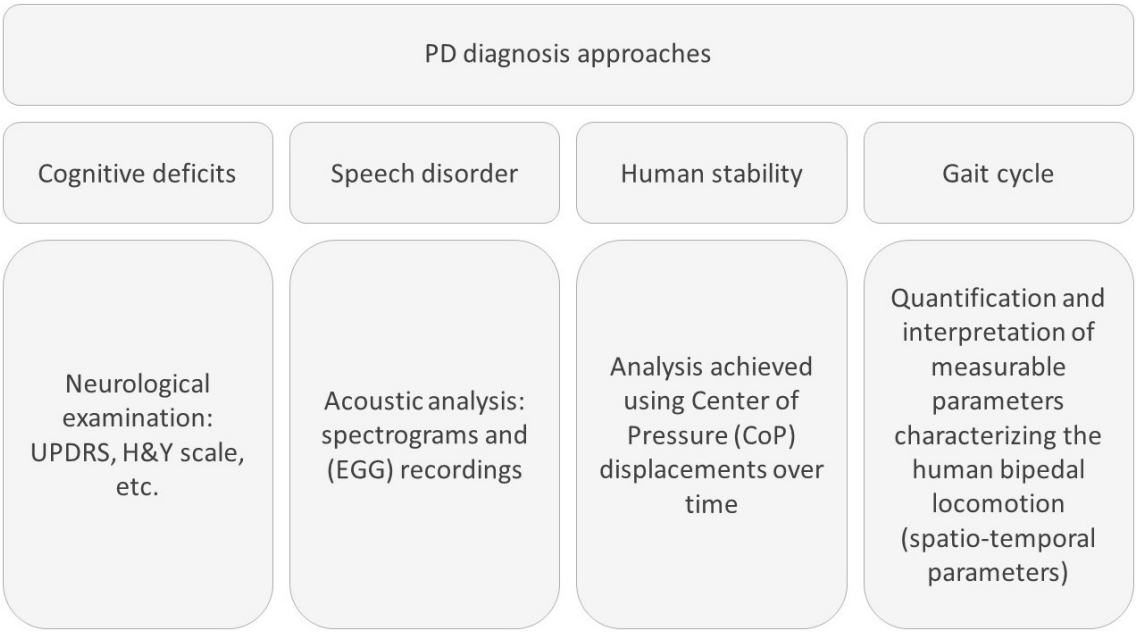

FIGURE 2.2: Different approaches of PD diagnosis

1. Cognitive deficit or cognitive impairment is a commonly used expression to describe any characteristic that impedes the cognitive process. In order to evaluate the disability and motor impairment in PD patients, several rating scales are used, such as the Unified Parkinson's Disease Rating Scale (UPDRS) [25], and the Hoehn and Yahr (H & Y) rating scale [26]. Other scales are based on the evaluation of the psychiatric manifestations [42] and quality of life [42, 43]. The UPDRS is a commonly used scale to assess impairment and disability [44, 45]. Studies using UPDRS to monitor the PD progression suggest that this progression is not linear and that the rate of deterioration is variable and faster in the early stage of PD and in PD patients suffering from Postural Instability and Gait Difficulty (PIGD) [46–48]. The H & Y scale ranging from 0 (no disease signs) to 5 (confinement to bed or wheelchair unless aided), is used to compare patients and provides a rough assessment of the evolution of the disease. A modified version of the H & Y scale, including stages 1.5 and 2.5, is used to take into account the intermediate progress of PD. Figure 2.3, summarizes the different stages of the H & Y and Modified H & Y scales.

Stages	Hoehn and Yahr Scale	Modified Hoehn and Yahr Scale
1	Unilateral involvement only usually with minimal or no functional disability	Unilateral involvement only
1.5	-	Unilateral and axial involvement
2	Bilateral or midline involvement without impairment of balance	Bilateral involvement without impairment of balance
2.5	-	Mild bilateral disease with recovery on pull test
3	Bilateral disease: mild to moderate disability with impaired postural reflexes; physically independent	Mild to moderate bilateral disease; some postural instability; physically independent
4	Severely disabling disease; still able to walk or stand unassisted	Severe disability; still able to walk or stand unassisted
5	Confinement to bed or wheelchair unless aided	Wheelchair bound or bedridden unless aided

FIGURE 2.3: PD stages according to H & Y and Modified H & Y scales [49]

2. Speech disorders or speech difficulties such as dysarthria (speech articulation difficulties) and dysphonia (impaired speech production) [33]. The most commonly used techniques to extract features that characterize alterations of vocalization in patients with PD are: the acoustic analysis that is based on spectrograms (visual representation of the spectrum of frequencies of sounds) and electroglottographic (EGG) recordings [2] [33]. The PD diagnosis based on speech disorders has been addressed in different studies [32–34].

3. Maintaining postural stability is a difficult task for patients suffering from PD. The analysis of human stability can be carried out using the Center of Pressure (CoP) displacements in the anteroposterior (AP) and mediolateral (ML) directions. Usually, many parameters and statistical measures are used to study the human motion in static posture, such as the maximum radius, mean radius, swept area, centroid, average CoP velocity, and maximum difference among all ML points and AP points [50].

4. Gait cycle or the way a human walks can also be affected by the Parkinson's disease. Gait alterations in patients with PD can strongly affect their ability to work, exercise, and engage in daily activities. A description of the human gait cycle

[2]EGG is a device used for the measurement of the degree of contact between the vibrating vocal folds during voice production, and therefore estimate the voice quality

along with the diagnosis of PD based on gait cycle are presented in the following sections.

2.4 Human gait analysis and gait cycle phases description

This section presents an analysis of human gait and describes the gait cycle phases.

2.4.1 Human gait analysis

Gait analysis is the systematic study of bipedal locomotion in human. This analysis encompasses quantification as well as interpretation of measurable parameters characterizing the human bipedal locomotion from a given gait pattern [51].

Spatio-temporal parameters are generally used to characterise the human walking [52].

The spatial parameters are:

- Step length: is the distance measured from the contact with the floor of one foot to the same contact of the other foot. It can also be defined as the distance between the two heels during double support.
- Stride length: is the distance measured between the initial contact of one foot and the next initial contact of the same foot. The stride corresponds to a two-step succession.
- Step width: is the distance between the axis of progression and the middle part of the heel.

The temporal parameters are:

- Heel strike: when the initial contact is with the heel. The initial contact is the instant in the gait cycle when the foot initially contacts the ground.
- Double and Single stance support: the first one implies a period of bilateral contact of the two feet with the ground while the second one corresponds to one contact with a single foot.

- Step period: is the time period for a step, and is measured from a specific event of a foot (usually the heel strike) to the same next event of the opposite foot.
- Cadence: is the rhythm of a person's walk, measured in number of steps per minute.
- Gait speed: is the product of the average step length by the cadence.

Gait analysis is an open and competitive topic that is attracting increasing interest in various multidisciplinary fields. In sport, such an analysis is a very useful tool in coaching for improving the performances of athletes and preventing injuries. Gait analysis can also aid clinicians in gait recovery process monitoring in subjects following operations or in course of processes of rehabilitation. In the rehabilitation, events distinguishing gait phases may be used as functional electrical stimulation control variables. Moreover, gait analysis can be exploited in the design and control of wearable assistive devices such as exoskeletons, prostheses and orthoses, used for walking assistance for elderly and subjects with paretic lower limbs. Gait analysis can also be used in healthcare monitoring for the detection of abnormal gait and estimation of fall risk. An abnormal gait can be seen as a symptom indicating neurodegenerative diseases progression. For example, the presence of gait abnormalities in the elderly, is frequently an important predictor of the risk of dementia development. Finally, the generation of walking models for human gait imitation based humanoid robots, is another potential application field of the human gait analysis [53].

The early work on gait analysis was conducted at the end of the 19th century and the first applications in biomedical engineering arisen with the availability of video camera systems [54–58]. Numerous gait laboratories have successfully developed and implemented a standard gait analysis method based on a force platform with the capability of measuring Ground Reaction Forces (GRFs) and on a multi-camera motion capture system [59, 60]. Yet, this standard method of gait analysis necessitates expensive equipment, specialized locomotion laboratories, and long-time of installation and post-processing. In addition, limitations have been observed in terms of the moving area and gait cycles for the observed subject. To overcome these limitations, other methods of gait analysis based on wearable sensors were proposed.

2.4.2 Human gait cycle description

Walking is a form of movement that represents the most important human physical activity because it is at the basis of several daily living activities. It represents a cyclical activity in which each stride (gait cycle) follows the other one continuously. The gait cycle describes how subjects walk; it represents a pattern of movement that is specific to each individual [53]. A gait cycle starts when the toe of the Right Foot (RFo) and the heel of the Left Foot (LFo) touch the ground simultaneously and ends with the same configuration.

The gait cycle is mainly divided into two phases: the stance phase and the swing phase. The stance phase represents the period during which the foot is in contact with the ground while the swing phase corresponds to the period during which the foot is in the air for the advancement of the leg. The initial contact is the beginning of the stance phase and the swing phase starts when the foot is lifted from the ground (Fig. 2.4)[61].

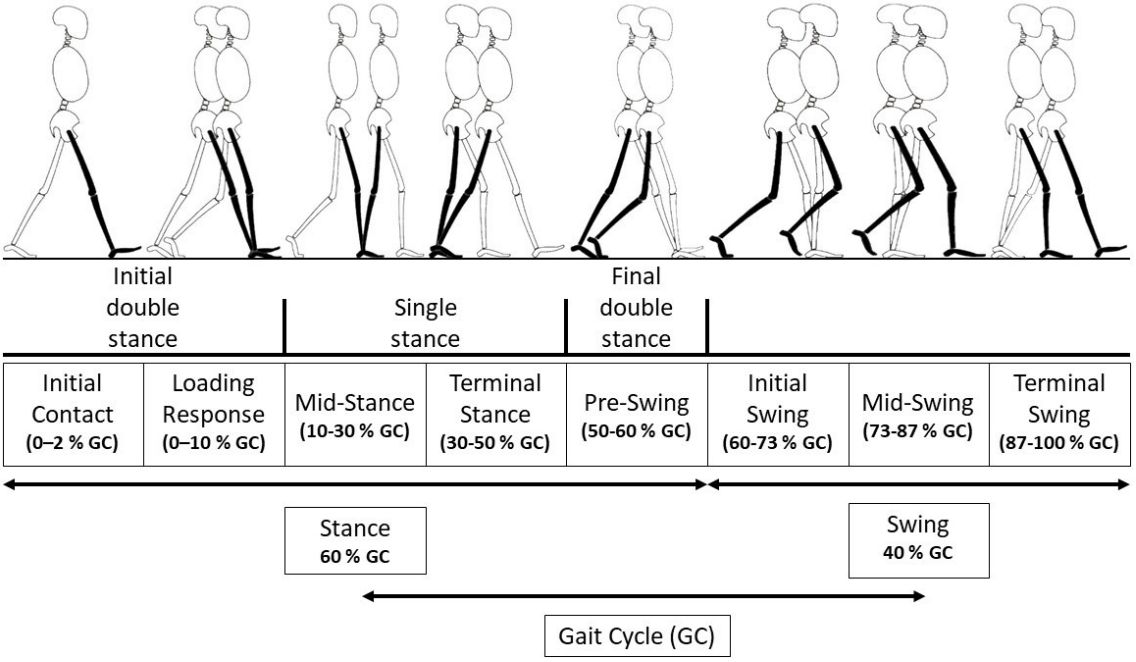

FIGURE 2.4: Gait cycle sub-phases [61]

Concerning the time percentage of each phase, the stance phase represents 60 % of the gait cycle time while the swing phase represents 40 % [62–64]. The exact duration of each phase changes according to the subject's walking velocity [65, 66]. In a normal walking pace (80 m/min), the stance and the swing phases represent, respectively, 62 % and 38 % of the gait cycle time. Furthermore, it can be noted that the walking speed

and the two phases durations have an inverse relationship ; swing and stance phases durations are shortened when the gait speed increases, and vice-versa.

The stance phase is generally subdivided into three intervals according to the sequence of contact between the two feet and the ground. The first and third intervals imply a period of bilateral contact of the two feet with the ground (double stance) while the second interval corresponds to one contact with a single foot (single stance) (Fig. 2.4)[61]. In the following, a brief description of these intervals is presented.

- Initial double stance occurs after initial contact when both feet are in contact with the ground.
- Single stance starts when the left foot is lifted from the ground to initiate its swing phase.
- Final double stance starts when the left foot touches the ground, and ends when the right foot is lifted from the ground to initiate its swing phase.

The timing for the stance intervals is as follows: 10 % for each double stance sub-phase and 40 % for the single stance. Since the single stance of one foot and the swing phase of the second one occur at the same time, they have the same duration (see Fig. 2.4).

As presented above, the stance phase and the swing phase are the main phases of the gait cycle, but in practice, the cycle can be divided up to eight sub-phases (functional patterns): five sub-phases in the stance phase and three sub-phases in the swing phase [61] (see Fig. 2.4). The eight gait cycle sub-phases are defined hereafter :

- Initial Contact (heel strike): is a short sub-phase that includes the moment the right foot contacts the floor. The duration of this sub-phase represents from 0 to 2 % of the gait cycle.
- Loading Response (foot flat): represents the initial double stance interval. It begins when the right foot touches the floor (heel strike) and continues until the left foot is lifted from the floor to initiate its swing phase. The sub-phase duration varies from 0 to 10 % of the gait cycle.

- Mid-Stance: It starts when the left foot leaves the floor and continues until the body center of gravity is aligned over the right foot. The duration of this sub-phase corresponds to 10 - 30 % of the gait cycle.

- Terminal Stance: It starts with heel rise and ends when the left foot touches the floor. The duration interval represents from 30 to 50 % of the gait cycle.

- Pre-Swing: It starts with initial contact (heel strike) of the left foot and ends with the toe-off of the right foot. The sub-phase duration corresponds to 50 - 60 % of the gait cycle.

- Initial Swing: It starts with lift of the right foot from the ground and continues until the swinging (right) foot is opposite to the stance (left) foot. The duration interval represents from 60 to 73 % of the gait cycle.

- Mid-Swing: it starts with the toe-off of the right foot and continues until the right foot is forward and the tibia [3] is in a vertical position. The duration of this sub-phase is estimated at 73 - 87 % of the gait cycle.

- Terminal Swing: it starts when the tibia is vertical and ends when the right foot touches the floor. The duration of this sub-phase represents from 87 to 100 % of the gait cycle.

The number of sub-phases studied varies from one study to another. In [67, 68], the authors take into consideration the eight gait cycle sub-phases. In [69], Nordin and Frankel consider a seven sub-phases gait cycle: initial contact, mid-stance, terminal stance, pre-swing, initial swing, mid-swing and terminal swing. In some early literature ([70]), the initial contact is considered as a part of the loading response sub-phase. In [53], authors take into consideration six sub-phases, by eliminating the initial contact and the initial swing sub-phases. In [71], Williamson and Andrews consider four stance sub-phases (the loading response, the mid-stance, the terminal stance and the pre-swing) and the swing phase. In [72], the gait cycle is divided into stance, heel-off, swing and heel-strike sub-phases. Finally, several researchers only consider the stance and swing phases in their studies, as in [73, 74].

[3] The larger of the two long bones in the lower leg

2.5 Gait cycle of Parkinsonian subjects

Parkinson's disease (PD) subjects usually suffer from gait alterations that increase with progression of the disease.

- **Freezing of gait**: Freezing of gait is defined as a brief, episodic absence or marked reduction of forward progression of the feet despite the intention to walk. This phenomenon is, in general, temporary, and the gait may be at a normal pace after few steps. This gait alteration can be triggered by contextual (eg. emotional, cognitive) and environmental factors, such as: walking through a doorway or a narrow passageway, changing directions, approaching one's destination (such as a chair or couch), crossing a street, and simply when a patient feels like he/she is being rushed [15]. For PD patients, gait freezing induces increased risk and frequency of falls [2].
- **Shuffling gait**: Subjects with PD may walk slowly with their chest bent forward, with short fast shuffling steps. This results in reduced stride length and walking speed. Subjects show also less arm and body movement which gives them a stiff appearance [75].
- **Festinating gait**: characterized by a short and fast stride. Short stride and fast step lead to a quite inefficient gait, which makes the walking person tired and frustrated [76].
- **Hypokinesia**: characterized by a small amplitude movements [77]. This alteration is associated with difficulties throughout the walking process, from preparing to initiation and finally performing walking. Execution of simultaneous and sequential of the walking movements is hampered [15].

These gait alterations increase the risk and the rate of fall. Falls may lead to severe injuries and fractures. The fear of falling is another consequence which results in a restriction of daily activities that in turn lead to a loss of independence and increased mortality. The fear of falling has psychological consequences, such as isolation with less social interactions and depression risk [77]. The effects of PD on the evolution of the stride-to-stride variability during a gait cycle have been extensively studied in the literature [78]. Yogev et al. [79] studied the cognitive function and the effects of different

types of dual tasks on the gait of subjects with PD. The outcomes of this study show that the executive function [80–82] is deteriorated in the subjects with PD. In [37], the authors discuss gait asymmetry (GA) in subjects with PD. The outcomes of this study show that when gait becomes impaired and less automatic, Gait Asymmetry apparently relies on cognitive input and attention. In the same context, Hausdorff et al. [38] focused on the gait dynamics to evaluate the effect of Rhythmic Auditory Stimulation (RAS), which consists of using musical stimuli to enhance the gait performance of neurological conditions subjects (e.g., subjects with PD). It has been shown that RAS promotes more automatic movement and reduces stride-to-stride variability in subjects with PD. The study conducted in [64], showed that the ability to maintain a steady gait with low stride-to-stride variability decreases in subjects with PD. In [39], the authors showed that swing time variability is independent of gait speed in subjects with PD; therefore, this can be used as a marker of rhythmicity and gait steadiness. The obtained results show also an increase in the variability of stride time and swing time at comfortable walking speeds for the subjects with PD compared to control subjects.

2.6 Gait assessment techniques

This section presents the semi-subjective and objective techniques used for gait analysis, as well as the different types of sensors used for measuring and estimating gait parameters.

2.6.1 Semi-subjective techniques

The tests and measurements traditionally used for analyzing gait parameters in clinical conditions are carried out by therapists by observing and evaluating the patient's gait-related parameters while he/she walks along a pre-determined circuit. Several semi-subjective techniques are traditionally used in clinics [83]:

- Timed 25-Foot Walk (T25-FW): known as the 25 foot walk test. During this test, therapist measures the time taken by the patient to walk a distance of 7.5 m in a straight line [84].

- Multiple Sclerosis Walking Scale (MSWS-12): is a self-assessment scale which measures the impact of multiple sclerosis on walking. It consists of 12 questions concerning the walking difficulties due to multiple sclerosis during the past 2 weeks [85].

- Tinetti Performance-Oriented Mobility Assessment (POMA): the protocol used in this assessment is as follows, (1) the patient is seated in a chair without armrests; (2) the patient is asked to stand up, if possible without leaning on the armrests, a balance test in the standing position is then performed; (3) the patient must turn 360°; (4) the patient must walk at least 3 meters forward, turn around and return back quickly to the chair. He must use his usual technical assistance (cane or walker); (5) the patient must sit on the chair [86]. This test allows to precisely evaluate gait disorders and elderly subjects' balance in daily life situations [83].

- Timed Get up and Go (TUG): in this test, the clinician measures the time taken by the subject to get up from a sitting position, walk a short distance, turn 180°, then return back to the chair and sit down again [87].

- Gait Abnormality Rating Scale (GARS): is a video-based analysis used to rate the subjects' gait according to 16 variables using a 4-point scale (0 = normal, 1 = mildly impaired, 2 = moderately impaired, 3 = severely impaired). These variables can be classified into: general categories (5 variables), lower extremity categories (4 variables), and trunk, head, and upper extremity categories (7 variables). The GARS is obtained by summing each of the individual variables. More impaired gait is characterized by a higher score [88].

- Extra-Laboratory Gait Assessment Method (ELGAM): is a method to quantify gait in the community or home. In this method several parameters are studied such as initial starting style of walking, walking speed, step length, static balance and ability to turn head during walking [89].

Tests and measurements used in semi-subjective techniques are usually followed by a self-assessment step in which the patient is asked to give a subjective evaluation of his/her gait quality. The aformentioned methods have the disadvantage of relying on subjective measurements that may have an incidence on the quality of diagnosis and treatment [83].

2.6.2 Objective techniques of gait analysis

With advances of sensor technologies, new techniques have been introduced as an alternative to semi-subjective techniques. These techniques have the advantage to provide a more reliable information related to gait parameters, and therefore, a more objective evaluation of gait quality as well as a more reliable diagnosis. The objective techniques of gait analysis differ from the semi-subjective ones by the use of different sensors for measuring and estimating the gait parameters. Sensors used for gait analysis can be classified into two main categories: non-wearable or wearable (Fig. 2.5).

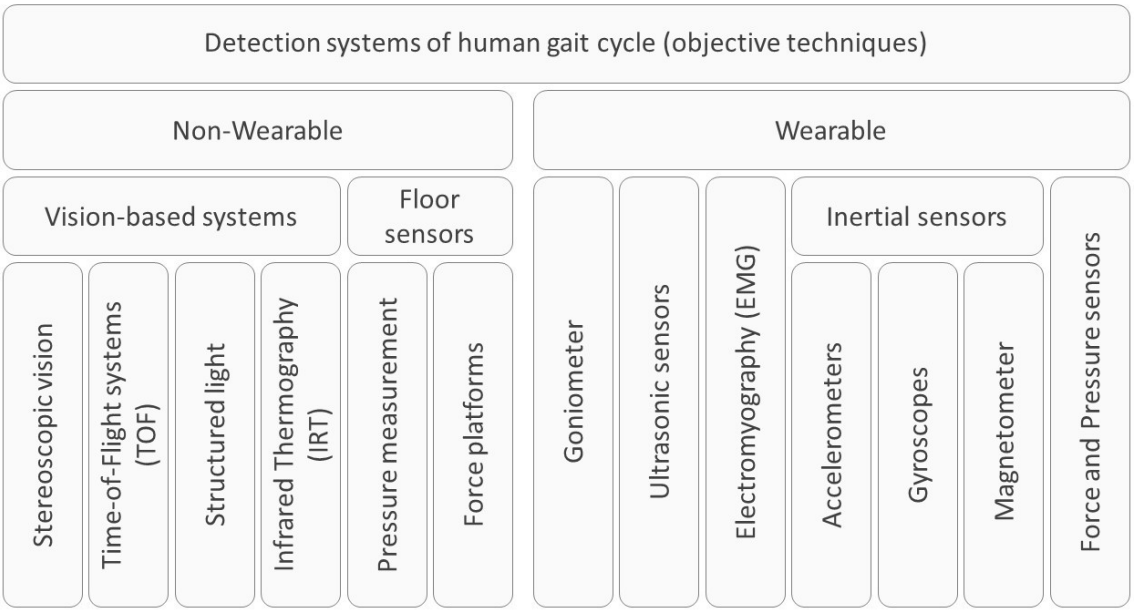

FIGURE 2.5: Sensors used for gait analysis: Wearable and Non-Wearable sensors.

Non-wearable sensors can be classified into two sub-categories. The first sub-category includes floor sensors such as force platforms and pressure-measurement systems; pressure sensors and Ground Reaction Force (GRF) sensors are used to extract gait information by measuring the force exerted by the subjects feet on the floor during walking. The second sub-category includes mainly vision-based systems such as optical motion capture (OMC) systems (Fig. 2.6). An OMC system consists of multiple optoelectronic cameras and allows an objective and accurate measurement of gait parameters. As alternative non-wearable sensors for gait analysis, infrared sensors, Time-of-Flight (ToF) cameras, laser range finders (LRF) placed at predefined positions [90] or mounted on robotic rollators are also used [91]. Non-wearable sensors are generally expensive and present several constraints that limit their use to instrumented and indoor environments.

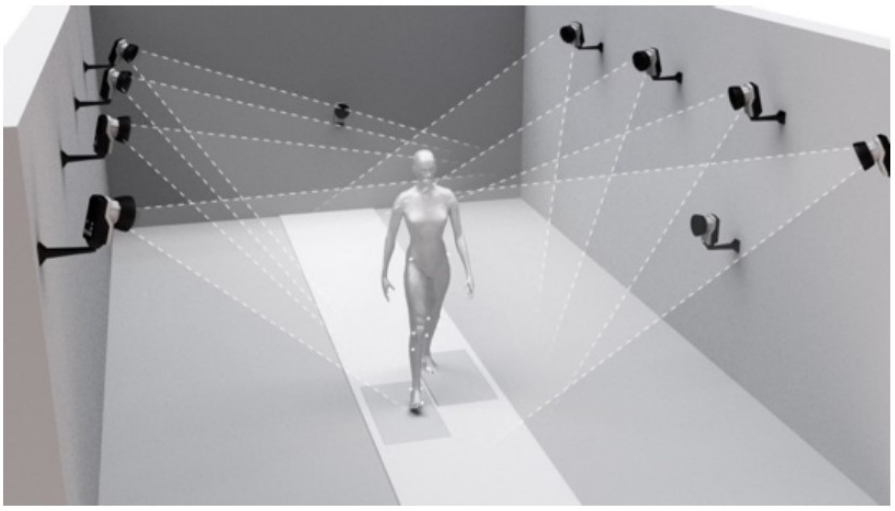

FIGURE 2.6: Example of an optical motion capture (OMC) system [99]

Among wearable sensors, foot pressure insoles or foot switches are the most commonly used since each specific pattern of the used sensor output can be associated with a gait phase [92–95]. Several other wearable sensors including inertial measurement units (IMUs) are also commonly used for gait analysis. An IMU typically includes 3D accelerometer, 3D gyroscope and 3D magnetometer. Placed at different key points of the human body, such as the feet, knees or hips, these sensors provide inertial quantities, i.e. linear accelerations and angular velocities that allow the estimation of different features of the gait cycle [71, 96–98]. Other types of sensors such as goniometers, ultrasonic sensors and EMG sensors, are also used. Wearable sensors are low-cost and do not require complex signal conditioning and post-processing. They are well-suited for long-term measurements and ambulatory gait analysis. Table 2.1 reports the wearable and non-wearable sensors commonly used in the study of PD.

2.6.2.1 Non-Wearable sensors

As mentioned above, the non-wearable sensors category can be divided into two sub-categories: the first one includes floor sensors while the second one includes mainly vision-based systems. The interest of these sensors for quantifying and analysing the different human gait aspects, has been demonstrated in numerous studies [83]. In the following, a brief description of the two sub-categories of non-wearable sensors is presented.

TABLE 2.1: List of the wearable and non-wearable sensors commonly used in PD study

Types	Sensors	Studies
Wearable sensors	In-shoe foot pressure system	[100]
	Goniometer	[101, 102]
	Electromyograph (EMG)	[101, 103–105]
	3D sensor detector	[105]
	Ultrasonic sensors	[106]
	Accelerometer	[102, 107, 108, 110]
	Gyroscope	[111, 112]
Non-wearable sensors	CCD camera	[113]
	Kinect sensors	[114]
	Infrared camera Vicon systems	[114]
	Panasonic NV-GS500 camcorders	[115]
	Microsoft 3D camera sensor based on ToF	[116]
	Microsoft Kinect	[117]
	ThermoVision Infrared Camera	[118]
	Motion analysis system	[119]
	Camera motion analysis system	[120]
	Force platform	[102, 119–122]

1. **Vision-based systems**: Typically, these systems are constituted by numerous analog or digital cameras that can be used to collect information related to the human gait (See Fig. 2.7). In [113], the authors propose a vision-based diagnostic system for recognizing gait patterns of PD subjects. Gait videos of PD and healthy subjects are used to evaluate the feasibility of the system in PD gait recognition. In [114], the authors use a Vicon three-dimensional motion analysis system (gold-standard) and a Kinect to detect simultaneously the movements of PD and healthy subjects.

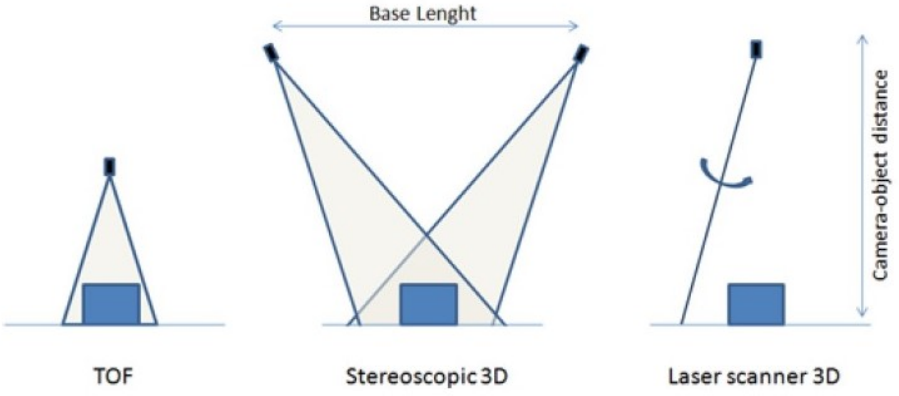

FIGURE 2.7: Different non-wearable sensors for gait analysis [83]

In the following, a summary of the different technologies used in vision-based system is presented:

- **Stereoscopic vision**: it can be used to determine the points depth in the scene from for example the midpoint of the line connecting their focal points. For this purpose, it is necessary to find the corresponding points in different images [83]. In [115], Pachoulakis et al. use motion capture techniques and a stereoscopic vision to obtain 3D skeletal motion data of PD and healthy subjects.
- **Time-of-Flight Systems (ToF)**: these systems exploit cameras using signal modulation. The principle of phase-shift is used for distances measurement [123]. In [116], Dror et al. propose an automatic assessment approach of PD from natural hands movements using a Microsoft 3D camera sensor based on Time of Flight (ToF) technology.
- **Structured Light**: is the process of projecting a light pattern (grid, plane, coded light, etc.) onto a scene. Depth and surface information of the objects in the scene are calculated by analysing the projection deformation of the pattern with respect to the initial projected pattern [83]. In [117], authors propose a method to detect and assess the severity of Levodopa-Induced Dyskinesia in PD using Kinect recordings of the patients. A depth image is produced by a standard structured light based Kinect camera.
- **Infrared Thermography (IRT)**: Its principle consists of creating visual images based on surface temperatures. This technique is used to measure precisely the infrared thermal intensity of the human body. In [118], the authors use a ThermoVision infrared camera to differentiate PD subjects from healthy subjects using hands thermographic recordings (Fig. 2.8).

2. **Floor Sensors**: Two types of systems can be distinguished: forces platforms and pressure-measurement platforms. These platforms are used to extract gait information by measuring the force and the pressure exerted by the subjects feet on the floor during walking. Pressure measurement platforms allow in addition to determine the location of the Center of Pressure (CoP). The force platform AMTI series OR6-7 of Biometrics France, shown in Fig. 2.9, is an example of commercial

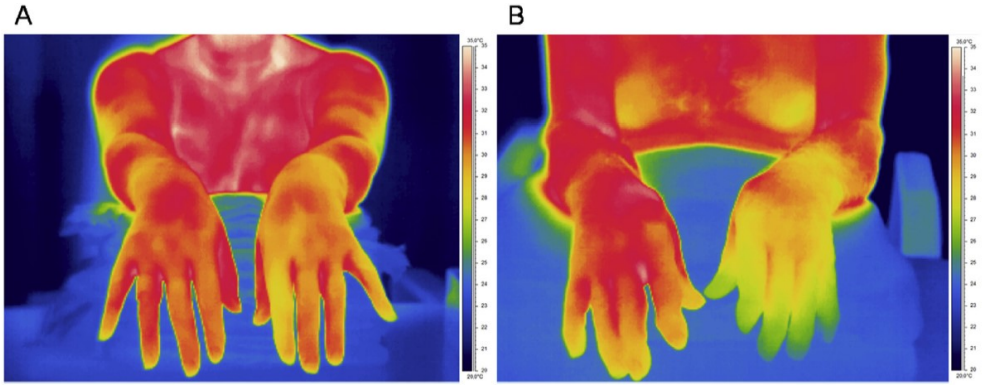

FIGURE 2.8: Hands thermographic recordings of (A) Healthy subjects and (B) PD subjects. The PD patient shows in (B) a thermal asymmetry between the two hands [118].

force platform [83]. This type of systems is used in PD diagnosis based on gait analysis [119–122].

(a) Force Plateform [83]

(b) Array of Force platforms

FIGURE 2.9: AMTI Force Plateforms

2.6.2.2 Wearable sensors

As mentioned above, in gait analysis, wearable sensors are placed on different parts of the human body, such as the hip, thigh, lower thigh, knee, and foot in order to measure different human gait characteristics (Figure 2.10). In the following paragraphs, a brief description of wearable sensors commonly used in the diagnosis of PD is presented.

1. **Goniometers** (See Fig. 2.11): These sensors are used to study the kinematics (angles) of joints such as knees, hips, ankles, and metatarsals [51, 83]. Goniometers have been used in several studies for PD diagnosis [101, 102].

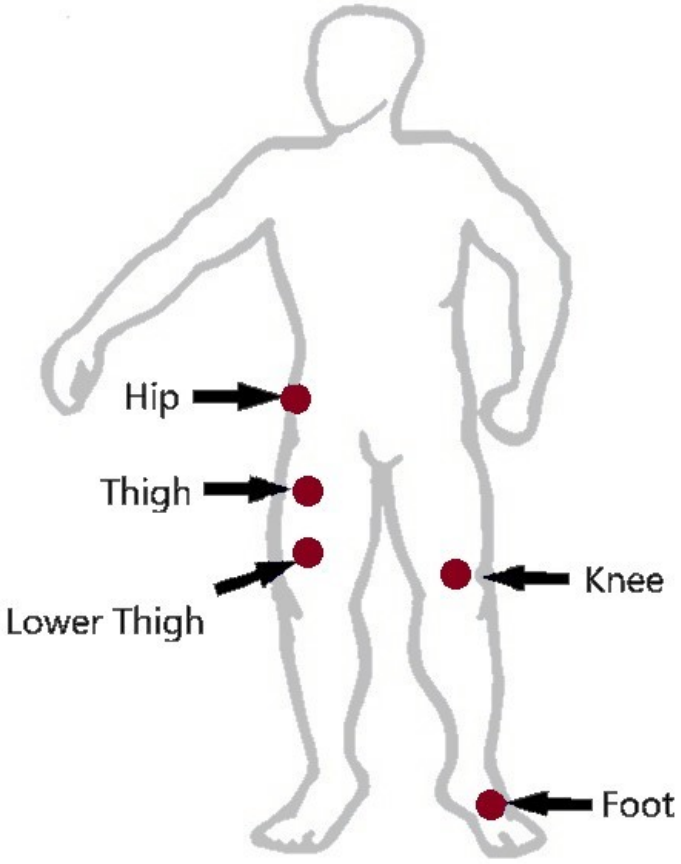

FIGURE 2.10: Placement of wearable sensors [124]

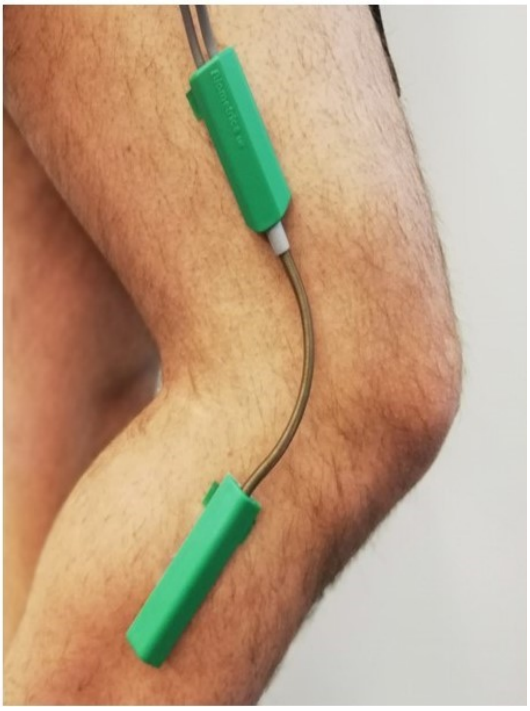

FIGURE 2.11: Goniometer for knee joint angle measurement

2. **Ultrasonic Sensors**: these sensors are generally used to measure spatial parameters such as stride length, step length, the separation distance between feet, and the distance between feet and the ground. This type of sensor is used in the assessment of human gait symmetry in PD patients [106]. In [125], authors use a foot-mounted ultrasonic sensor for extracting the following gait phases: heel-strike, heel-off, toe-off and mid-swing (see Fig. 2.12).

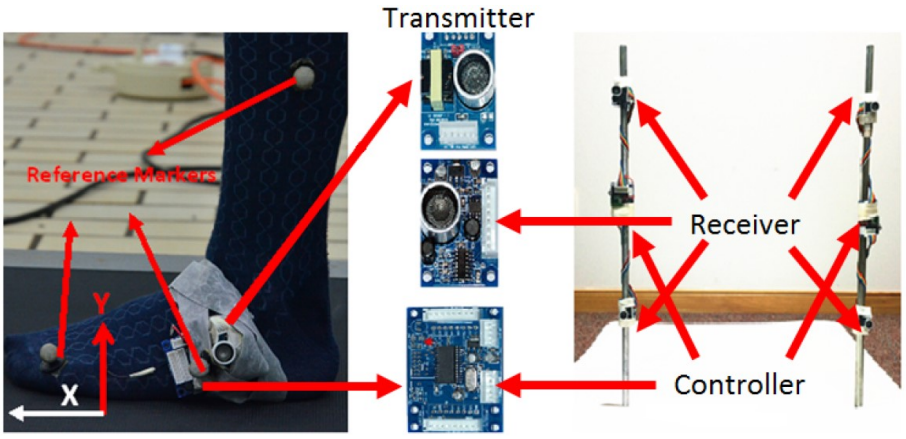

FIGURE 2.12: Hardware system of the foot-mounted Ultrasonic sensor system [125]

3. **Electromyography (EMG)** (see Fig. 2.13): EMG consists of measuring the electrical activity of voluntary or involuntary muscle contraction. In [103], EMG is used to analyse the temporal pattern and the magnitude of the electromyographic activity of PD subjects lower limb muscles just before freezing, in comparison with the normal and pre-stop strides [83]. Other studies used EMG in the same context as [104, 105].

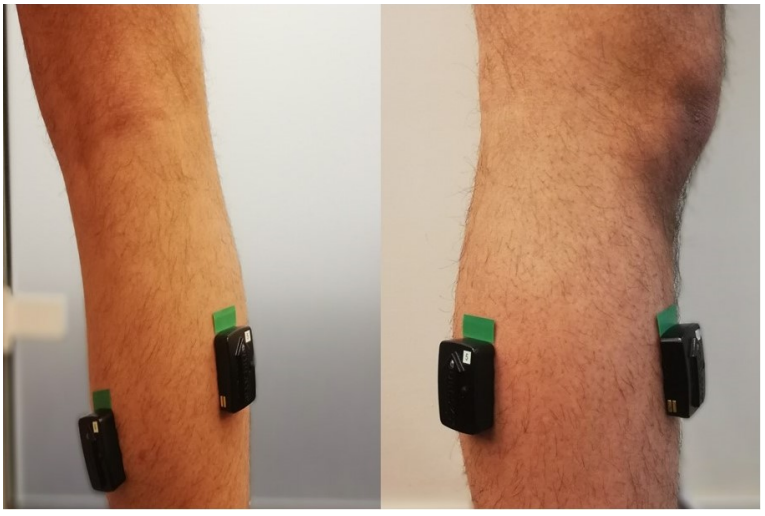

FIGURE 2.13: Electromyography (EMG) sensors

4. **Inertial Sensors**: These sensors allow measuring the velocity, orientation, acceleration, and gravitational forces of an object, through a combination of gyroscopes, accelerometers and occasionally magnetometers. Accelerometers and gyroscopes can be used to measure the signals characterizing the gait phase (see Fig. 2.14). To carry out the gait analysis, the feet accelerations can be then measured during the walk, by attaching these accelerometers to the feet [51]. Accelerometers are used in PD assessments and monitoring in [107, 108]. Gyroscope are used for gait cycle detection in subject with PD in [109].

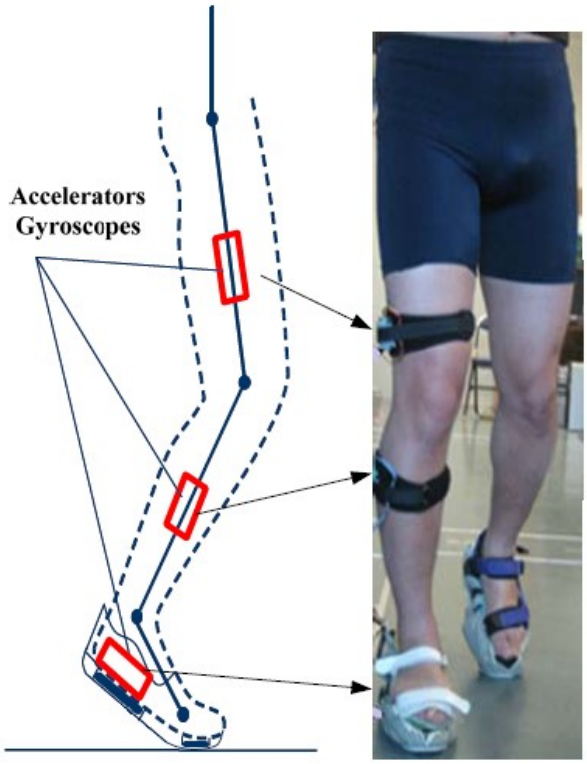

FIGURE 2.14: Gyroscopes for kinematic measurment [51]

In the category of inertial sensors, MTx units series from Xsens company are well known commercial products (see Fig. 2.15). Each unit includes typically a tri-axial accelerometer, a gyroscope and a magnetometer, to measure respectively, the 3D acceleration, the 3D angular velocity and the local Earth magnetic field vector. These units can be connected in series using the Xbus Master [124].

5. **Force and Pressure Sensors**: These sensors are generally in-shoe measurement systems that are based on the same principle as floor sensors, but have the advantage that they are well-suited for long-term measurements and ambulatory gait

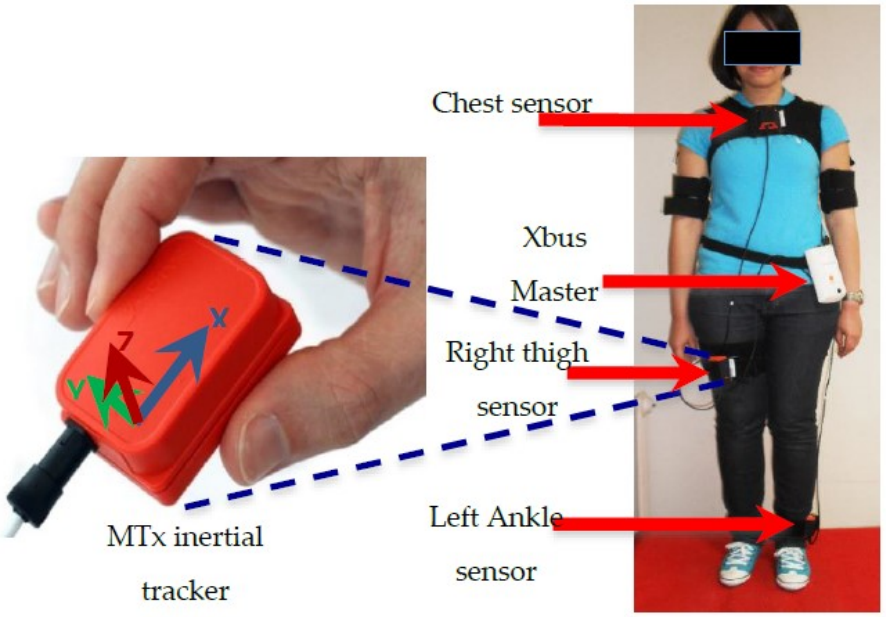

FIGURE 2.15: Xsens (MTx) inertial tracker and sensors placement [124]

analysis. In the category of force and pressure sensors, F-scan from Tescan is a well-known commercial in-shoe pressure measurement system that allows wireless recording of pressure and force measurements during walking (Fig. 2.16 and 2.17). F-scan quantifies the subject's plantar pressure from 960 sensels [4], arranged in columns and rows on the sensor. The F-scan operates at a scan rate of up to 100 Hz for each sensor.

FIGURE 2.16: The Tekscan F-scan Force Sensitive Resistors (FSR) insoles [131]

[4] individual pressure sensing locations

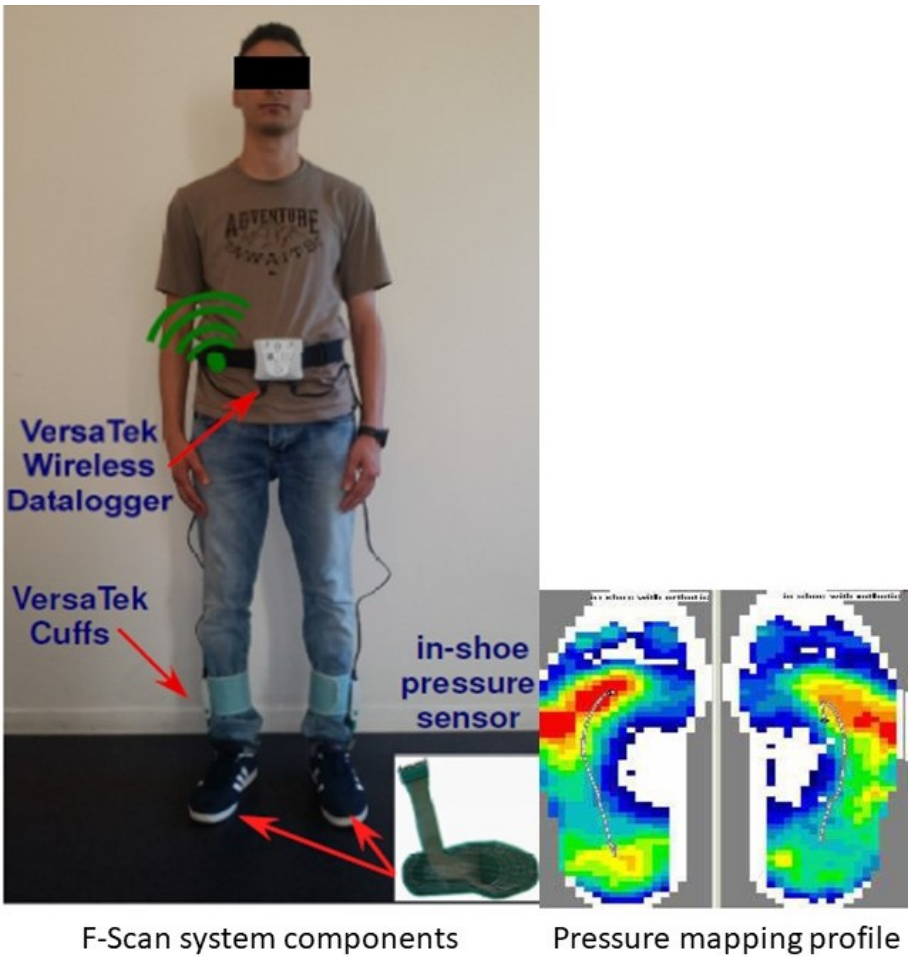

FIGURE 2.17: F-Scan measurement system [53]

In [100], Jean et al. study the classification of the spatial-temporal image of plantar pressure (STIP) obtained using an in-shoe dynamic foot pressure system. In [110], Mariani et al. propose an approach based on in-shoe wearable sensors to provide measurements that characterize the mobility symptoms of PD during Timed Up and Go (TUG) and gait tests. The following spatio-temporal parameters were used in the study: swing width, turning, path length and their inter-cycle variability. Likewise, the vertical and horizontal Ground Reaction Forces were used in [128–130]. Other studies exploiting vertical Ground Reaction Forces (vGRFs) will be presented in the next chapter (Fig. 2.18).

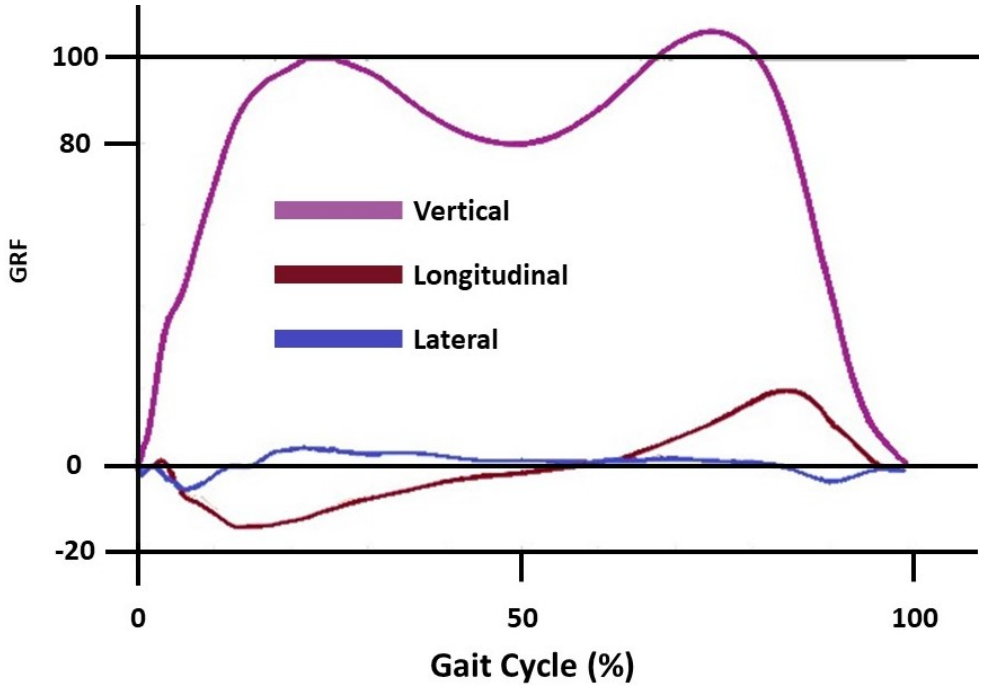

FIGURE 2.18: Vertical, longitudinal, and lateral components of the Ground Reaction Forces (GRF) during gait cycle [132].

2.7 Positioning of the thesis

In this chapter, we presented the general context of the thesis. We first gave a brief description of Parkinson's disease, its symptoms, along with the approaches commonly used for the diagnosis. Currently, the diagnosis made by doctors to assess the severity level of PD is conducted using various methods based on the assessment of cognitive deficits, speech disorders, human stability, gait cycle, etc. [133]. The absence of specific test for the Parkinson's disease makes it challengeable to diagnose subjects suffering from this disease. In addition, signs and symptoms similar to those of Parkinson's disease may have other causes, such as dementia with Lewy bodies, progressive supranuclear palsy, and certain types of stroke. Similar symptoms can also be observed in the case of exposure to some toxins, intake of some antipsychotic medication, as well as a head injury. This might further complicate the PD diagnosis using only qualitative criteria such as bradykinesi, hypertonia, depression, pain, fatigue, etc. Hence, machine learning based tools have been recently the subject of great interest to assist physical doctors in their daily diagnosis process. Furthermore, the study of gait parameters such as step length, step frequency and velocity is useful in understanding the mechanism of human motor control and in recognizing neurological disease progression. In this context, the

study of the gait cycle has been strongly applied to evaluate gait pattern disorders [133]. This thesis exploits gait cycle analysis to diagnose PD. Gait disturbances are often observed with the PD progression. Therefore, the main objective of this thesis is to provide an efficient machine learning tool that aims at supporting physiotherapists in the diagnosis process by exploiting the most relevant features extracted from gait cycle. The challenge is to achieve an accurate classification between healthy and PD subjects, and also, between subjects with different levels of severity of the disease. For this purpose, two possible improvements of the diagnosis accuracy are investigated. The first one consists of considering only the most relevant spatio-temporal features from the clinical point of view among those extracted from vGRFs signals during walking. The second possible way of improvement is to exploit the repeatability of gait cycle in PD subjects and more precisely the similarity of stance phases time-series in unidimensional and multidimensional cases.

Chapter 3

Data-driven approach to aid Parkinson's disease diagnosis

3.1 Introduction

In this chapter, we propose a data-driven approach for Parkinson's disease diagnosis. We present firstly the general background including data pre-processing (features computation, feature extraction and feature selection) followed by presentation of the main supervised and unsupervised classification approaches used in this study. An online dataset of vertical Ground Reaction Forces (vGRFs) data collected from gait cycle is used [1].

The rest of this chapter is organized as follows: Section 3.2 presents the methodological background of the study, in particular, (1) the feature extraction and feature selection processes, (2) the supervised and unsupervised classification approaches, as well as (3) the performance evaluation metrics. Section 3.3 is dedicated to the related works. Sections 3.4 and 3.5 present the implementation of the above-mentioned methodology for the PD diagnosis.

3.2 General background

This section presents the standard phases that are commonly used in the machine learning process. These phases include: data acquisition and preprocessing, feature extraction and selection, classification and performance evaluation. In the following, a systematic review of the feature extraction/selection, classification and performance evaluation methods is presented.

3.2.1 Pre-processing

Data pre-processing is one of the most important steps in the data mining process. It consists of filtering data, replacing the missing and outlier's values and extracting/selecting features. To extract features from raw data, windowing techniques are generally used, which consist of dividing sensor signals into small time segments. Segmentation and classification algorithms are then applied respectively to each window. Three types of windowing techniques are usually used: (i) sliding window where signals are divided into fixed-length windows; (ii) event-defined windows, where pre-processing is necessary

[1] PhysioNet dataset

to locate specific events, which are further used to define successive data partitioning and (iii) class-defined windows where data partitioning is based on the detection of class changes. The sliding window approach is well-suited to real-time applications since it does not require any pre-processing treatments [134].

3.2.1.1 Features computation

Signal characteristics such as time-domain and frequency-domain features are widely used for feature calculation. Time-domain features include mean, median, variance, skewness, kurtosis, range, etc. Peak frequency, peak power, spectral power on different frequency bands and spectral entropy are generally included in the frequency-domain features. Time-domain and frequency-domain features that are commonly used, are presented in the table below (Figure 3.1)

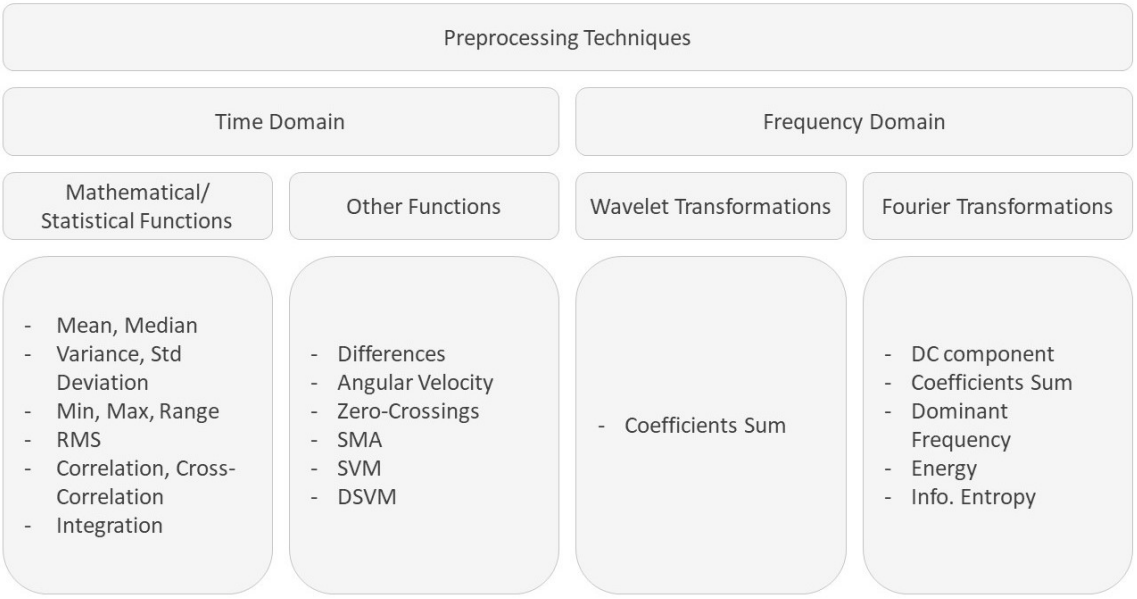

FIGURE 3.1: Time-domain and frequency-domain features [135].

3.2.1.2 Features Selection

Feature selection consists of selecting a subset of relevant features from the original feature set [136]. To differentiate between samples, classification algorithms need representative features. Using inappropriate or redundant features may deteriorate the performance of a classification algorithm. This may result in a curse of the dimensionality problem and a decrease of classifier performance, therefore, selecting a reduced number

of features, which have optimal discriminative power between classes, is a significant phase in data mining. The feature selection is defined as a process of searching a subset of appropriate features from the original set. Feature selection is an important step in the use of machine-learning algorithms as it reduces computation time and complexity while improving the overall classification rate.

Liu et al. [137] categorized the feature selection process in a three-dimensional framework into a data mining task, an evaluation criterion, and a search strategy. The feature selection process is generally categorized into three categories: filter methods [137], wrapper methods [138] and hybrid methods [139]. Filter methods operate directly on the dataset by exploiting the intrinsic properties of the features. These methods rank a set of selected features according to the estimated weights of each feature. It should be noted that filter methods do not use any classifier in the selection process. Unlike filter methods, wrapper methods, which often yield better results, use a classifier to evaluate the selected subsets based on their predictive accuracies. Finally, the hybrid methods select the most relevant subset based on the use of some internal parameters of the machine-learning algorithm. In these methods, no validation step is required in the process of feature selection.

3.2.1.3 Features Extraction

The combination of original features is an alternative way of selecting a subset of relevant features. This technique consists of combining the original features set in order to define a new relevant features set. In other words, feature extraction is the transformation of high-dimensional data into a meaningful representation data of reduced dimensionality. The main advantage of feature extraction is that it facilitates classification and visualization of high-dimensional data.

The most popular technique for feature extraction is principal component analysis (PCA) [140], which is a linear technique that consists of transforming the original features (generally inter-correlated) into new mutually uncorrelated features. These new features are the so-called principal components. The main idea behind PCA is to remap the original features into a low dimensional space in which the principal components are arranged according to their variance (from largest to lowest). The principal components that contribute to very low variance are omitted.

Linear Discriminant Analysis (LDA) allows also extracting features through a linear transformation. LDA is closely associated to principal component analysis (PCA) since these two methods try to find linear combinations of variables, which best represent the data [141]. The LDA method projects the original features points into a new space of lower dimension that maximizes the between-class separability while minimizing their within-class variability unlike PCA which, does not take into account any difference in classes.

The independent component analysis (ICA) [142] is another feature extraction technique commonly used on non-Gaussian data. This technique was initially developed to provide solution to the Blind Source Separation (BSS) problem. ICA searches for projections of original features such that the probability distributions of the projected data are statistically independent. The ICA algorithm aims at finding independent components, such as the original features that can be expressed as a linear combination of those components.

Another feature extraction method used in data mining is Factors Analysis (FA). In the FA method, the original features can be grouped according to their correlation. However, FA determines the group of features that are highly correlated but have small correlations with features in other groups by some factors.

3.2.2 Classification Techniques

The features extracted/selected from the raw sensor data are used as inputs of the classification algorithms. In general, the classification task requires learning a decision rule or a function associating the inputs data to the classes. There are two main directions in machine learning techniques: supervised and unsupervised approaches [142–144]. Supervised learning approaches for classification such as Artificial Neural Networks [143], Support Vector Machines (SVM) [145], require entirely labeled activity data. The unsupervised learning approaches, such as those based on Gaussian Mixture Models (GMM) allow to infer automatically the labels from the data.

In the following sections, we briefly describe the classification techniques used in this study (k-Nearest Neighbours (k-NN), Decision Trees (DT), Random Forests (RF), Naive

Bayes (NB), Support-vector machines (SVM), Gaussian Mixture Methods (GMM) and k-Means).

- **k-Nearest Neighbours (k-NN)**

  k-Nearest Neighbours (k-NN) [142, 144] is a supervised classification technique that can be seen as a direct classification method because it does not require a learning process. It just requires the storage of the whole data. To classify a new observation, the k-NN algorithm uses the principle of similarity (distance) between the training set and a new observation to classify. The new observation is assigned to the most common class through a majority vote of its k-Nearest Neighbours. The distance of the neighbors of an observation is calculated using a distance measurement called similarity function such as Euclidean distance. Moreover, one should note that when using the k-NN approach and a new sample is assigned to a class, the computation of distances (i.e., the computation time) increases as a function of the existing examples in the dataset [146].

- **Decision Trees (DT)**

  The decision trees is a supervised classification method [147] that is simple, effective and easy to interpret. A DT finds nonlinear relationships between the inputs and outputs of the classifier. A DT is an iterative classifier that separates variables into branches and nodes. The nodes are composed of one root node and diverse inertial nodes and leaves. Several algorithms have been used for DT construction including the Classification and Regression Tree (CART) [147], Iterative Dichotomiser (ID3) [148] and C4.5 [149], etc.

- **Random Forests (RF)**

  Random Forests (RF) [147] consists of a combination of decision trees. It improves the classification performance of a single-tree classifier by combining the bootstrap aggregating (bagging) method and randomization in the selection of partitioning data nodes in the construction of decision trees. The assignment of a new observation vector to a class is based on a majority vote of the different decisions provided by each tree constituting the forest. However, RF needs huge amount of labeled data to achieve good performances.

- **Naive Bayes (NB)**

  Naive Bayes (NB) is another simple supervised machine learning model based on the Bayes theorem [150, 151] with independence assumptions between observation data. NB's main advantage is that its learning model is simple and does not require any complicated iterative parameter estimation. Despite its simplicity, the NB model can outperform more sophisticated machine learning models.

- **Support Vector Machines (SVM)**

  Support Vector Machines (SVM), introduced by Vapnik [152], is a classifier derived from statistical learning theory. This well-known machine learning technique minimizes an empirical risk (as a cost function) and at the same time, maximizes the margin between the so-called separating hyperplane and the data.

  In their standard formulation, SVM are linear classifiers. However, non-linear classification can be achieved by extending SVM by using kernels methods [153]. The key idea of kernels methods is to project the data from the original data space to a high dimensional space called feature space by using a given non-linear kernel function. A linear separation in the resulting feature space can then be achieved by using the Cover's theorem [154]. Moreover, SVM is a binary classifier; therefore, to ensure a multi-class classification, pairwise classifications can be used (one SVM is defined by a class against all a convex others, for all optimization classes), which makes it time-consuming especially in the case of a large amount of data.

- **Gaussian Mixture Models (GMM)**

  A Gaussian Mixture Models (GMM) is a probabilistic approach, generally used in an unsupervised classification. Unlike standard probabilistic models based on approximating the data by a single Gaussian component density, GMM uses a weighted sum of finite Gaussian component densities. The parameters of GMM (the proportions, the mean vectors and the covariance matrices of the Gaussian components) are estimated using the expectation-maximization (EM) algorithm [155]. One of the drawbacks of this model is that in many cases the GMM does not guarantee the convergence to the global minimum and a particular attention needs to be given to the initialization of the EM algorithm.

- **k-Means**

  k-Means is a well-known unsupervised classification technique that can cluster n objects into k classes. k-Means clustering minimizes the distortion measure the total intra-cluster variance as a cost function. This consists of iteratively finding the cluster centroids, and then assigning the data according to their distance (e.g., Euclidean) to the cluster centroids, until convergence. One of the known limitations of k-Means is that it may have poor performance in the case of overlapping clusters (classes) and it does not define a density on the data and cannot therefore measure the uncertainty regarding the data classification, particularly in the overlap regions.

3.2.3 Performance evaluation

3.2.3.1 Generalization performance

The validation consists of the model evaluation derived from the learning step. It is important to measure the generalization error on examples that were not used in the learning process. Thus, it is necessary to divide all available data into two sets [156]:

- Learning set ($\mathcal{S}$) whose data will be used to build the model.
- Test set ($\mathcal{V}$) whose data will be used only to evaluate the performance of the obtained model.

There are several methods (called re-sampling techniques) that are used to assess the generalization ability of the obtained model. These techniques are applied with the assumption that the dataset used consists of independent and identically distributed (i.i.d) realizations:

1. **Hold out**: this validation technique consists of dividing the available data into two subsets (the learning set ($\mathcal{S}$) and the test set ($\mathcal{V}$)) without any common data. A fairly large number of data is required in the test set to estimate the generalization error with good accuracy, thereby reducing the number of data available for learning [157]. Often 70% of the data are kept for the learning and 30% are

used for the test. All the learning and test sets are randomly selected from the available data.

2. **K-fold cross-validation**: the initial set is divided into K disjointed subsets of approximately identical size (N/K), where N represents the total number of samples of the whole available data [158]. Each of these subsets is used as a test set while the others $(K-1)$ subsets are used for learning. The optimal value of K is the one that yields the highest score (minimum generalization error) of cross-validation.

3. **Stratified K-fold cross-validation**: several works have introduced the stratified re-sampling scheme in cross-validation, in order to respect the distribution of classes in each iteration. The underlying idea is to reduce the variability of the models produced after each learning step. Nevertheless, some authors [159] believe that this strategy is only truly effective if the initial data sample was extracted in a stratified manner from the initial dataset, i.e. the probabilities of occurrence of each class were explicitly respected when constructing the sample.

4. **Leave One Out**: this method is a special case of cross-validation in which $K = N$ [159, 160]. This technique requires repeating N times the classification method on $(N-1)$ observations making it prohibitive in terms of computation time but necessary when the number of samples is not high.

5. **Bootstrap** [161]: The Bootstrap is a relatively recent method compared to the other methods mentioned above. This method was initially developed to estimate certain statistical parameters such as mean, variance, etc. In the case of model selection, the parameter that is estimated is the generalization error. However, what is specific to the Bootstrap is that the generalization error is not estimated directly: but rather is estimated using the difference between the generalization error and the learning error on a subset of data extracted from the initial dataset.

3.2.3.2 Classifier performance evaluation

To evaluate the performance of the different classification techniques, the following metrics are commonly used:

- **Confusion matrix**: in the field of statistical learning, a confusion matrix is a table that allows the visualization of the performance of a classification method.

It also makes it easy to see if the classification method confuses several classes. Each column of the confusion matrix represents the instances of an estimated class while each row represents instances of a true class. Table. 3.1 shows a confusion matrix in the case of a binary classification.

		Obtained class	
		Positive	Negative
True class	Positive	T_p	F_n
	Negative	F_p	T_n

TABLE 3.1: Confusion matrix in the case of a binary classification.

where T_n (true negatives) represents the correct classifications of negative examples, T_p (true positives) represents the correct classifications of positive examples. F_n (false negatives) and F_p (false positives) represent, respectively the positive examples incorrectly classified into the negative classes and the negative examples incorrectly classified into the positive classes.

- **Accuracy**: The accuracy measure is used to evaluate the classifiers performances. In fact, this metric measures the proportion of correctly classified examples. In the case of binary classification, the accuracy can be expressed as follows:

$$Accuracy = \frac{T_p + T_n}{T_p + T_n + F_p + F_n} \tag{3.1}$$

The accuracy measure does not take into account the unbalanced datasets. In this case, the accuracy is particularly biased to favour the majority classes. Thus the following evaluation criteria are considered: the average of the accuracy rate and its standard deviation (STD), precision, recall, and F-measure.

- **F-measure**: The F-measure is defined as the combination of two criteria, the precision and the recall, which are defined as follows:

$$Precision = \frac{T_p}{T_p + F_p} \tag{3.2}$$

$$Recall = \frac{T_p}{T_p + F_n} \tag{3.3}$$

The F-measure is calculated as follows:

$$F - measure = \frac{(1+\beta^2).Recall.Precision}{(\beta^2.Recall + Precision)} \tag{3.4}$$

Where β is a weighting factor that controls the degree of importance of recall/-precision. This parameter is a positive real number. In this study, β is set to 1 to give the same importance to both recall and precision.

3.3 Related works

Classification of patients with PD has been extensively studied based on the use of ground reaction force sensors placed in shoes [128–130]. For example, the PD classification in [128] is based on vGRFs and uses a simple threshold-based classifier. However, this method has disadvantages due to its sensitivity to the choice and tuning of the threshold values [156]. In [128], Su et al. introduced measures of gait asymmetry by comparing the ground reaction force (GRF) features of both the left and right limbs. The effectiveness of the proposed measures was evaluated by differentiating between the walking patterns of patients with PD and healthy subjects, respectively. The differentiation was done through threshold-based and Multi-Layer Perceptron (MLP) models. A classical cross-validation procedure has been used to estimate the classifier performances; the dataset has been randomly divided into three subsets that are: training (80%), validation (10%) and test (10%) subsets.

Machine learning based approaches to classify patients with PD can be divided into two learning approaches: supervised and unsupervised [162]. In [129], patients with PD and healthy control subjects were classified using gait analysis through deterministic learning theory. This classification approach consists of two phases: a training phase and a classification phase. In the classification phase, a bank of dynamic estimators was constructed from all the training data. The results show that this approach achieves an accuracy rate of 96.39%. In [163], to classify subjects with PD, vGRFs obtained from idiopathic subjects with PD were used to extract wavelet-based features, which, in turn, were used as inputs of a neural network with weighted fuzzy membership functions (NEWFM). In [164], extracted features from gait signal measurements acquired through eight ground-reaction force sensors placed underneath each foot, and SVM-based algorithm were used to classify 93 subjects with PD and 73 healthy control subjects. The

results show that the proposed approach achieved an accuracy of 91.20% at diagnosing the subjects with PD. In [130], SVM-based algorithm and extracted/selected feature form time series-based information such as stride intervals, swing intervals' measurements acquired through force-sensitive resistor sensors were used. The classification accuracy for patients with PD was approximately 89.33%. In [73], the stride interval density and its sub-phases (swing and stance intervals) were estimated using the non-parametric Parzen-window method and least squares SVM (LS-SVM). The obtained classification rate was approximately 90.32%.

Khorasani et al. [165] used a hidden Markov model (HMM) with Gaussian mixtures to classify patients with PD and healthy subjects. The proposed method allows achieving an accuracy of 90.3%. In [166], to classify subjects with PD and healthy subjects, a nearest-mean scaled classifier was used, with the following features as classifier inputs: variance of the stride signal, mean of phase signal, variance of phase signal, regression error, and Petrosian dimension for both feet. This approach resulted in a classification accuracy of 95.6%. In [167], IMU gait measurement sequences sampled during walking are encoded as hidden Markov models (HMMs) to extract their dynamics. The distance between HMMs is learned and employed in a standard nearest neighbour classifier. This approach achieved an accuracy of 85.51%. A Q-back propagated time delay neural network classifier was proposed in [168] to monitor and predict the severity of gait disturbances in subjects with PD by analyzing the instability in their walking patterns. The dataset used includes data from three PD research studies [169]. The results show that the classification accuracy on the three sub-datasets reached 91.49%, 92.19% and 90.91%, respectively. In [170], Ertugrul et al. proposed an approach built using shifted one-dimensional local binary patterns and machine learning. The statistical features extracted as: energy, skewness, correlation, coefficient of variation, entropy and kurtosis. These features were classified using Naive Bayes, multilayer perceptron, partial C4.5 decision trees (PART), random forests, Bayes Network, logistic regression, a rule learner method and functional tree methods. The best accuracy rate was 88.88% obtained using the multilayer perceptron classifier. In [171], an RF algorithm was used for classification, and a set of features in the time and frequency domains were extracted. The classification accuracy when all features subsets were used reached 98.04%.

Joshi et al. [74] presented an approach that combined wavelet analysis and an SVM to distinguish Parkinson's subjects from healthy ones using gait cycle variability. The

results showed that adopting the wavelet transform approach resulted in a classification rate of 90.32%. In [172], the parameters of approximate entropy, normalized symbolic entropy, and signal turn counts were computed to measure stride fluctuations in patients with PD. To implement gait pattern classification, Wu et al. employed generalized linear regression analysis and an SVM. The experimental results showed that the SVM achieved an accuracy of 84.48%. In [173], several supervised classifier methods including SVM, RF, k-NN and DT were compared in terms of the classification performances. Furthermore, this study compared different kernel functions, including linear, Gaussian, quadratic and cubic. The results show that the SVM with the cubic kernel outperformed the other classifiers and achieved an accuracy of 93.6%. In [174], linear discriminant analysis and k-Means were used to classify and cluster subjects with PD and healthy control subjects. The goal of the authors was to study the effect of neurodegenerative diseases (i.e., Parkinson's disease) on mobility and gait in comparison with healthy control subjects. In [175], k-Means was used with the objective of discriminating patients with PD from control subjects. Finally, in [165, 176], Parkinson's disease diagnosis was made based on gait recognition using GMM. Table 3.2 presents a synthetic review of studies on PD diagnosis.

The most of aforementioned studies are mainly based on the use of time-domain and frequency-domain features to diagnose Parkinson's disease. However, such features could not be easily linked to a clinical indicator. In this chapter, the main objective is to develop a useful tool to aid the diagnosis of Parkinson's disease using clinical-based features extracted from vertical Ground Reaction Forces (vGRFs). This tool is mainly devoted to being used in a clinical environment to support physiotherapists in the PD diagnosis process. Hence, in this study, only clinical-based features are considered.

TABLE 3.2: Synthetic review of studies on PD diagnosis.

References	Sensors	Sensors Type	Method	Validation Methods	Accuracy
Jean et al., 2008 [100]	In-shoe dynamic foot pressure	Wearable	SVM	15-fold cross-validation	91.73%
Cho et al., 2009 [113]	CCD camera	Non wearable	MDC	Not specified	95.49%
Muniz et al., 2010 [121]	Force platform	Non wearable	LR, PNN, SVM	Bootstrap method	91–94%
Wu and Krishnan, 2010 [73]	Force sensors	Wearable	LS-SVM	Leave-one-out	90.32%
Sarbaz et al., 2011 [166]	Force sensors	Wearable	Nearest mean scaled	70% (train), 30% (test)	95.6%
Daliri, 2012 [130]	Force sensors	Wearable	SVM	50% (train), 50% (test)	89.33%
Lee et al., 2012 [163]	Force sensors	Wearable	NEWFM	50% (train), 50% (test)	74–77%
Daliri, 2013 [164]	Force sensors	Wearable	SVM	50% (train), 50% (test)	84–91%
Khorasani et al., 2014 [165]	Force sensors	Wearable	HMM with GM	Leave-one-out	90.3%
Dror et al., 2014 [116]	Microsoft 3D camera sensor	Non wearable	SVM	leave-one-out	100%
Dyshel et al., 2015 [117]	Microsoft Kinect For Windows SDK	Non wearable	SVM	5-fold cross-validation	-
Su et al., 2015 [128]	Force sensors	Wearable	Threshold-based and MLP models	80% (train), 10% (Valid.), 10% (test)	72%
Zeng et al., 2016 [129]	Force sensors	Wearable	RBF NN	5-fold cross-validation	96.39%
Jane et al., 2016 [168]	Force sensors	Wearable	Q-BTDNN	cross-validation	90–92%
Ertugrul et al., 2016 [170]	Force sensors	Wearable	BayesNT, NB, LR, MLP, PART, Jrip, RF, and FT	10-folds cross-validation	87–88%
Cuzzolin et al., 2017 [167]	IMU sensors	Wearable	HMM	cross-validation	85.51%
Aici et al., 2017 [171]	Force sensors	Wearable	RF	10-fold cross-validation	74–98%
Joshi et al., 2017 [74]	Force sensors	Wearable	SVM	Leave one-out	90.32%
Wu et al., 2017 [172]	Force sensors	Wearable	SVM	Leave one-out	84.48%
Alam et al., 2017 [173]	Force sensors	Wearable	SVM, RF, k-NN, and DT	Leave one-out	85–95%
Bhoi et al., 2017 [174]	Force sensors	Wearable	k-Means	-	-
Aharonson et al., 2018 [175]	Force sensors and accelerometer	Non wearable	k-Means	-	-
Haji Ghassemi et al., 2018 [176]	IMU sensors	wearable	GMM	-	-

3.4 Parkinson's disease classification

In this section, we present the implementation of the above-mentioned methodology for the PD diagnosis. An online dataset of vertical Ground Reaction Forces (vGRFs) data collected from gait cycle is used. A classification engine assigns subjects to healthy or Parkinsonian classes. The diagnosis process involves four steps: data pre-processing, feature extraction and selection, data classification and performance evaluation. Figure 3.2 shows the synopsis of this methodology by presenting the steps involved in Parkinson's Disease classification.

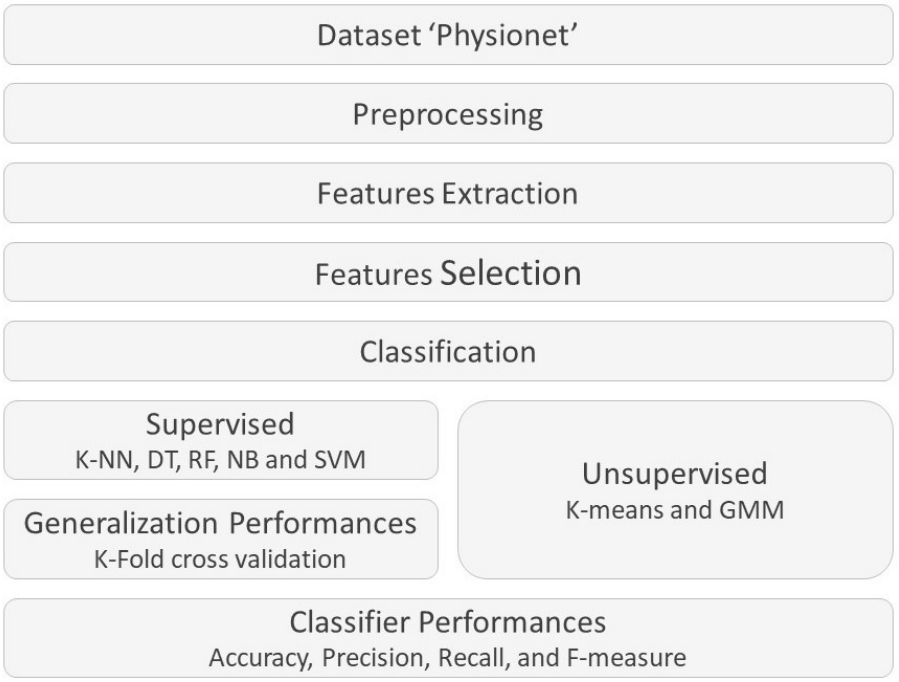

FIGURE 3.2: Synopsis of the used methodology.

3.4.1 Dataset Description

The gait dataset used in this study was obtained from the PhysioNet web site [169]. It contains gait data of 93 patients suffering from Parkinson's disease and 72 healthy subjects. The average age of both categories is approximately 66 years. Males constitute 63% of the subjects with PD and 55% of the healthy subjects. This dataset contains three different sub-datasets. The first one, provided by Yogev et al. [79], contains the gait data of 29 people with PD and 18 healthy subjects. The second one, provided by Hausdorff et al. [38], includes the gait data of 29 people with PD and 25 healthy

individuals. The third one, provided by Frenkel-Toledo et al. [177], contains the gait data of 35 people with PD and 29 healthy people. Table 3.3 shows the number of subjects in each sub-dataset with respect to the severity level of PD according to the H & Y scale.

	Sub-datasets		
Severity	Yogev et al. [79]	Hausdorff et al. [38]	Frenkel-Toledo et al. [177]
H & Y=2	15	12	28
H & Y=2.5	8	13	7
H & Y=3	6	4	0

TABLE 3.3: Number of subjects in each sub-dataset with respect to the severity level of PD according to the H & Y scale.

Each dataset includes vGRF measurements collected from eight force sensors (Ultraflex Computer DynoGraphy, Infotronic Inc., Hong Kong, China) placed under each foot of the subjects as shown in Figure 3.3.

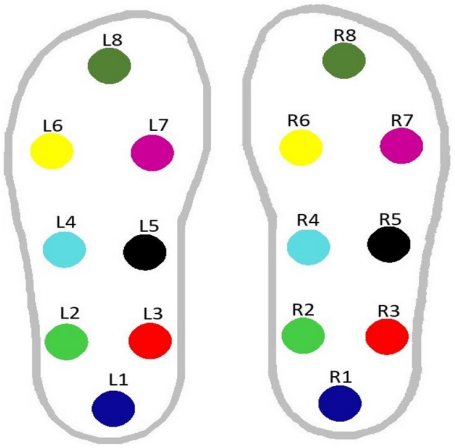

FIGURE 3.3: Placement of the 16 sensors under both feet.

The vGRF signals are sampled at a frequency of 100 Hz. To create the different sub-datasets, the participants were asked to walk at their typical walking pace on level ground for periods ranging from 25 min for distances ranging from 25 m to 77 m. These three studies differ in their measurement protocols. Subjects in [79] were asked to walk under different dual tasking conditions. Subjects in [38] were asked to walk with and without Rhythmic auditory stimulation (RAS) condition, while, in study [177], subjects were asked to walk with and without assistance by using a wheeled walker on a motorized treadmill. It should be noticed that the subjects who participated in the three studies

[38, 79, 177] were either healthy subjects or subjects suffering from PD, excluding any other walking pathologies. In addition to the sixteen signals provided by the vGRFs sensors, the dataset also includes two signals that represent the sums of the eight sensor outputs for each foot. Demographic information, measures of disease severity on the Hoehn and Yahr (H & Y) scale, the Unified Parkinson's Disease Rating Scale (UPDRS) and the Time Up and Go test (TUG) are also included in this sub-dataset. Figure 3.4 presents the sum of the signals from the eight left and eight right superposed sensors of two subjects, one healthy and one diseased.

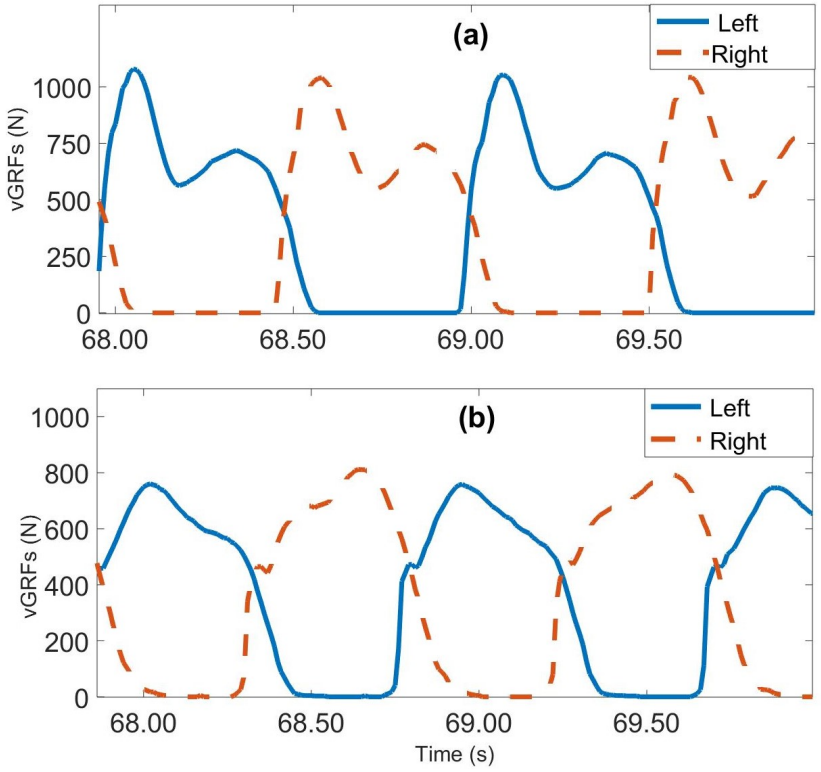

FIGURE 3.4: vGRFs measured on left foot (blue) and right foot (red); (**a**) healthy subject, (**b**) subject with PD.

3.4.2 Data preprocessing

In this study, we used the two signals representing the sums of the 8 sensor outputs from each foot. Rather than using each sensor signal, the use of these two signals allows the detection of the stance and swing phase in high precision. Moreover, these two signals can reflect the overall conditions of fluctuation from one aspect of gait dynamics [129]. As described in [38], the subjects were asked to perform a round trip along a walkway, which can reveal the presence of outliers in gait parameters. The recorded gait

data during the turn-around phase were removed manually. This phase was removed manually, because the duration of this phase and the duration between two phases are different in the same subject, making its automatically removed more difficult. In addition to the turn, the first and last 20 seconds were removed to ignore starting and stopping effects. An analysis of the collected vGRFs shows signal fluctuations in some cases. Sensors used during the experimentation are not ideal sensors, which makes these fluctuations more important during the swing phase by recording non-zero vGRF values. To address this issue, a 10-point median filter is applied. Fig. 3.5 shows the application of the pre-processing phase on the vGRFs signal for one of the subjects.

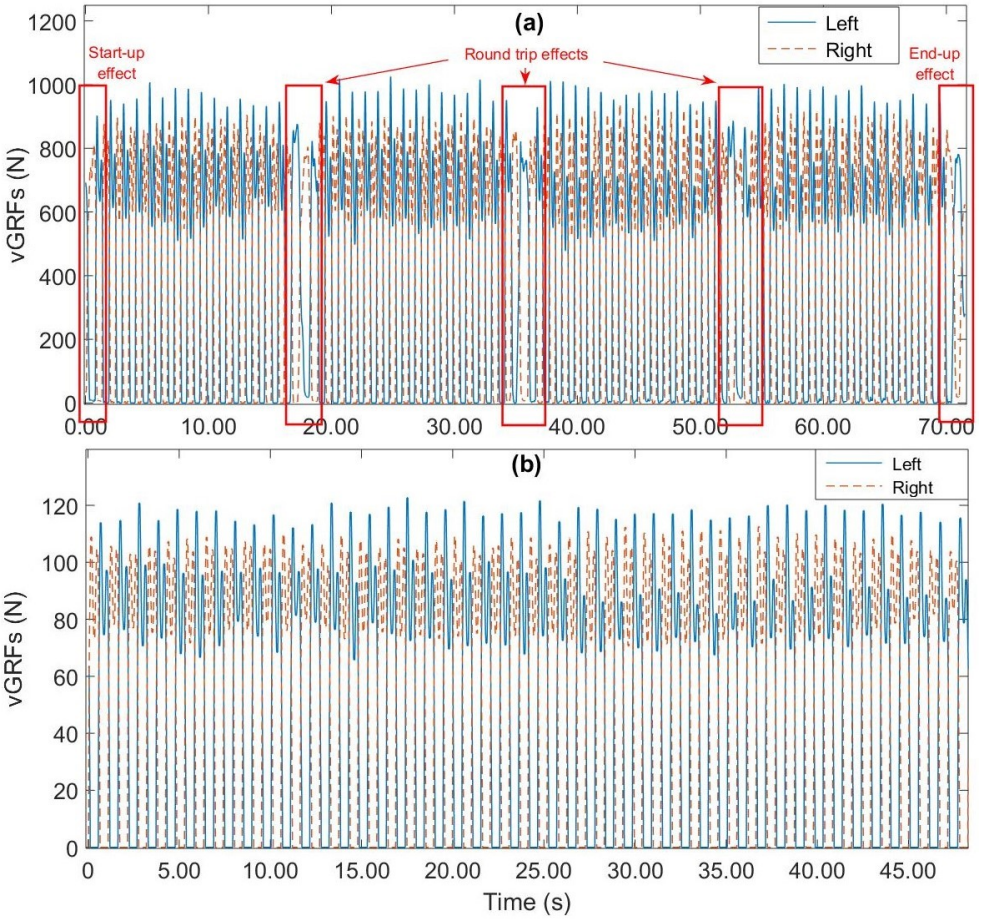

FIGURE 3.5: Example of vGRF data pre-processing; (**a**) raw vGRFs data; (**b**) processed vGRF data.

3.4.3 Results of feature extraction process

In this study, the most relevant spatiotemporal features from the clinical point of view are extracted from vGRF signals [37, 39, 64, 79, 178, 179]. The extracted features are:

- **Duration (s) of the Stride Time**: the amount of time from initial contact of the foot, to the next contact of the same foot with the same configuration [37, 39, 179].
- **Duration (s) of the Swing Time**: the amount of time when the foot is in the air [39, 79, 178, 179].
- **Percentage (%) of the Swing Time**: $100 \times \frac{Duration\ (s)\ of\ Swing\ Time}{Duration\ (s)\ of\ Stride\ Time}$. [64, 79]
- **Duration (s) of the Double Stance Time**: the time when both feet are in contact with the ground [64].
- **Percentage (%) of the Double Stance Time**: $100 \times \frac{Duration\ (s)\ of\ Double\ Stance\ Time}{Duration\ (s)\ of\ Stride\ Time}$ [64].
- **Short swing time**: For each subject, we determine which foot had the shorter swing times by comparing the swing durations of each foot [37].
- **Long swing time**: For each subject, we determine which foot had the longer swing times by comparing the swing durations of each foot [37].
- **Gait asymmetry**: $100 \times |ln(\frac{Short\ Swing\ Time}{Long\ Swing\ Time})|$ according to this definition, a gait asymmetry value of 0 implies a perfect gait symmetry, and the more the value is higher the more the degree of gait asymmetry is greater [37].
- **Mean**: the average of each previous feature.
- **Coefficient of variations (CV)**: $100 \times \frac{STD\ of\ each\ feature}{Mean\ of\ each\ feature}$ (calculated for each previous feature)
- **Standard Deviation (STD)**: calculated for the following features: duration (s) of the stride time, duration (s) of the swing time, percentage (%) of the swing time, short swing time, and long swing time.
- **Coefficient of variation of the gait asymmetry**: $100 \times |ln(\frac{CV\ of\ the\ Short\ Swing\ Time}{CV\ of\ the\ Long\ Swing\ Time})|$. This measure reflects the potential left-right differences in the stride-to-stride variability of each leg [37].

A total of nineteen features are considered (see Table 3.4).

TABLE 3.4: List of the nineteen extracted features.

Features References	Extracted Features	Explanation
1	Coefficients of Variation in percentage (%) of the Swing Time of the left foot	$100 \times \frac{Standard\ Deviation\ in\ percentage\ (\%)\ of\ the\ Swing\ Time\ of\ the\ left\ foot}{Mean\ in\ percentage\ (\%)\ of\ the\ Swing\ Time\ of\ the\ left\ foot}$ [64, 79]
2	Coefficients of Variation in duration (s) of the Swing Time of the left foot	$100 \times \frac{Standard\ Deviation\ in\ duration\ (s)\ of\ the\ Swing\ Time\ of\ the\ left\ foot}{Mean\ in\ duration\ (s)\ of\ the\ Swing\ Time\ of\ the\ left\ foot}$ [37]
3	Coefficients of Variation in duration (s) of the Stride Time of the left foot	$100 \times \frac{Standard\ Deviation\ in\ duration\ (s)\ of\ the\ Stride\ Time\ of\ the\ left\ foot}{Mean\ in\ duration\ (s)\ of\ the\ Stride\ Time\ of\ the\ left\ foot}$ [79]
4	Coefficients of Variation in percentage (%) of the Swing Time of the right foot	$100 \times \frac{Standard\ Deviation\ in\ percentage\ (\%)\ of\ the\ Swing\ Time\ of\ the\ right\ foot}{Mean\ in\ percentage\ (\%)\ of\ the\ Swing\ Time\ of\ the\ right\ foot}$ [64, 79]
5	Coefficients of Variation in duration (s) of the Swing Time of the right foot	$100 \times \frac{Standard\ Deviation\ in\ duration\ (s)\ of\ the\ Swing\ Time\ of\ the\ right\ foot}{Mean\ in\ duration\ (s)\ of\ the\ Swing\ Time\ of\ the\ right\ foot}$ [37]
6	Coefficients of Variation in duration (s) of the Stride Time of the right foot	$100 \times \frac{Standard\ Deviation\ in\ duration\ (s)\ of\ the\ Stride\ Time\ of\ the\ right\ foot}{Mean\ in\ duration\ (s)\ of\ the\ Stride\ Time\ of\ the\ right\ foot}$ [79]
7	Coefficients of Variation of the Short Swing Time	$100 \times \frac{Standard\ Deviation\ of\ the\ Short\ Swing\ Time}{Mean\ of\ the\ Short\ Swing\ Time}$ [37]
8	Coefficients of Variation of the Long Swing Time	$100 \times \frac{Standard\ Deviation\ of\ the\ Long\ Swing\ Time}{Mean\ of\ the\ Long\ Swing\ Time}$ [37]
9	Coefficients of Variation of the Gait Asymmetry	$100 \times \lvert ln\left(\frac{Coefficient\ of\ Variation\ of\ the\ Short\ Swing\ Time}{Coefficient\ of\ Variation\ of\ the\ Long\ Swing\ Time}\right)\rvert$ [37]
10	Mean in percentage (%) of the Swing Time of the left foot	$100 \times \frac{Duration\ (s)\ of\ Swing\ Time\ of\ the\ left\ foot}{Duration\ (s)\ of\ Stride\ Time\ of\ the\ left\ foot}$ $(Mean\ of\ the\ Percentage\ (\%)\ of\ the\ Swing\ Time\ of\ the\ left\ foot)$ [64, 79]

TABLE 3.4: *Cont.*

Features References	Extracted Features	Explanation
11	Mean in duration (s) of the Swing Time of the left foot	*Time of the left foot was in the air* (*Mean of the duration (s) of the Swing Time of the left foot*) [37, 39, 179]
12	Mean in duration (s) of the Stride Time of the left foot	*Time from initial contact of the Left foot to subsequent contact of the same foot* (*Mean of the duration (s) of the Stride Time of the left foot*) [39, 79, 178, 179]
13	Mean in percentage (%) of the Swing Time of the right foot	$100 \times \frac{Duration\ (s)\ of\ Swing\ Time\ of\ the\ right\ foot}{Duration\ (s)\ of\ Stride\ Time\ of\ the\ right\ foot}$ (*Mean of the Percentage (%) of the Swing Time of the right foot*) [64, 79]
14	Mean in duration (s) of the Swing Time of the right foot	*Time of the right foot was in the air* (*Mean of the duration (s) of the Swing Time of the right foot*) [37, 39, 179]
15	Mean in duration (s) of the Stride Time of the right foot	*Time from initial contact of the right foot to subsequent contact of the same foot* (*Mean of the duration (s) of the Stride Time of the right foot*) [39, 79, 178, 179]
16	Mean in percentage (%) of the Double Stance Time	$100 \times \frac{Duration\ (s)\ of\ Double\ Stance\ Time}{Duration\ (s)\ of\ the\ Stride\ Time}$ (*Mean in percentage (%) of the Double Stance Time*) [64]
17	Mean of the Short Swing Time	*compare Swing Time between the Right and the Left foot, then distribut it according to the Short Swing Time Criteria* (*Mean of the Short Swing Time*) [37]
18	Mean of the Long Swing Time	*compare Swing Time between the Right and the Left foot, then distribut it according to the Long Swing Time Criteria* (*Mean of the Long Swing Time*) [37]
19	Mean of the Gait Asymmetry	$100 \times \left\lvert ln\left(\frac{Short\ Swing\ time}{Long\ Swing\ time}\right)\right\rvert$ (*averaged of the Gait Asymmetry*) [37]

3.5 Results and Discussion

In this section, different classification methods have been implemented for the purposes of the classification of subjects with PD. Moreover, the results of the features selection method as well as the performance of the different classification algorithms are presented and discussed. Note that in this study, the three sub-datasets are used separately. Five supervised classification methods, namely k-Nearest Neighbours (k-NN), Support Vector Machines (SVM), Decision Trees (CART), Random Forests (RF), and Naive Bayes (NB), as well as two unsupervised techniques, namely Gaussian Mixture Models (GMM), and k-Means, are compared using standard evaluation metrics. Both supervised and unsupervised methods, take as inputs the extracted and selected features from raw data. These results will be used as standard results to compare them with results that will be obtained in the next contribution.

3.5.1 Parameters settings

Each classification technique requires one or several parameters that control (affect) the prediction outcome of the classifier. Choosing the best values for these parameters is difficult and involves finding a trade-off between the model's complexity and its generalization ability. In this study, finding parameter settings is conducted using a grid search. A grid search consists of adapting a grid of values (2D or 3D, depending on the number of model parameters) and incrementing each parameter by a fixed interval until the optimal values of the parameters are found. For example, for a model with two parameters a and b, the procedure consists of varying parameter a in a predefined interval $[a_{min}, a_{max}]$ using an increment of $\triangle a$ and parameter b in the interval $[b_{min}, b_{max}]$ with an increment of $\triangle b$. For each vector of values (a, b), the models performance in terms of recognition rate is evaluated, and the vector that yields the best accuracy is selected. The advantage of this method is that it allows the optimal parameters within the chosen intervals to be selected, but it is expensive in terms of computation time.

The selected parameters for each model are described below:

3.5.1.1 Supervised methods

- A k-NN with Euclidean distance is applied to the three sub-datasets (Yogev, Hausdorff and Frenkel-Toledo). The number of neighbours is determined by varying k from 2 to 10. The optimal k values for the Yogev, Hausdorff and Frenkel-Toledo sub-datasets are, respectively, 5, 3 and 7.

- The CART algorithm is used for the DT model. The CART uses the Gini index to find the best construction and the best partition of the tree.

- For the RF model, the number of trees is varied between 10 and 200. The optimal numbers of trees for the Yogev, Hausdorff and Frenkel-Toledo sub-datasets are, respectively, 110, 100 and 100.

- For the NB model, a normal distribution is used to model the conditional probability of the observation data and classes for the three sub-datasets.

- For the SVM model, a non-linear model with polynomial kernel function (degree 3) is used for the two first sub-datasets, and a linear model is used for the third sub-dataset.

3.5.1.2 Unsupervised methods

- For the GMM model, the diagonal Gaussian function is used for the Frenkel-Toledo sub-dataset, and the full Gaussian function is used for the other two sub-datasets.

- For k-Means, the only parameter to tune is the number of classes. The number of classes is equal to two (Healthy and PD subject classes)

Each sub-dataset is divided into training and testing sets according to a 10-fold cross-validation procedure. For the supervised approaches, the labels are used during the

learning phase. Then, during the testing phase, the labels estimated by each classifier are matched with the reference labels (true labels) to evaluate the classification performance. Unlike the supervised models, the unsupervised models are trained using only the extracted features; no reference labels are used; instead, the labels are used only for classification evaluation purposes. Note that all extracted features and just the selected features are used as classifier input. As described above, a wrapper approach using an RF classifier [147] is used. This algorithm allows reordering the extracted features according to their relevance percentage. In this study, a set of 5 features representing 80% of the cumulative relevance is selected for each sub-dataset.

3.5.2 Parkinson's disease classification results

3.5.2.1 Results of feature selection process

In this subsection, the performance of the different classification techniques are presented and discussed. Note that, in this study, the three sub-datasets are analyzed separately. Table 3.5 summarizes the results of the feature selection process by presenting the five selected features for each sub-dataset. In the following sections, we use references to the features listed in Table 3.5 as substitutes for their names. These features are used as the input of each classifier. The features referred to as 6, 7 and 13 are included in the feature combination obtained from the Yogev and Hausdorff sub-datasets. We found that this combination was the most effective in achieving the highest correct classification rate for these two sub-datasets. A combination of the features referred to as 7 and 11 are obtained from the first and third sub-datasets. Moreover, the combination of the features referred to as 7, 8 and 19 (derived from the former two) yields good performance on the Frenkel-Toledo sub-dataset.

Table 3.6 shows the obtained results in terms of accuracy for the different classifiers with and without feature selection. This table presents the obtained accuracy and its standard deviation from the three sub-datasets (Yogev, Hausdorff and Frenkel-Toledo). Table 3.6 also shows, that using only the features obtained from the feature selection process as classifier inputs leads to improving the overall accuracy rate with respect to the case where all the extracted features were used. For the Yogev sub-dataset, improvements of approximately 5%, 4%, 2%, 3%, 2%, 10% and 3% can be observed when

Table 3.5: The five most relevant features from each sub-dataset obtained using the RF feature selection process.

	Features Ref.	Selected Features
Yogev et al.	13	Mean in percentage (%) of the Swing Time of the right foot
	7	Coefficient of Variation of the Short Swing Time
	10	Mean in percentage (%) of the Swing Time of the left foot
	6	Coefficient of Variation in duration (s) of the Stride Time of the right foot
	11	Mean in duration (s) of the Swing Time of the left foot
Hausdorff et al.	7	Coefficient of Variation of the Short Swing Time
	5	Coefficient of Variation in duration of the Swing Time of the right foot
	4	Coefficient of Variation in percentage (%) of the Swing Time of the right foot
	13	Mean in percentage (%) of the Swing Time of the right foot
	6	Coefficient of Variation in duration (s) of the Stride Time of the right foot
Frenkel-Tol. et al.	7	Coefficient of Variation of the Short Swing Time
	19	Mean of the Gait Asymmetry
	11	Mean in duration (s) of the Swing Time of the left foot
	8	Coefficient of Variation of the Long Swing Time
	9	Coefficient of Variation of the Gait Asymmetry

using k-NN, CART, RF, NB, SVM, k-Means and GMM respectively. Almost the same improvements can be observed for the Hausdorff (3%, 5%, 3%, 10%, 4%, 4% and 6%, respectively) and Frenkel-Toledo (5%, 4%, 3%, 3%, 2%, 3% and 8%, respectively) sub-datasets. This outcome can be explained by the fact that the feature selection process, by providing the best combination of relevant features for the classification algorithm, improves the classification performance with respect to both healthy subjects and PD subjects. Moreover, by analyzing the performance of each classifier with and without feature selection, it can be noted that, in the case of k-NN and CART with selected features, an improvement of 5% for the three sub-datasets is observed compared to the results obtained when using all extracted features. In the case of RF and SVM with selected features, an improvement of 3% can be observed for the three sub-datasets compared to the results obtained using all features. However, a greater improvement can be observed in the case of the Hausdorff sub-dataset (10%). Regarding the unsupervised

classifiers, k-Means shows an improvement of 3% in the case of Hausdorff and Frenkel-Toledo sub-datasets. Regarding the Yogev sub-dataset, using k-Means with selected features allows achieving a significant improvement about 10%. A significant improvement can be also noted in the case of GMM when using Hausdorff and Frenkel-Toledo. Finally, there is also a slight improvement in the case of the Yogev sub-dataset. GMM using selected features achieves an improvement about 3%. These results show that the selected features can further increase the discriminative capability of the different classifiers (supervised and unsupervised). It is worth noting that using selected features as classifier inputs allows not only the improvement of the classification performance but also a significant reduction of the computational time both in the training and testing steps.

TABLE 3.6: Accuracy and its standard deviation (STD) obtained with/ without the use of the feature selection process, for each sub-dataset.

	Features Selec.		**Supervised**					**Unsupervised**	
		Perf.	**k-NN**	**CART**	**RF**	**NB**	**SVM**	**k-Means**	**GMM**
Yogev et al.	With	Accuracy	85.39%	82.10%	85.6%	75.64%	85.02%	63.72%	64.77%
		STD	3.49%	3.25%	3.23%	2.91%	4.26%	4.20%	12.64%
	Without	Accuracy	80.13%	77.94%	83.66%	72.58%	82.44%	53.72%	61.39%
		STD	5.50%	4.32%	4.40%	4.10%	1.50%	1.10%	11.55%
Hausdorff et al.	With	Accuracy	91.39%	84.82%	88.77%	77.22%	87.70%	55.12%	65.12%
		STD	2.83%	3.66%	2.30%	4.06%	3.26%	3.59%	11.08%
	Without	Accuracy	88.47%	79.10%	85.57%	67.13%	83.93%	51.07%	58.93%
		STD	2.84%	2.89%	2.35%	3.26%	1.30%	2.09%	8.43%
Frenkel-Tol. et al.	With	Accuracy	81.49%	79.01%	81.98%	78.97%	80.23%	57.19%	65.31%
		STD	4.68%	3.72%	4.19%	4.86%	4.80%	3.98%	12.12%
	Without	Accuracy	76.75%	74.68%	79.51%	75.56%	78.47%	53.75%	57.34%
		STD	4.91%	4.87%	3.91%	5.74%	1.33%	4.61%	3.97%

3.5.2.2 Classification results

Tables 3.7–3.9 show the classifier performances in terms of accuracy with standard deviation, precision, recall and F-measure when using the selected features with the Yogev,

Hausdorff and Frenkel-Toledo sub-datasets. A comparison of the classifier performances shows that RF, k-NN and SVM achieve almost similar accuracy while outperforming the other classifiers with the Yogev and Frenkel-Toledo sub-datasets. The same observation can be made when considering the F-measure metric. On the Yogev sub-dataset, k-NN achieves the best recall performance followed by SVM, NB, RF, k-Means and CART. However, in terms of precision, the RF classifier provides the best rate, followed by SVM, CART, k-NN, NB and k-Means. GMM exhibits the worst rate. On the Frenkel-Toledo sub-dataset, k-NN, SVM and k-Means have similar recall performances, followed by NB, RF, CART and GMM. In terms of precision, RF achieves a higher rate, followed by SVM, NB, k-NN and CART, all with similar rates. Again, GMM and k-Means exhibit the worst performances. Finally, on the Hausdorff sub-dataset, k-NN achieves the highest accuracy, followed by RF, SVM, CART and NB. Regarding the F-measure metric, k-NN and SVM achieve almost similar performance, similar to RF and NB. In terms of recall, k-NN and SVM provides the best rates. In contrast, in terms of precision, k-NN shows the highest rate, followed by SVM, RF, CART and NB. The worst precision, recall and F-measure rates were obtained in the case of k-Means and GMM. By comparing supervised and unsupervised methods, it can be noted that supervised ones outperform unsupervised methods.

Table 3.7: Accuracy and its STD, Precision, Recall and F-measure for each classifier in the case of Yogev et al. sub-dataset.

Perf.	**Supervised**					**Unsupervised**	
	k-NN	**CART**	**RF**	**NB**	**SVM**	**k-Means**	**GMM**
Accuracy	85.39%	82.10%	85.65%	75.64%	85.02%	63.72%	64.77%
STD	3.49%	3.25%	3.23%	2.91%	4.26%	4.20%	12.64%
Precision	79.88%	80.93%	84.53%	66.99%	82.08%	50.79%	43.18%
Recall	87.67%	75%	78.33%	80.83%	82.83%	76.87%	49.37%
F-Measure	83.59%	77.85%	81.31%	73.26%	82.45%	61.17%	46.07%

By analyzing the result differences observed between the different sub-datasets, it can

Table 3.8: Accuracy and its STD, Precision, Recall and F-measure for each classifier in the case of Hausdorff et al. sub-dataset.

Perf.	**Supervised**					**Unsupervised**	
	k-NN	**CART**	**RF**	**NB**	**SVM**	**k-Means**	**GMM**
Accuracy	91.39%	84.82%	88.77%	77.22%	87.70%	55.12%	65.12%
STD	2.83%	3.66%	2.30%	4.06%	3.26%	3.59%	11.08%
Precision	84.85%	77.99%	82.12%	71.56%	82.32%	18.98%	22.17%
Recall	66.16%	57.83%	51.50%	58.50%	67.33%	42.40%	25.20%
F-Measure	74.34%	66.41%	63.30%	64.37%	74.07%	26.22%	23.59%

Table 3.9: Accuracy and its STD, Precision, Recall and F-measure for each classifier in the case of Frenkel-Toledo et al. sub-dataset.

Perf.	**Supervised**					**Unsupervised**	
	k-NN	**CART**	**RF**	**NB**	**SVM**	**k-Means**	**GMM**
Accuracy	81.49%	79.01%	81.98%	78.97%	80.23%	57.19%	65.31%
STD	4.68%	3.72%	4.19%	4.86%	4.80%	3.98%	12.12%
Precision	79.53%	78.90%	82.80%	79.68%	79.83%	51.90%	58.27%
Recall	85.83%	76.33%	78.67%	82.33%	85.50%	85.86%	57.24%
F-Measure	82.56%	77.59%	80.68%	80.98%	82.56%	64.69%	57.75%

be noticed that almost all classifiers (supervised and unsupervised) show their best results in the case of the Hausdorff et al. sub-dataset. It can be also noticed that the results obtained in the case of Yogev et al; sub-dataset. are better than those obtained for Frenkel-Toledo et al. sub-dataset. This can be explained by the fact that the number of PD subjects with low severity is more important in the case of Frenkel-Toledo sub-dataset (28 among 35), followed by the Yogev et al. sub-dataset (15 among 29). Finally, the Hausdorff et al. sub-dataset includes the lower number of PD subjects with low severity (12 among 29). Unlike the number of PD subjects with low severity, the

number of PD subjects with high severity is more important in the case of the Hausdorff sub-dataset (17 among 29) followed by the Yogev et al. sub-dataset (14 among 29). Finally, the Frenkel-Toledo et al. sub-dataset includes the lower number of PD subjects with high severity (7 among 35). It is worth noting that the subjects with low severity (beginning stage of the disease) may be considered by the classifiers, in some cases, as healthy subjects. However, the PD subjects with high severity can be easily distinguished from healthy subjects.

To analyse the confusion that can occur in the classification step, global confusion matrices obtained using the different classifiers under 10-fold cross-validation on each sub-dataset (Yogev, Hausdorff and Frenkel-Toledo) are given in Table 3.10.

In most cases, the classifiers recognize subjects with PD better than they do with healthy subjects, particularly on the Yogev and Hausdorff sub-datasets. This can be explained by the fact that the number of healthy subjects in Yogev and Hausdorff sub-datasets is smaller than the number of subjects with PD (see Table 3.10). This imbalance in terms of the number of subjects may have affected the classifier performances because they cannot capture the specificities of the under-represented classes. On the Yogev sub-dataset (Table 3.10), the biggest percentage of misclassified healthy subjects is between 13% and 21%, which means that, among the 18 healthy subjects, three were classified as having PD. Most of the supervised methods classified 10 to 15% of subjects with PD as healthy, which means that, among the 29 subjects with PD, only four were misclassified. On the Hausdorff sub-dataset (Table 3.10), the percentage of misclassified healthy subjects varies from 14% to 27%, i.e., that, among 25 healthy subjects, 6 subjects were classified as having PD, whereas, in the case of supervised classifiers (except NB), 1 to 8% of subjects with PD were classified as healthy. This result means that, among the 29 subjects with PD, only two subjects were misclassified. In the Frenkel-Toledo sub-dataset, the number of healthy subjects is 29, whereas the number of PD ones is 35. Note that, in almost all cases, the healthy subjects are better recognized than are subjects with PD. Table 3.10 shows that the percentage of misclassified healthy subjects is between 14% and 23%, which means that, among the 29 healthy subjects, six subjects were classified as having PD. In contrast, 13 to 25% of subjects with PD were classified as healthy, which means that, among the 35 subjects with PD, eight subjects were misclassified. To explain this outcome, we observed that most of the subjects with PD

TABLE 3.10: Global confusion matrix obtained using the different classifiers in the case of each sub-datasets.

			Obtained Classes													
			Supervised								Unsueprvised					
			k-NN		CART		RF		NB		SVM		k-Means		GMM	
			Healthy	PD	Healthy	PD	Healthy	PD	Healthy	PD	Healthy	PD	Healthy	PD	Healthy	PD
Yogev et al.	True Classes	Healthy	86.68%	13.32%	78.1%	21.9%	81.28%	18.72%	78.6%	21.4%	83.88%	16.12%	71.53%	28.47%	55.64%	44.36%
		PD	15.9%	84.1%	13.9%	86.1%	10.0%	90.0%	27.4%	72.6%	13.7%	86.3%	44.07%	55.93%	26.1%	73.9%
			Healthy	PD	Healthy	PD	Healthy	PD	Healthy	PD	Healthy	PD	Healthy	PD	Healthy	PD
Hausdorff et al.	True Classes	Healthy	85.07 %	14.93 %	77.64 %	22.36 %	78.94 %	21.06 %	72.44 %	27.56 %	82.3 %	17.7 %	51.84 %	48.16 %	54.74 %	45.26 %
		PD	2.29 %	97.71 %	8.0 %	92.0 %	1.4 %	98.6 %	18.0 %	82.0 %	6.9 %	93.1 %	41.6 %	58.4 %	24.5 %	75.5 %
			Healthy	PD	Healthy	PD	Healthy	PD	Healthy	PD	Healthy	PD	Healthy	PD	Healthy	PD
Frenkel-Tol. et al.	True Classes	Healthy	85.5%	14.5%	76.32%	23.68%	77.44%	22.56%	82.8%	17.2%	85.5%	14.5%	80.95%	19.05%	57.24%	42.76%
		PD	22.5%	77.5%	18.3%	81.7%	13.4%	86.6%	24.86%	75.14%	25.06%	74.94%	66.57%	33.43%	26.62%	73.38%

who were misclassified as healthy subjects were in the beginning stage of the illness, according to the H & Y scale. The Yogev sub-dataset includes six subjects among 15 with a severity of 2 according to the H & Y scale, while the Hausdorff and Frenkel-Toledo sub-datasets include four and seven subjects among 12 and 28, respectively, with a severity of 2. Considering the misclassified healthy subjects, they were in the three sub-datasets mostly elderly, overweight, or had levels similar to that of PD on the TUG test.

It is clear that comparing algorithm performance across different studies is a difficult task for many reasons. This difficulty is mainly related to: (i) the type of sensors used to quantify PD activities, (ii) the performance evaluation criteria (specificity, recall, precision, F-measure, accuracy, etc.), and (iii) the validation procedure (leave one out, P-fold, bootstrap). In this study, we have limited the comparison to the studies in literature considering the Physionet dataset. Table 3.11 summarizes the most relevant works for PD diagnosis using Physionet dataset. It can be noticed that almost all related studies use statistical features (time-domain and frequency-domain features) as classifier inputs. It can be also observed that the proposed methodology outperforms major state-of-the-art performances. Certainly, using time-domain and frequency-domain features may lead, in certain studies, to a higher accuracy rate; however, such features could not be easily linked to a clinical indicator. As such tools are devoted to being used in a clinical environment to support doctors in the PD diagnosis process, it is necessary to use clinical-based features. Therefore, the main advantage of the proposed method is the use of only clinical-based gait features. On the other hand, we can notice a drawback related to the fact of not considering the family history and the medical history of the different subjects. Such information could lead to a more accurate PD diagnosis.

TABLE 3.11: Classification accuracy results obtained in recent related studies based on PhysioNet datasets.

References	Gait parameters features	Classifiers	Accuracy
Sarbaz et al. 2012 [166]	Time domain	Nearest mean scaled classifier	95.6%
Daliri 2012 [130]	Time domain	SVM	89.33%
Lee et al. 2012 [163]	frequency domain	NEWFM	74-77%
Daliri 2013 [164]	Time domain	SVM	84-91%
Khorasani et al. 2014 [165]	Raw gait data	HMM with GM	90.3%
Ertugrul et al. 2016 [170]	Entropy, Energy, Correlation, Coefficient of Variation, Skewness and Kurtosis	BayesNT, NB, LR, MLP, PART, Jrip, RF, and FT	87-88%
Jane et al. 2016 [168]	Left and right vGRFs signals	Q-BTDNN	90-92%
Wu et al. 2017 [172]	ApEn, NSE, STC	SVM	84.48%
Alam et al. 2017 [173]	Time and Frequency domain	SVM	85-95%
Aici et al. 2017 [171]	Time and Frequency domain	RF	74-98%
Proposed methodology	Time domain	k-NN, CART, RF, SVM, k-Means, GMM	80-91%

3.6 Conclusion

We firstly presented the general background including data pre-processing (features computation, feature extraction and feature selection) as well as the main supervised and unsupervised classification approaches in this study. We implemented several classification methods used to recognize PD based on vGRFs collected from gait cycles. This chapter discusses the complete structure of the PD recognition process: from data acquisition to performance evaluation. First, data acquisition and sensor placement are addressed. Then, feature extraction and selection processes are presented. Finally, we presented a comparison of five supervised methods (k-NN, CART, RF, NB and SVM) and two unsupervised methods (k-Means and GMM). The five selected features were used as classifier inputs. The classifiers are compared in terms of classification rate (accuracy) and its standard deviation (STD), precision, recall and F-measure. Their generalization performance is then assessed using the 10-fold cross-validation. The supervised classification approaches yield more efficient results, as it can be expected since they use labeled data in the learning phase. k-NN, RF and SVM provide good results in terms of accuracy and F-measure.

Chapter 4

CDTW-based classification for Parkinson's Disease diagnosis

4.1 Introduction

This chapter presents the Continuous Dynamic Time Warping (CDTW) technique for Parkinson's Disease (PD) diagnosis classification using gait cycle similarities. The proposed approach exploits the principle of the repetition of gait cycle patterns to discriminate healthy subjects from PD subjects. To evaluate the repeatability of a given gait cycle, it is first necessary to extract a gait feature that better characterize the walking activity. Such feature can be expressed either in a global framework (the whole gait cycle is described using a feature vector (chapter 3)) or using a temporal description (i.e. the gait cycle is represented using time-series). The repetition of gait cycles is evaluated using the similarity of the time-series corresponding to stance phases estimated by applying the CDTW technique. The CDTW distances, extracted from gait cycles, are used as inputs of a binary classifier discriminating healthy subjects from PD subjects.

Euclidean and squared Euclidean distances are used to express the CDTW. Different classification methods are evaluated, including four supervised methods: k-Nearest Neighbours (k-NN), Decision Tree (DT), Random Forest (RF), and Support Vector Machines (SVM), and two unsupervised ones: Gaussian Mixture Model (GMM), and k-Means.

The rest of this chapter is organized as follows: Section 4.2 presents a brief synthesis on the time-series similarity evaluation techniques. Section 4.3 focuses particularly on the Dynamic Time Warping technique and its extension to the Continuous Dynamic Time Warping (CDTW). Section 4.4 shows the state of the art related to the use of DTW to analyze the gait cycle. Section 4.5 shows the data pre-processing for PD classification. In section 4.6, the obtained results in terms of PD classification are presented and discussed.

4.2 Time series similarity measures

Different measures of similarity (or metrics) between time series exist. Depending on the context of use, a simple Euclidean distance (or other standard Lp) may be effective [180], but is limited to comparing time series of the same size and without time deformation. In this section, several techniques of time series similarity measures are

presented: lock-step measures (Euclidean distance), feature-based measures (Fourier coefficients), model-based measures (auto-regressive), and elastic measures (DTW, EDR[1], and TWED[2]). For more details about time series similarity, the reader is invited to refer to the following references [181–187].

- **Euclidean:** Dissimilarity between two examples of time series can be estimated using any L_n norm such that:

$$d_{L_n}(u, v) = \left(\sum_{i=1}^{M} (u_i - v_i)^n \right)^{\frac{1}{n}} \tag{4.1}$$

  where n is a positive integer, M denotes the time series length, while u_i and v_i represent respectively the $i-th$ element of time series u and v. Measures based on L_n norms correspond to the lock-step measures group [183]. It consists of comparing samples having exactly the same temporal location. In addition, the size of the time-series u_i and v_i should be the same, otherwise, one time-series should be re-sampled to match the other one. Note that for $n = 2$, we obtain the Euclidean distance.

- **Fourier Coefficients:** A simple extension of the Euclidean distance consists in representing the time series by their Fourier Coefficients (FC) as follows:

$$d_{Fc}(u, v) = \left(\sum_{i=1}^{\theta} (\widehat{u}_i - \widehat{v}_i)^2 \right)^{\frac{1}{2}} \tag{4.2}$$

  Where $\widehat{u}_i$ and $\widehat{v}_i$ are pairs of complex values designating the $i-th$ Fourier coefficient of $\widehat{u}$ and $\widehat{v}$, the discrete Fourier transforms (DFT) of the raw time-series. θ represents the actual number of the considered coefficients. Due to DFT symmetry, only half of the coefficients ($\theta = M/2$) are required. According to Parseval theorem [188], the Euclidean distance between FCs is equivalent to the standard Euclidean distance between the raw time series [189].

- **Learning-models**: Another alternative to compute feature-based time series similarities is to use time series models [185, 187]. The idea here is to compute a

[1]EDR: Edit Distance on Real sequences
[2]TWED: Time-Warped Edit Distance

similarity value based on the parameters of the two time series learned model. In the literature, several studies have exploited the idea of using learning model to estimate the similarity between time series [181, 190–193].

- **Edit Distance on Real sequences (EDR):** EDR corresponds to the extension of the original Levensthein distance [194] to real-valued time series. EDR has the ability to handle local time shifting and removes the noise effects by quantizing the distance between a pair of elements to two values, 0 and 1. Moreover, assigning penalties to the unmatched parts improves its accuracy [195]

- **Dynamic Time Warping (DTW):** Dynamic time warping (DTW) [196, 197] is one of the well known used approach to assess the similarity between two time series. It has been used in different applications [198], [199], [200], [201], etc. DTW is based on an optimal alignment (or 'warping') of the time series in the temporal domain while minimizing the accumulated cost of this alignment that can be obtained using dynamic programming. More details about the formalization of the DTW are given in section 4.3.

  Several techniques derived from DTW are used in the literature. For instance, the Derivative DTW (DDTW) technique, that overcomes the limitations of DTW minimization criterion [202]: (1) the Piecewise Dynamic Time Warping (PDTW), that effectuates warping on a reduced dimensionality representation of the data [203]; (2) the Iterative Deepening Dynamic Time Warping (IDDTW) [204], that aims at calculating DTW only for candidate sequences in the dataset that are likely to be similar to the considered query [203]; (3) the Weighted DTW (WDTW), which is a DTW based on penalties; the WDTW penalizes points with higher phase difference between reference/ testing point to avoid minimum distance distortion caused by outliers [205]; (4) the FastDTW, that uses a multi-level approach, in which a solution is projected recursively from a coarse resolution and refines the projected solution [187]; (5) the Continuous DTW (CDTW) technique, that allows the matching between sample point of one of the two time-series and another point between two samples of the other time-series [206].

- **Time-warped edit distance (TWED):** TWED is slightly different from Dynamic Time Warping or Edit Distance on real sequences algorithms. In particular, TWED comprises a mismatch penalty parameter and introduces a parameter that

controls a kind of stiffness of the elastic measure [186]. It is worth noting that TWED is able to take into account, in its original formulation, the time stamp differences. As a result, TWED allows dealing with time series having different sampling rates [181].

4.3 Dynamic Time Warping (DTW)

4.3.1 Dynamic Time Warping (DTW) formulation

This subsection describes the Dynamic Time Warping (DTW) technique used to calculate the similarity between two time-series. Let $u(i), i = 1, 2, ..., m$ and $v(j), j = 1, 2, ..., n$ be two univariate time-series. An $m \times n$ matrix d_{global} is calculated whose $ij-th$ element being $d_{local}(i, j) = (u(i) - v(j))^2$. $d_{local}(i, j)$ is the local distance between elements $u(i)$ and $v(j)$ (Figure 4.1).

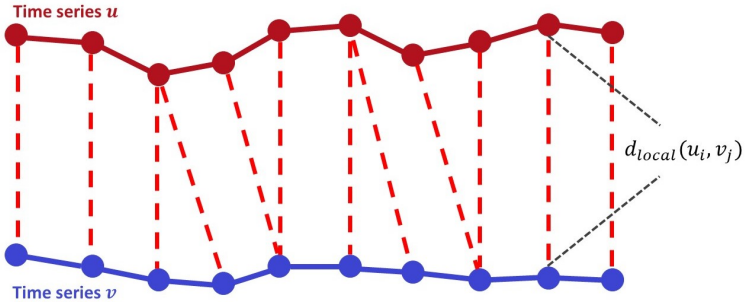

FIGURE 4.1: An example of DTW for two univariate time-series u and v [207].

$\mathcal{W}$ is the warping (corresponding path) between u and v, which could be expressed as follows:

$$\mathcal{W} = \begin{pmatrix} w_u(k) \\ w_v(k) \end{pmatrix}, k = 1, 2, ..., p \tag{4.3}$$

Where $w_u(k)$ and $w_v(k)$ are the indexes in time-series u and v respectively, and p is the length of the warping path. $(w_u(k), w_v(k))'$ indicates that the $w_u(k)$ th element in time series u corresponds to the $w_v(k)$ th element in time series v (mapping between $w_u(k)$ th and $w_v(k)$ th). The warping path will be generated under the following constraints:

1. **Boundary Condition**: As shown in figure 4.2(c), the warping path starts at $\mathcal{W}(1) = (1, 1)'$ and ends at $\mathcal{W}(p) = (m, n)'$.

2. **Continuity**: The adjacent elements $\mathcal{W}(k)$ and $\mathcal{W}(k + 1)$ of the path $\mathcal{W}$ must respect the following continuity constraints:

$$w_u(k + 1) - w_u(k) \leq 1$$
$$w_v(k + 1) - w_v(k) \leq 1$$

3. **Monotonicity**: The adjacent elements $\mathcal{W}(k)$ and $\mathcal{W}(k + 1)$ of the path $\mathcal{W}$ must respect the following monotonicity constraints:

$$w_u(k + 1) - w_u(k) \geq 0$$
$$w_v(k + 1) - w_v(k) \geq 0$$

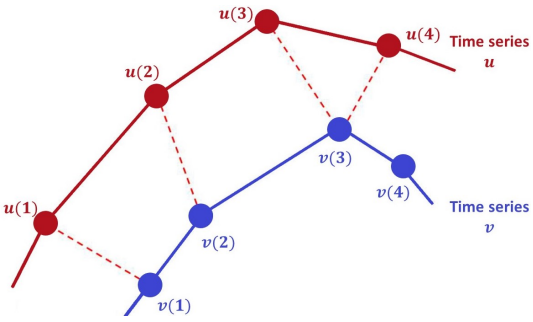

(a) Matching of two time-series using DTW.

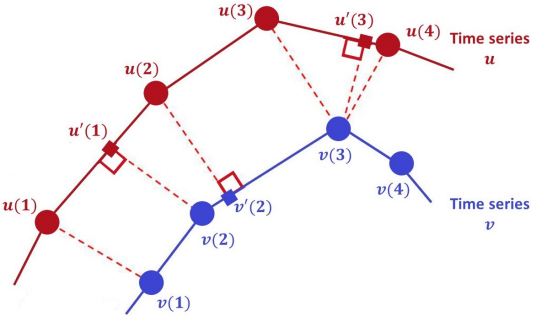

(b) Matching of two time-series using CDTW; where the points in small squares represent the matching points that differ from the sample points.

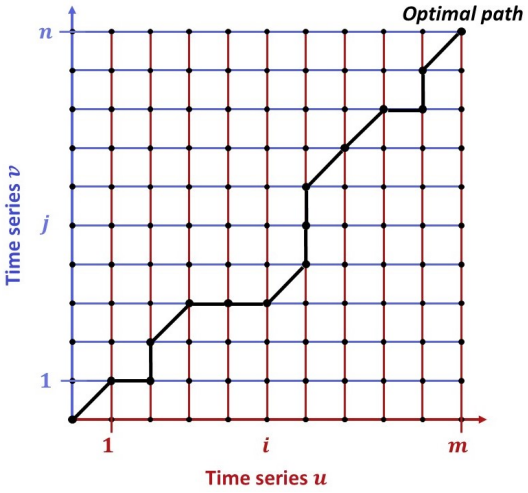

(c) Warping path obtained using DTW.

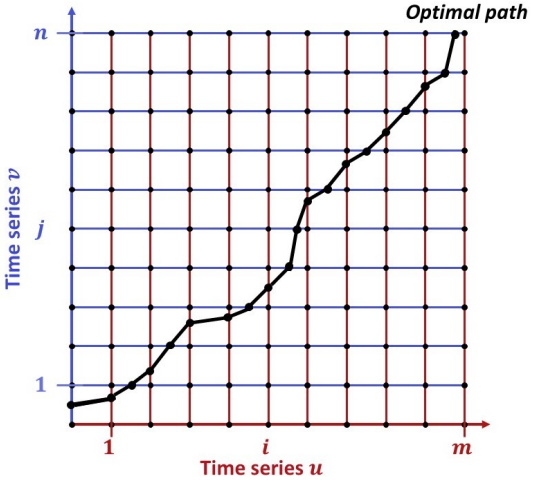

(d) Warping path obtained using CDTW.

FIGURE 4.2: Example illustrating the difference between DTW and CDTW [207, 208].

It is worthy noting that there are several warping paths that could satisfy the above constraints. $DTW(u, v)$ is used to represents the optimal warping path, which is the minimal distance between time series u and v that could be found through a dynamic programming algorithm.

$$\begin{cases} \mathcal{D}(i,j) = d_{global}(i,j) + min\{\mathcal{D}(i-1,j-1), \mathcal{D}(i-1,j), \mathcal{D}(i,j-1)\} \\ DTW(u,v) = min\{\mathcal{D}(m,n)\} \end{cases} \tag{4.4}$$

$\mathcal{D}(i,j)$ denotes the minimal cumulated distance in matrix $\mathcal{D}$ from $(0,0)$ to (i,j).

Once the optimal warping path has been computed based on the above dynamic programming equation, the time series u and v can be formulated using the following equations $\overline{u}$ and $\overline{v}$:

$$\begin{cases} \overline{u}(k) = u(w_u(k)) \\ \overline{v}(k) = v(w_v(k)) \end{cases}, k = 1, 2, ..., p \tag{4.5}$$

Where $\overline{u}$ and $\overline{v}$ represent the warped time-series u and v, respectively. The DTW Euclidean distance between u and v could be expressed using the two new time series $\overline{u}$ and $\overline{v}$ as follows:

$$\mathcal{DTW}(u,v) = \sum_{k=1}^{p} (\overline{u}(k) - \overline{v}(k))^2 \tag{4.6}$$

Figure 4.2(c) illustrates the matching process on the 'warping plane', by representing $w_u(k)$ on the x-axis, and $w_v(k)$ on the y-axis. The path on this warping plane is represented by the warping function $\mathcal{W}$. The set of sample points on u and v defines a grid on the warping plane. When the warping path crosses one vertex (i,j) of the grid, it means that the point $u(i)$ corresponds to the point $v(j)$.

In the DTW technique, a discrete solution is provided for the warping function $\mathcal{W}$; i.e. the warping functions $w_u(k)$ and $w_v(k)$ take discrete values in $k = 1, ..., p$. Moreover, this technique allows for the warping path to pass only through the points of the grid.

By using the recursion equation (4.4), the optimal path could be easily computed. For each node of the plane (i,j), the minimum cumulated cost is calculated sequentially by

column-wise or row-wise. The previous node that yields to the minimum cost is saved. The node with minimum cost is searched in the last column or row. By backtracking the saved nodes, the optimum warping path is then generated.

4.3.2 Continuous Dynamic Time Warping (CDTW) formulation

The major limitation of the DTW technique is the use of discrete points in the mapping of the two time-series. Furthermore, this technique does not give the best 'optimal' warping path. To improve this technique, Munich et al. [208], proposed the Continuous DTW (CDTW) technique by applying the process of mapping in the continuous domain. In this case, the distortion function $\mathcal{W}$ can take non-integer values as the solution of the equation 4.4. The CDTW differs from the standard DTW by the fact that a sample point in one of the time-series could match a point in-between two samples in the other time-series (see Fig. 4.2(b)). Therefore, the warping path could go through points between the grid nodes (see Fig. 4.2(d)). As it regards the recursion equation 4.4, the only difference lies in the fact that if $w_u(k)$ takes integer values in the set $\{1, ..., m\}$, then $w_v(k)$ could take non-integer values, and vice-versa.

The intermediate matching points are obtained using interpolation model for the two time-series [208]. To obtain a closed and simple form of the equations for the recursion, a linear interpolation model between sample points is used in this study. As shown in Figure 4.2(b), the sample point $v(2)$ is mapped to a new point $u'(1)$ which is obtained using an orthogonal projection of $v(2)$ onto the segment $[u(1), u(2)]$. The linear model has the interest of greatly simplifying the computation of the intermediate matching points resulting from the orthogonal projection. It's worth noting that the similarity measurement used in CDTW is similar to that of the standard DTW [208]. Figure 4.2 illustrates the principle of the DTW and CDTW.

From Figure 4.3, using the orthogonal projection of sample point $u(i-1)$ of the time-series u onto the segment $[v(j-1), v(j)]$, and conversely the orthogonal projection of sample point $v(j)$ of the time-series v onto the segment $[u(i-1), u(i)]$, the coordinates of the intermediate matching points $v(f)$, $u(e)$ can be expressed as follows:

$$u : \begin{cases} e = (i-1) + r_u.\dfrac{\triangle_i}{\triangle_1} = (i-1) + \dfrac{r_u}{\triangle_u} \\ u(e) = u(i-1) + r_u.\dfrac{\triangle_u}{\triangle_1} = u(i-1) + r_u \end{cases} \tag{4.7}$$

With

$$\triangle_i = (i) - (i-1) = 1$$
$$\triangle_u = u(i) - u(i-1)$$
$$\triangle_1 = \sqrt{\triangle_i^2 + \triangle_u^2} = \sqrt{\triangle_u^2} = \triangle_u$$
$$r_u = \frac{((j) - (i-1)).\triangle_i + (v(j) - u(i-1)).\triangle_u}{\triangle_1} = \frac{((j) - (i-1))}{\triangle_u} + (v(j) - u(i-1))$$

$$v : \begin{cases} f = (j-1) + r_v.\dfrac{\triangle_j}{\triangle_2} = (j-1) + \dfrac{r_v}{\triangle_v} \\ v(f) = v(j-1) + r_v.\dfrac{\triangle_v}{\triangle_2} = v(j-1) + r_v \end{cases} \tag{4.8}$$

With

$$\triangle_j = (j) - (j-1) = 1$$
$$\triangle_v = v(j) - v(j-1)$$
$$\triangle_2 = \sqrt{\triangle_j^2 + \triangle_v^2} = \sqrt{\triangle_v^2} = \triangle_v$$
$$r_v = \frac{((i-1) - (j-1)).\triangle_j + (u(i-1) - v(j-1)).\triangle_v}{\triangle_2} = \frac{((i-1) - (j-1))}{\triangle_v} + (u(i-1) - v(j-1))$$

4.4 Gait cycle similarity evaluation using Dynamic Time Warping (DTW)

DTW technique has been exploited in the literature for gait cycle analysis. For instance, in Helwig et al. [209], the DTW and DDTW techniques are exploited to temporally align gait cycle data for biomechanical and clinical applications. The ability of these techniques to perform a precise temporal alignment is assessed when mapping a test gait cycle trajectory to a reference trajectory. In [210], authors applied the DTW technique

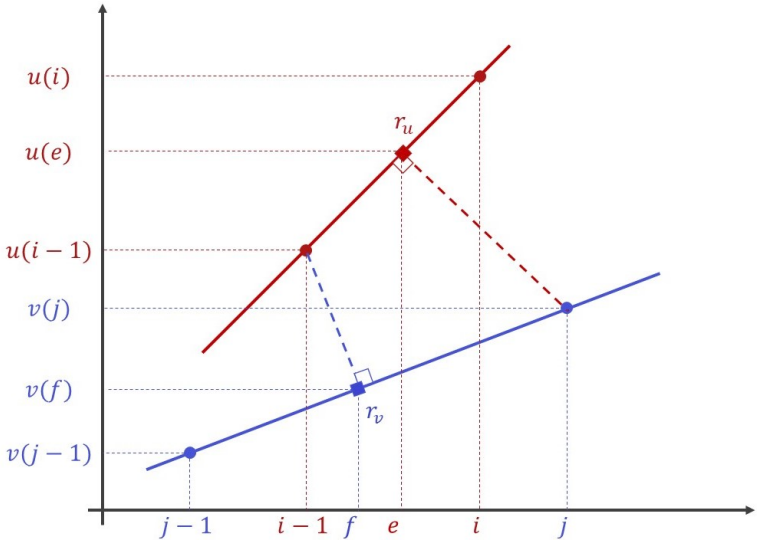

FIGURE 4.3: An example of the linear interpolation between samples of time-series using the CDTW.

to characterize pattern of walking extracted from video sequences depicting walking persons. In [211], authors propose to use the DTW technique to match between training sets and test sets of features characterizing the gait pattern. In Kale et al. [212], the dynamic time-warping (DTW) approach is used to deal with the naturally-occurring changes in walking speed. Different gait features representing a person's gait are extracted from the silhouette image of a walking person. Switonski et al. use in [213] the nearest neighbours classification scheme with DTW based motion similarity assessment to recognize the kinematic motion data characterizing the gait. In [214], Muscillo et al. use Dynamic Time Warping (DTW) and Derivative Dynamic Time Warping (DDTW) approaches to recognize daily living activities such as walking, climbing and descending stairs using accelerometer data.

4.5 Data pre-processing for PD classification

This section shows the data pre-processing and consists of two subsections: (1) Feature extraction step achieved using the CDTW technique to evaluate, for each foot, the similarity between the stance phase of each gait cycle and those of the other cycles. (2) Feature selection step where CDTW-based features and standard spatio-temporal features, as computed in chapter 3, are used to select the optimal subset of the features

that allow obtaining the best classification rate. These steps are briefly described in the following :

4.5.1 Features extraction

Before assessing the similarity of the gait cycles, a threshold-based approach is applied to each of the recorded gait time-series of the left foot and the right foot taken separately, to extract swing and stance phases. Only stance phases have been considered since vGRFs values in swing phases are equal to zero (see Fig. 4.4).

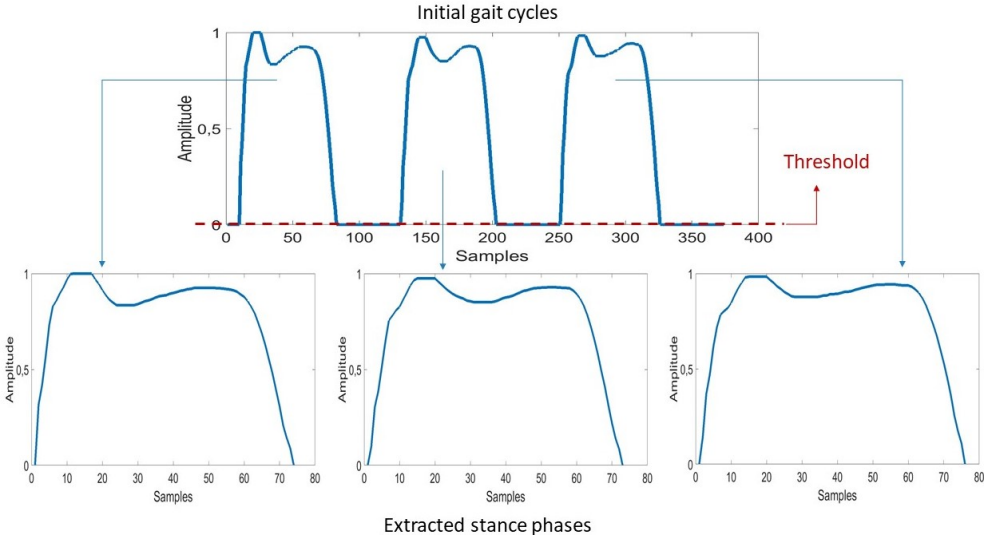

FIGURE 4.4: Stance phases extraction

The feature extraction step proposed in our approach, uses the CDTW technique to evaluate for each foot the similarity between its stance phases. Two CDTW distance vectors characterizing this similarity are then extracted from the stance phases; a distance vector is associated to each foot. By using the mean and the STD of each CDTW distance vector, four features are thus considered: The four features are Mean of the CDTW distance of the left foot, Mean of the CDTW distance of the right foot, STD of the CDTW distance of the left foot, STD of the CDTW distance of the right foot.

Figures 4.5(a) and 4.5(b) show the matching between the time-series of two right foot stance phases in the case of a healthy subject and a subject with PD. One can observe that the stance phases of the healthy subject are almost similar (figure 4.5(a)), unlike those of the subject with PD (4.5(b)).

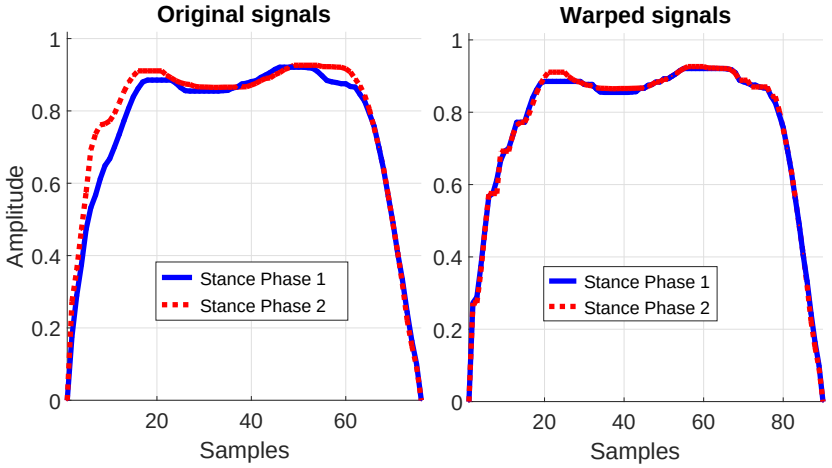

(a) Healthy subject

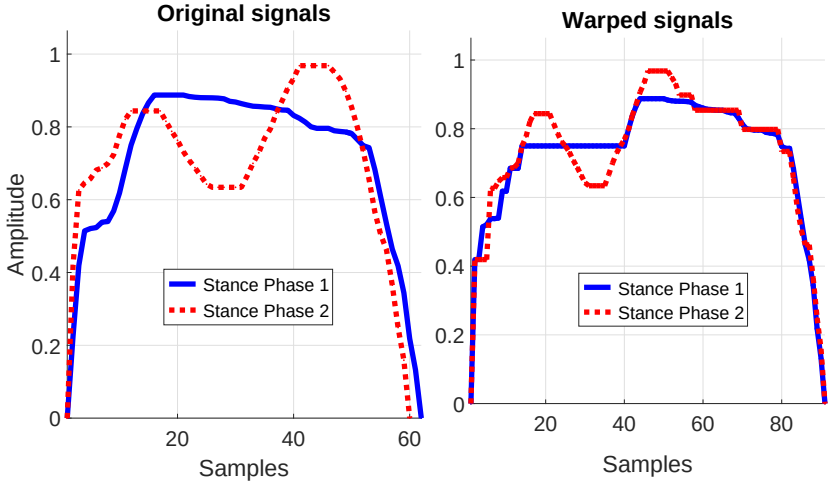

(b) PD subject

FIGURE 4.5: Matching between the times-series of two right foot stance phases (a) healthy subject, (b) PD subject.

The obtained 'optimal' warping paths are shown in white in figures 4.6(a) and 4.6(b). The intensity of the gray color represents the value of the CDTW distance; the more the gray is darker the more the distance is higher, and vice-versa. The black lines represent the 'optimal' warping paths in the case of two identical stance phases. In the case of a healthy subject, the 'optimal' warping path is very close to the one obtained with two identical stance phases (figures 4.6(a)). Conversely, for a subject with PD, the 'optimal' warping path is highly deformed and relatively far from the one obtained in the case of two identical stance phases (figures 4.6(b)).

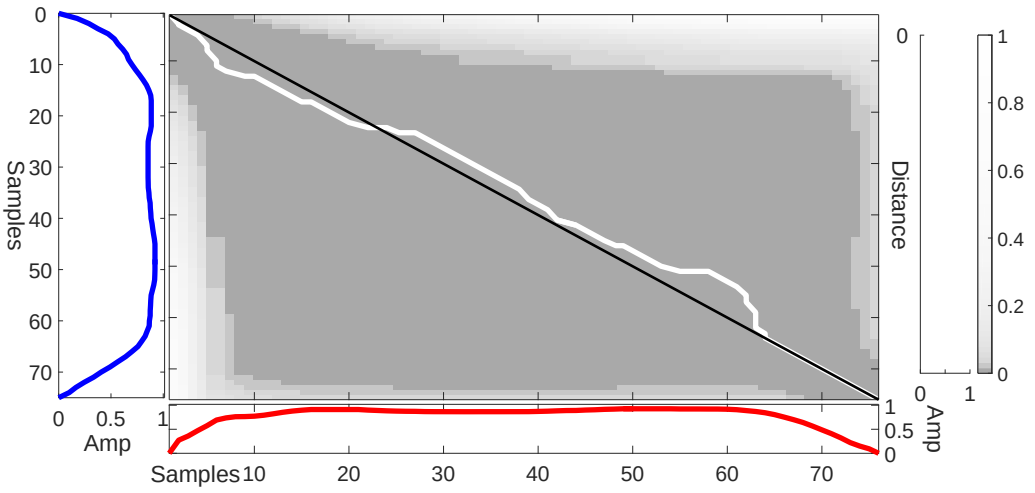

(a) Healthy subject

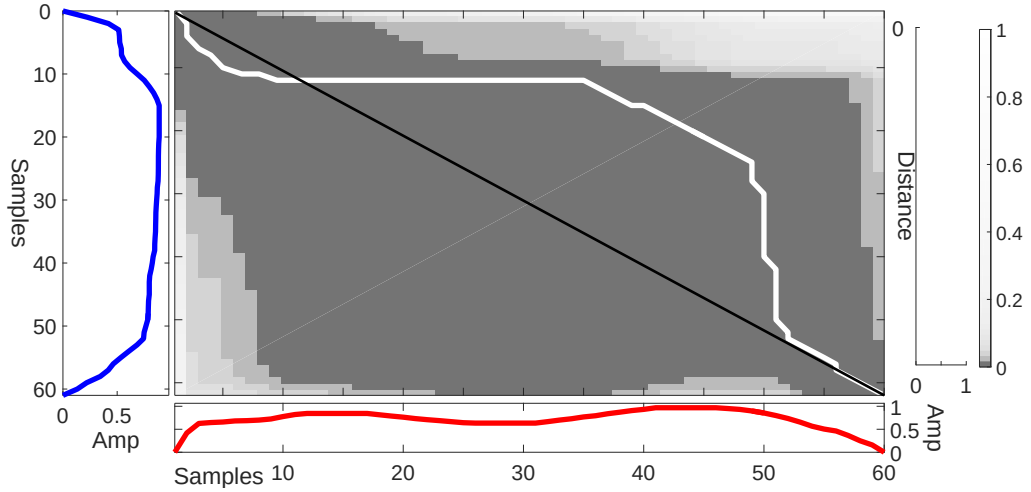

(b) PD subject

FIGURE 4.6: Optimal paths:(a) healthy subject, (b) PD subject.

4.5.2 Features selection

Four features that represent the mean and the STD of the CDTW distance of each of both feet, are considered in addition to nineteen standard (spatio-temporal) features, to form a set of twenty three features (see Table 4.1). From this set, a wrapper-based method is used to derive an optimal subset of 4-selected features. This wrapper method consists of two steps: subset generation step using exhaustive search method and evaluation step using k-NN algorithm to assess the classification performance of the generated subset.

Features	References	Extracted features
Spatio-temporal features (Standard features)	1	Coefficients of Variation in percentage (%) of the Swing Time of the Left foot
	2	Coefficients of Variation in duration (s) of the Swing Time of the Left foot
	3	Coefficients of Variation in duration (s) of the Stride Time of the Left foot
	4	Coefficients of Variation in percentage (%) of the Swing Time of the Right foot
	5	Coefficients of Variation in duration (s) of the Swing Time of the Right foot
	6	Coefficients of Variation in duration (s) of the Stride Time of the Right foot
	7	Coefficients of Variation of the Short Swing Time
	8	Coefficients of Variation of the Long Swing Time
	9	Coefficients of Variation of the Gait Asymmetry
	10	Mean in percentage (%) of the Swing Time of the Left foot
	11	Mean in duration (s) of the Swing Time of the Left foot
	12	Mean in duration (s) of the Stride Time of the Left foot
	13	Mean in percentage (%) of the Swing Time of the Right foot
	14	Mean in duration (s) of the Swing Time of the Right foot
	15	Mean in duration (s) of the Stride Time of the Right foot
	16	Mean in percentage (%) of the Double Stance Time
	17	Mean of the Short Swing Time
	18	Mean of the Long Swing Time
	19	Mean of the Gait Asymmetry
CDTW Features	20	Mean of the CDTW distance of the Left foot
	21	Mean of the CDTW distance of the Right foot
	22	STD of the CDTW distance of the Left foot
	23	STD of the CDTW distance of the Right foot

TABLE 4.1: List of the twenty three extracted features.

4.6 Results and discussion

In this section, the results of the classification between healthy and PD subjects are presented and discussed. Four supervised classifiers are considered: k-Nearest Neighbours (k-NN), Support Vector Machines (SVM), Decision Trees (CART), Random Forests (RF), and Naive Bayes (NB). Two unsupervised classifiers were also evaluated: Gaussian Mixture Models (GMM), and k-Means.

The tuning of the classifier parameters used in this section is similar to the one applied

in section 3.5 chapter 3. Also, it should be noted that 10-fold cross-validation technique was applied to evaluate the performances of the classifiers. Two types of distances were evaluated in the application of the CDTW: squared Euclidean and Euclidean [215] .

For the performance evaluation of the different classification methods, the following metrics were used: accuracy rates and their STD, precision, recall, and F-measure.

4.6.1 PD classification using CDTW-based features

Each classification technique requires one or several parameters that control (affect) the prediction outcome of the classifier. Choosing the best values for these parameters is difficult and involves finding a trade-off between the model's complexity and its generalization ability. In this study, finding parameter settings is conducted using a grid search. For more details, please refer to chapter 3, section 3.5.1. Table 4.2 shows the tuned parameters for each of the used classifier.

	Classifiers	**Sub-datasets**	**Distances**	
			Sq. Euclidean	**Euclidean**
Supervised	k-NN	Yogev	k=3	k=10
		Hausdorff	k=2	k=5
		Frenkel-Toledo	k=2	k=3
	DT	Yogev	'Cart' Algorithm	
		Hausdorff		
		Frenkel-Toledo		
	RF	Yogev	T=90	T=95
		Hausdorff	T=200	T=75
		Frenkel-Toledo	T=300	T=100
	SVM	Yogev	Polynomial	Polynomial
		Hausdorff	Polynomial	Polynomial
		Frenkel-Toledo	Linear	Polynomial
Unsupervised	k-Means	Yogev	Number of classes=2	
		Hausdorff		
		Frenkel-Toledo		
	GMM	Yogev	Full Gaussian	Full Gaussian
		Hausdorff	Full Gaussian	Full Gaussian
		Frenkel-Toledo	Diagonal Gaussian	Full Gaussian

TABLE 4.2: Tuned parameters in each classifier in two used distance types.

The obtained classification results in terms of accuracy rates and their standard deviations (STD), precision, recall and F-measure using the CDTW distance based on squared Euclidean and Euclidean distance metrics, in the case of Yogev et al., Hausdorff et al., and Frenkel-Toledo et al. sub-datasets are shown in tables 4.3, 4.4, and 4.5, respectively. It is worth noting that the use of Euclidean distance improves the accuracy rates with respect to the ones obtained using the squared Euclidean.

The accuracy rate improvement obtained using the Euclidean distance varies from 4 to 12 % in the case of Yogev's sub-dataset. This improvement varies from 2 to 5 % in the case of Hausdorff's sub-dataset and from 6 to 12 % in the case of Frenkel-Toledo's sub-dataset. Moreover, it could be noted that the GMM achieves the best improvement which reaches 12 % in the case of Yogev's sub-dataset. Also, SVM achieves this higher improvement (5 %) in the case of Hausdorff's sub-dataset; k-NN, CART and SVM which reached 12 % in the case of Frenkel-Toledo's sub-dataset.

Better performances are obtained in the case of the Hausdorff's sub-dataset since, as discussed in chapter 3, this dataset is composed in proportion of more subjects with high severity, which makes it possible to obtain a better separability between the PD subjects class and the healthy subjects class.

Regarding the performance of classifiers, the same trends can be observed as in Chapter 3. Indeed, the best accuracy rates are obtained with SVM in the case of Yogev's sub-dataset (98.60 %), with k-NN in the case of Hausdorff's sub-dataset (99.33 %), and with SVM in the case of Frenkel-Toledo's sub-dataset (99.53 %). The same observation can be made when considering the Precision, Recall and F-measure metrics.

Table 4.6 shows the performances in terms of accuracy rates and their STD, using Euclidean-based CDTW distance. These performances have been compared to those obtained using 5 features selected among 19 standard features (see subsection 3.4.3 chapter 3). Results reported in table 4.6 show that the use of CDTW distance based features gives the best classification performances. It can be noted that for the three datasets with CDTW features, SVM and k-NN classifiers, achieve the best performances, while, with standard features, RF and k-NN classifiers, achieve the best performances. The accuracy rate obtained using these two classifiers ranges from 97 to 99 %. The accuracy rate ranges from 68 to 77 % using unsupervised classifiers. The accuracy rate improvement obtained with k-NN and SVM classifiers varies from 7 to 19 %.

Distances	Perf.	Supervised				Unsupervised	
		k-NN	**CART**	**RF**	**SVM**	**k-Means**	**GMM**
Sq. Euclidean	Accuracy	92.88 %	82.96 %	89.35 %	93.57 %	67.79 %	65.58 %
	STD	2.03 %	3.99 %	2.62 %	2.61 %	1.10 %	7.23 %
	Precision	93.22 %	82.09 %	90.01 %	93.33 %	63.53 %	64.86 %
	Recall	91.55 %	80.85 %	87.03 %	92.93 %	62.75 %	65.84 %
	F-measure	92.38 %	81.46 %	88.49 %	93.13 %	63.14 %	65.35 %
Euclidean	Accuracy	**97.32 %**	**92.36 %**	**96.18 %**	**98.60 %**	**74.88 %**	**77.44 %**
	STD	1.60 %	3.39 %	1.95 %	0.49 %	1.12 %	7.15 %
	Precision	97.23%	92.03 %	96.29 %	98.77 %	74.49 %	78.97 %
	Recall	97.04 %	91.47 %	95.48 %	98.25 %	76.18 %	80.70 %
	F-measure	97.13 %	91.75 %	95.88 %	98.51 %	75.33 %	79.82 %

TABLE 4.3: Accuracy rates and their STD, Precision, Recall and F-measure obtained using different distance metrics - Yogev's sub-dataset.

Distances	Perf.	Supervised				Unsupervised	
		k-NN	**CART**	**RF**	**SVM**	**k-Means**	**GMM**
Sq. Euclidean	Accuracy	97.52 %	88.82 %	90.02 %	95.03 %	65.29 %	73.97 %
	STD	1.04 %	3.09 %	1.98 %	1.85 %	2.13 %	4.90 %
	Precision	94.73 %	84.01 %	89.62 %	92.12 %	53.55 %	54.46 %
	Recall	98.29 %	80.2 %	78.46 %	92.75 %	54.46 %	52.97 %
	F-measure	96.48 %	82.05 %	83.67 %	92.44 %	54.01 %	53.71 %
Euclidean	Accuracy	**99.33 %**	**92.65 %**	**95.64 %**	**99.09 %**	**68.68 %**	**77.11 %**
	STD	0.67 %	2.74 %	1.56 %	0.26 %	0.26 %	8.21 %
	Precision	98.58 %	88.82 %	97.13 %	98.02 %	57.35 %	65.23 %
	Recall	99.44 %	88.71 %	89.35 %	99.28 %	59.11 %	65.46 %
	F-measure	99.01 %	88.77 %	93.08 %	98.64 %	58.22 %	65.34 %

TABLE 4.4: Accuracy rates and their STD, Precision, Recall and F-measure obtained using different distance metrics - Hausdorff's sub-dataset.

Distances	Perf.	Supervised				Unsupervised	
		k-NN	**CART**	**RF**	**SVM**	**k-Means**	**GMM**
Sq. Euclidean	Accuracy	86.02 %	80.02 %	82.59 %	87.32 %	60.47 %	67.19 %
	STD	3.09 %	6.44 %	4.92 %	2.99 %	2.13 %	8.65 %
	Precision	86.62 %	80.79 %	83.07 %	87.20 %	66.99 %	70.43 %
	Recall	86.75 %	80.04 %	81.99 %	87.42 %	62.91 %	68.76 %
	F-measure	86.69 %	80.41 %	82.52 %	87.31 %	64.89 %	69.59 %
Euclidean	Accuracy	**98.21 %**	**92.03 %**	**94.05 %**	**99.53 %**	**71.56 %**	**73.12 %**
	STD	1.38 %	4.83 %	2.37 %	0.75 %	3.88 %	4.53 %
	Precision	98.25 %	92.02 %	94.48 %	99.54 %	75.52 %	81.14 %
	Recall	97.99 %	91.89 %	93.68 %	99.51 %	73.23 %	75.40 %
	F-measure	98.12 %	91.95 %	94.08 %	99.53 %	74.36 %	78.16 %

TABLE 4.5: Accuracy rates and their STD, Precision, Recall and F-measure obtained using different distance metrics - Frenkel-Toledo's sub-dataset.

	Features	Perf.	Supervised				Unsupervised	
			k-NN	**CART**	**RF**	**SVM**	**k-Means**	**GMM**
Yogev	CDTW	Accuracy	97.32 %	92.36 %	96.18 %	98.60 %	74.88 %	77.44 %
		STD	1.60 %	3.39 %	1.95 %	0.49 %	1.12 %	7.15 %
	Standard	Accuracy	85.39 %	82.10 %	85.65 %	85.02 %	63.72 %	64.77 %
		STD	3.49 %	3.25 %	3.23 %	4.26 %	4.20 %	12.64 %
Hausdorff	CDTW	Accuracy	99.33 %	92.65 %	95.64 %	99.09 %	68.68 %	77.11 %
		STD	0.67 %	2.74 %	1.56 %	0.26 %	0.26 %	8.21 %
	Standard	Accuracy	91.39 %	84.82 %	88.77 %	87.70 %	55.12 %	65.12 %
		STD	2.83 %	3.66 %	2.30 %	3.26 %	3.59 %	11.08 %
Frenkel-Toledo	CDTW	Accuracy	98.21 %	92.03 %	94.05 %	99.53 %	71.56 %	73.12 %
		STD	1.38 %	4.83 %	2.37 %	0.75 %	3.88 %	4.53 %
	Standard	Accuracy	81.49 %	79.01 %	81.98 %	80.23 %	57.19 %	65.31 %
		STD	4.68 %	3.72 %	4.19 %	4.80 %	3.98 %	12.12 %

TABLE 4.6: Accuracy rates and their STD obtained using the CDTW distance features (4 features) and the standard features (5 features)

4.6.2 PD classification based on feature selection

In order to study the effect of using the CDTW-based features with respect to the use of standard features, we have applied a feature selection process of the total 23 features including, on one hand, the 4 CDTW-based features as shown in subsection 4.5.1 and calculated based on the Euclidean distance metric, and on the other hand, the 19 standard (spatio-temporal) features.

Table 4.7 shows the optimal feature parameters for each sub-dataset. In the case of Yogev's sub-dataset, the selected feature parameters include three CDTW-based features (that are Mean of the CDTW distance of the Left foot, Mean of the CDTW distance of the Right foot, and STD of the CDTW distance of the Right foot) and one standard spatio-temporal parameter that is the mean of the gait asymmetry whereas, for the two remaining sub-datasets, the four CDTW-based features were selected exclusively. These results confirm that among the total computed features, the CDTW-based features are the most relevant ones in terms of classification accuracy rates.

Sub-datasets	**Selected Features**
Yogev	Mean of the Gait Asymmetry
	Mean of the CDTW distance of the left foot
	Mean of the CDTW distance of the right foot
	STD of the CDTW distance of the right foot
Hausdorff	Mean of the CDTW distance of the left foot
	Mean of the CDTW distance of the right foot
	STD of the CDTW distance of the left foot
	STD of the CDTW distance of the right foot
Frenkel-Toledo	Mean of the CDTW distance of the left foot
	Mean of the CDTW distance of the right foot
	STD of the CDTW distance of the left foot
	STD of the CDTW distance of the right foot

TABLE 4.7: The four selected features, obtained from the exhaustive selection, for each sub-dataset

4.7 Conclusion

In this chapter, we proposed a new approach for the aid of the diagnosis of Parkinson's Disease (PD). This approach exploits the fact that usually the walking of healthy subject is characterised by repetition of gait cycles, whereas that of PD ones show significant variations from one gait cycle to another. For this purpose, a measure of similarity between these cycles carried out using the Continuous Dynamic Time Warping (CDTW) technique is proposed. By using the mean and the STD of each CDTW distance vector, four features are considered: Mean of the CDTW distance of the Left foot, Mean of the CDTW distance of the Right foot, STD of the CDTW distance of the Left foot, STD of the CDTW distance of the Right foot. In order to study the effect of using the CDTW based features with respect to the use of standard features, we have applied a feature selection process of the total 23 features including, on one hand, the 4 CDTW based features and on the other hand the 19 standard (spatio-temporal) features. The obtained results showed that the use of CDTW-based features improves significantly the classification accuracy rates for discriminating healthy subjects from subjects with PD.

Chapter 5

Multidimensional CDTW-based classification for Parkinson's Disease diagnosis

5.1 Introduction

This chapter describes the extension of the CDTW technique, proposed in chapter 4, to calculate the similarity between time-series during the stance phases in the multidimensional domain.

The formulation of the CDTW in multidimensional domain is presented firstly and then applied to the PD subjects classification. Several supervised/unsupervised classification methods have been implemented and evaluated. Different cases were considered with respect to the number of classes in each sub-dataset, which correspond to the severity degree of PD according to H & Y scale.

5.2 Multidimensional CDTW formulation

In the previous chapter, Continuous Dynamic Time Warping (CDTW) based features are introduced to evaluate the gait cycle similarity using unidimensional time-series. Recall that only the mean value of eight force sensors placed under each foot are considered in this case and consequently the estimation of the force interaction between the foot and the ground is limited to only one mean value per foot. Therefore, multidimensional Continuous Dynamic Time Warping (CDTW) based features are introduced in this chapter for a more accurate measure of similarity between stance phases times-series. The aim is to have a better discrimination between subjects according to the H & Y scale. In this chapter, for each foot we consider eight force signals provided by the vGRFs sensors (fig. 3.3, chapter 3) as well as their mean value to form in total a vector of nine signals per foot. In the following, we first present the formulation of the DTW in the multidimensional domain [216].

Formally, let $U = (u_1, u_2, ..., u_l, ..., u_d)$ and $V = (v_1, v_2, ..., v_l, ..., v_d)$ two multidimensional time-series, where $u_l = (u_l(1), u_l(2), ..., u_l(i), ..., u_l(m))$ and $v_l = (v_l(1), v_l(2)$ $, ..., v_l(j), ..., v_l(n))$ represent the $l\ th$ unidimensional time-series. d represents the number of signals per foot, $i = 1, 2, ..., m$, $j = 1, 2, ..., n$ where m and n represent respectively the lengths of the time series U and V that could be represented under the following matrices.

$$U = \begin{bmatrix} u_1(1) & u_1(2) & ... & u_1(i) & ... & u_1(m) \\ u_2(1) & u_2(2) & ... & u_2(i) & ... & u_2(m) \\ \vdots & \vdots & \vdots & \vdots & \vdots & \vdots \\ u_l(1) & u_l(2) & ... & u_l(i) & ... & u_l(m) \\ \vdots & \vdots & \vdots & \vdots & \vdots & \vdots \\ u_d(1) & u_d(2) & ... & u_d(i) & ... & u_d(m) \end{bmatrix}$$

$$V = \begin{bmatrix} v_1(1) & v_1(2) & ... & v_1(j) & ... & v_1(n) \\ v_2(1) & v_2(2) & ... & v_2(j) & ... & v_2(n) \\ \vdots & \vdots & \vdots & \vdots & \vdots & \vdots \\ v_l(1) & v_l(2) & ... & v_l(j) & ... & v_l(n) \\ \vdots & \vdots & \vdots & \vdots & \vdots & \vdots \\ v_d(1) & v_d(2) & ... & v_d(j) & ... & v_d(n) \end{bmatrix}$$

By generalizing the formulation of the local distance in the unidimensional case to the multidimensional case, the local distance $d_{local}(U(i), V(j))$ between the time-series elements in the multidimensional domain, is calculated using the squared Euclidean distance as follows:

$$d_{local}(U(i), V(j)) = \sum_{l=1}^{d} (u_l(i) - v_l(j))^2 \tag{5.1}$$

Where $U(i)$ and $V(j)$ represent the i^{th} and the j^{th} columns of U and V respectively. Then the optimal alignment path between the two time series U and V corresponds to the minimum distance warping path that is calculated based on the $d_{local}(U(i), V(j))$.

In the multidimensional case, the cumulated distance could be expressed as follows:

$$\mathcal{D}(i,j) = d_{local}(U(i), V(j)) + min \begin{cases} \mathcal{D}(i-1, j-1) \\ \mathcal{D}(i-1, j) \\ \mathcal{D}(i, j-1) \end{cases} \tag{5.2}$$

Where $\mathcal{D}(1,1) = d_{local}(U(1), V(1))$ represents the initial condition.

The optimal warping path $\mathcal{W}$ corresponds to the minimum sum of distance from $(1,1)$ to (m,n), which indicates how the two multidimensional time series U and V stretch or shrink along the time axis [216]. In the following, two new multivariate time-series $\overline{U}$ and $\overline{V}$ are calculated as follows:

$$\begin{cases} \overline{U}(k) = U(w_u(k)) \\ \overline{V}(k) = V(w_v(k)) \end{cases}, k = 1, 2, ..., p \tag{5.3}$$

Where p denotes the length of the warping path.

Using the warping path $\mathcal{W}$, the original U and V will be mapped to $\overline{U}$ and $\overline{V}$. Thus, the multidimensional DTW distance measure can be expressed as follows [216]:

$$\begin{aligned} DTW(U,V) = \sum_{k=1}^{p} d_{local}(U(w_u(k)), V(w_v(k))) = \sum_{k=1}^{p} d_{local}(\overline{U}(k), \overline{V}(k)) \\ = \sum_{k=1}^{p} (\overline{U}(k) - \overline{V}(k))^2 \end{aligned} \tag{5.4}$$

Note that the previous formulation concerns the standard multidimensional DTW. In the same way as for the unidimensional CDTW, the Multidimensional Continuous DTW (MCDTW) can be formulated by considering the process of mapping used in multidimensional DTW in the continuous domain. As in the case of unidimensional CDTW, intermediate points are added in the time-series by linear interpolation.

Figure 5.1 illustrates the matching process between the multidimensional time-series during the stance phases of the right foot in the case of one healthy subject and one PD subject. In this study, nine signals per foot are considered and correspond to the data collected from the eight sensors placed under each foot as well as their mean value. Figure 5.2 shows the optimal warping paths in the case of one healthy subject and one PD subject. It can be noticed that the obtained warping path for PD subject shows similar deformation curvature of the unidimensional one.

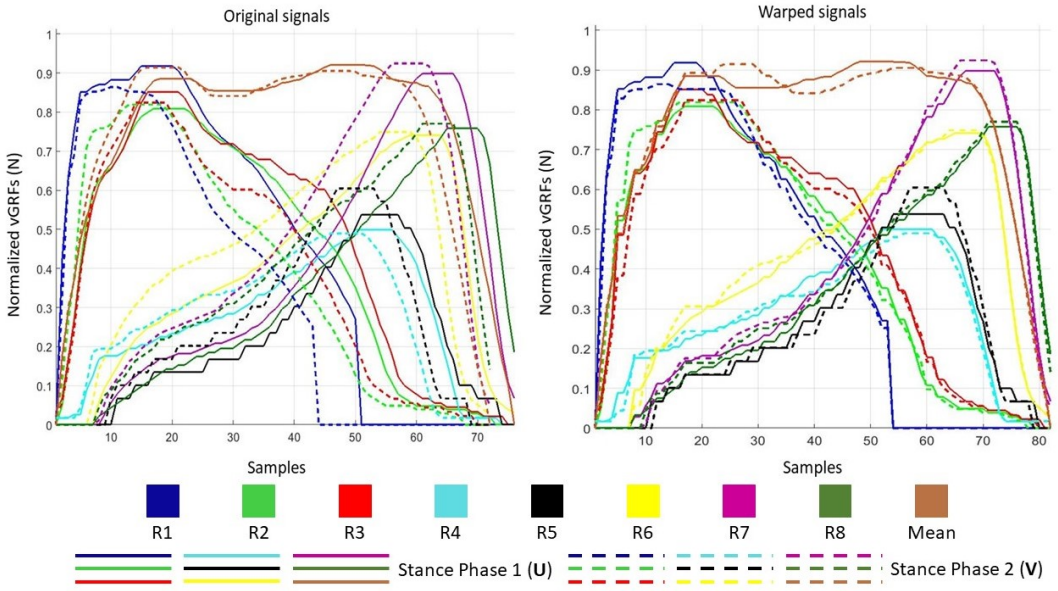

(a) Healthy subject

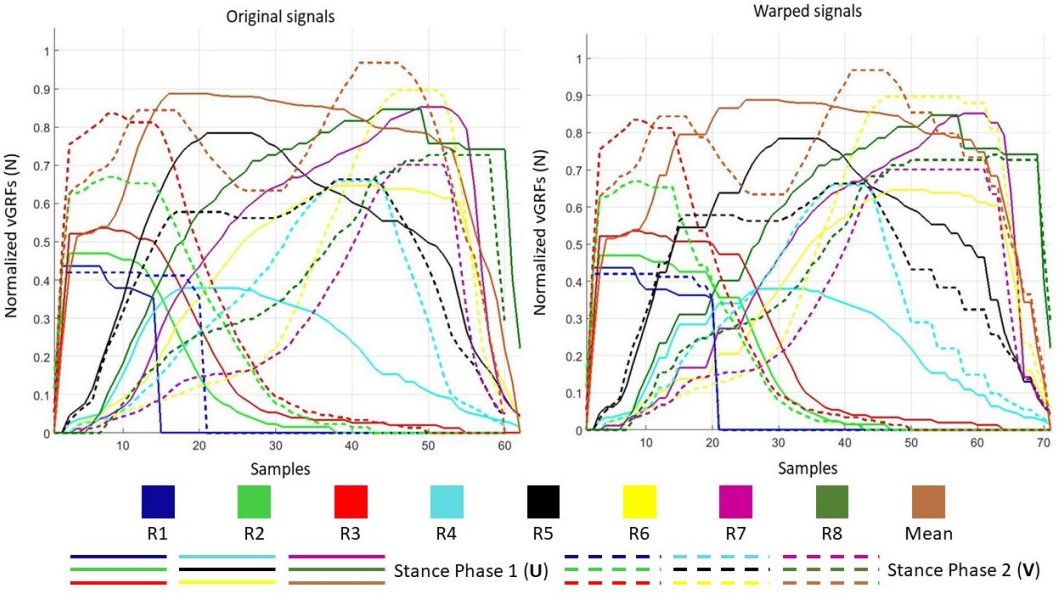

(b) PD subject

FIGURE 5.1: Results obtained from the matching between the times-series, in the multidimensional CDTW case, of two right foot stance phases according to: (a) healthy subject, (b) PD subject

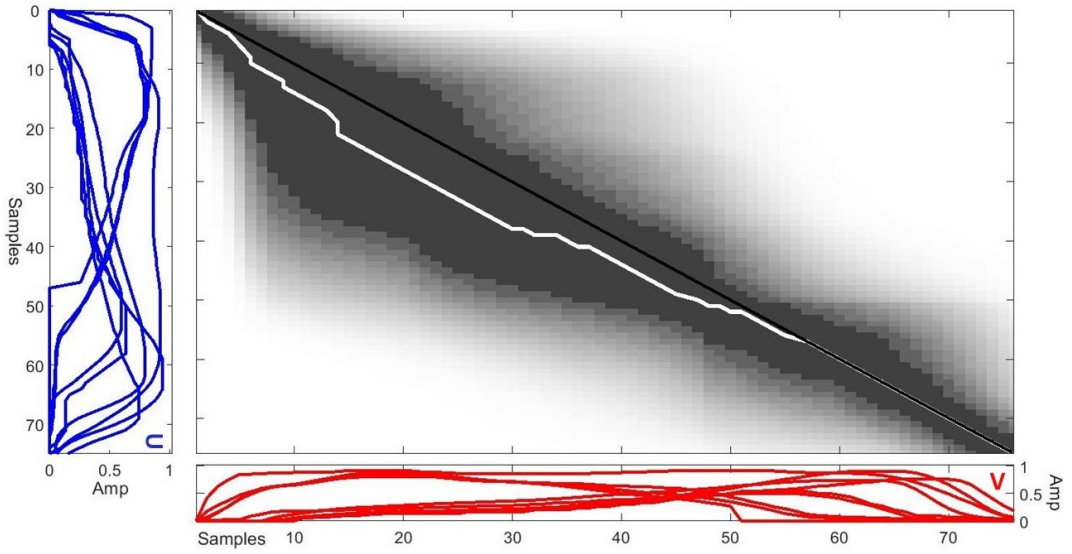

(a) Healthy subject

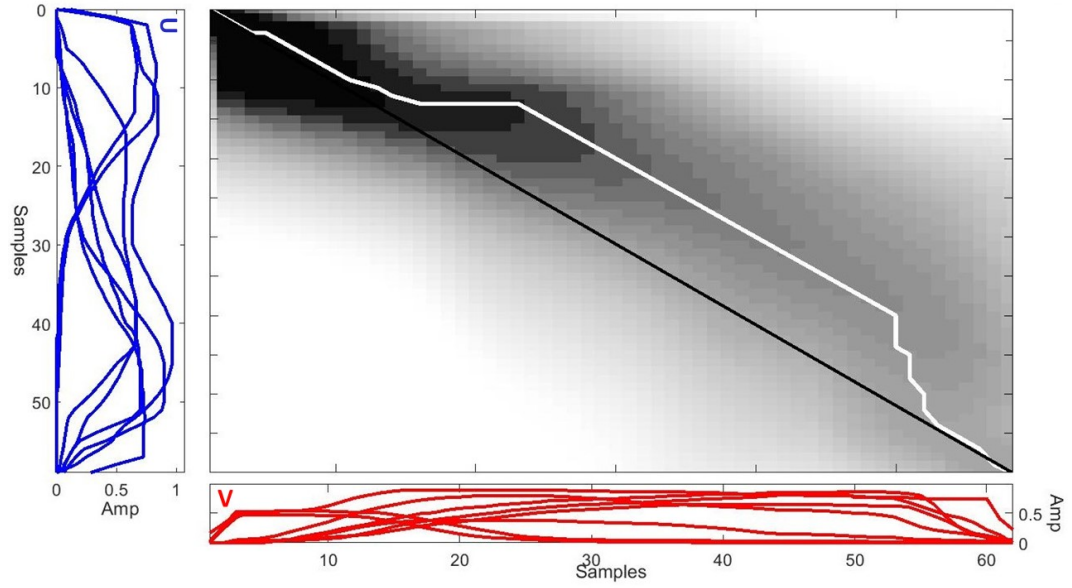

(b) PD subject

FIGURE 5.2: Optimal paths obtained in the multidimensional CDTW case: (a) healthy subject, (b) PD subject

5.3 PD subjects classification using multidimensional CDTW-based features

In this chapter, four CDTW-based features were used for classification purposes due to the fact that those features have shown the best performances in terms of classification rates (see chapter 4, section 4.6).

Several classification methods have been implemented and evaluated that are:

- Four supervised methods, namely, k-Nearest Neighbours (k-NN), Decision Tree (CART), Random Forest (RF), and Support Vector Machine (SVM).
- Two unsupervised methods, namely, k-means and Gaussian Mixture Model (GMM)

In this study, different cases were considered with respect to the number of classes for classification purposes:

- **Case 1)** class 1: healthy subjects; class 2: all PD subjects (3 sub-datasets)
- **Case 2)** class 1: healthy subjects; class 2: PD subjects having the severity H & Y =2 and H & Y =2.5 ; class 3: PD subjects having the severity H & Y =3 (2 sub-datasets: Yogev and Hausdorff)
- **Case 3)** class 1: healthy subjects; class 2: PD subjects having the severity H & Y =2; class 3: PD subjects having the severity H & Y =2.5; class 4: PD subjects having the severity H & Y =3 (2 sub-datasets: Yogev and Hausdorff). Class 1: healthy subjects; class 2: PD subjects having the severity H & Y =2; class 3: PD subjects having the severity H & Y =2.5 (Frenkel-Toledo's sub-dataset).

Table 5.1 shows the classes in each sub-dataset with respect to the severity level of PD according to the H & Y scale.

Sub-datasets	Yogev				Hausdorff				Frenkel-Toledo		
Severity on H & Y	0	2	2.5	3	0	2	2.5	3	0	2	2.5
Classes	1	2	3	4	1	2	3	4	1	2	3

TABLE 5.1: Classes in each sub-dataset with respect to the severity level of PD according to the H & Y scale.

5.3.1 Parameter settings

The tuning of the classifier' parameters used in this section is similar to the one applied in section 3.5-chapter 3. 10-fold cross-validation technique is used to evaluate the performances of the classifiers. The classifier parameters were tuned using a grid search based method. Tables 5.2, 5.3 , 5.4 show the optimal parameters for each of the used classifier.

	Classifiers	Sub-datasets	Distances	
			Sq. Euclidean	**Euclidean**
Supervised	k-NN	Yogev	k=2	k=4
		Hausdorff	k=2	k=2
		Frenkel-Toledo	k=4	k=3
	DT	Yogev	'CART' Algorithm	
		Hausdorff		
		Frenkel-Toledo		
	RF	Yogev	T=100	T=120
		Hausdorff	T=90	T=110
		Frenkel-Toledo	T=100	T=90
	SVM	Yogev	Polynomial	
		Hausdorff		
		Frenkel-Toledo		
Unsupervised	k-Means	Yogev	Number of classes=2	
		Hausdorff		
		Frenkel-Toledo		
	GMM	Yogev	Full Gaussian	
		Hausdorff		
		Frenkel-Toledo		

Table 5.2: Optimal parameters of the different classifiers (case 1)

	Classifiers	Sub-datasets	Distances	
			Sq. Euclidean	**Euclidean**
Supervised	k-NN	Yogev	K=5	K=6
		Hausdorff	K=5	K=5
	DT	Yogev	'CART' Algorithm	
		Hausdorff		
	RF	Yogev	T=80	T=130
		Hausdorff	T=100	T=100
	SVM	Yogev	Polynomial	
		Hausdorff		
Unsup.	k-Means	Yogev	Number of classes=3	
		Hausdorff		
	GMM	Yogev	Full Gaussian	
		Hausdorff		

Table 5.3: Optimal parameters of the different classifiers (case 2)

	Classifiers	Sub-datasets	Distances	
			Sq. Euclidean	Euclidean
Supervised	k-NN	Yogev	K=5	K=4
		Hausdorff	K=5	K=5
		Frenkel-Toledo	K=4	K=4
	DT	Yogev	'CART' Algorithm	
		Hausdorff		
		Frenkel-Toledo		
	RF	Yogev	T=100	T=120
		Hausdorff	T=100	T=100
		Frenkel-Toledo	T=100	T=100
	SVM	Yogev	Polynomial	
		Hausdorff		
		Frenkel-Toledo		
Unsupervised	k-Means	Yogev	Number of classes=4	
		Hausdorff	Number of classes=4	
		Frenkel-Toledo	Number of classes=3	
	GMM	Yogev	Full Gaussian	
		Hausdorff		
		Frenkel-Toledo		

TABLE 5.4: Optimal parameters of the different classifiers (case 3)

5.3.2 Results and discussion

Tables 5.5, 5.6, and 5.7 show the classifiers performances in terms of accuracy and its standard deviation, precision, recall and f-measure in the first case (Section 5.3). A comparison of the classifiers performances, shows that k-NN and SVM outperform both supervised and unsupervised classifiers by achieving almost the same accuracy rate (between 96.33 % and 99.92 %) independently from the type of distance used in the computation of the CDTW distances. The same observation can be made when considering the other metrics (precision, recall, and F-measure).

		Supervised				Unsupervised	
	Perf.	**k-NN**	**CART**	**RF**	**SVM**	**k-Means**	**GMM**
Sq. Euclidean	Accuracy	97.15 %	90.75 %	94.45 %	**97.79 %**	72.79 %	67.91 %
	STD	1.66 %	1.71 %	2.36 %	**0.86 %**	3.01 %	6.08 %
	Precision	96.47 %	89.85 %	90.08 %	**97.50 %**	76.87 %	68.96 %
	Recall	97.49 %	90.43 %	93.96 %	**97.80 %**	77.38 %	58.91 %
	F-measure	96.98 %	90.14 %	94.02 %	**97.65 %**	77.12 %	63.54 %
Euclidean	Accuracy	99.76 %	94.24 %	98.71 %	**99.88 %**	75.81 %	77.79 %
	STD	0.5 %	2.66 %	1.18 %	**0.38 %**	7.88 %	12.92 %
	Precision	99.75 %	93.39 %	98.93 %	**99.84 %**	77.68 %	80.63 %
	Recall	99.75 %	94.07 %	98.34 %	**99.91 %**	79.21 %	81.93 %
	F-measure	99.75 %	93.73 %	98.64 %	**99.88 %**	78.44 %	81.28 %

TABLE 5.5: Accuracy and its std, precision, recall and f-measure for each classifier in the multidimensional CDTW (case 1) - Yogev's sub-dataset.

		Supervised				Unsupervised	
	Perf.	**k-NN**	**CART**	**RF**	**SVM**	**k-Means**	**GMM**
Sq. Euclidean	Accuracy	**98.10 %**	91.23 %	92.36 %	97.52 %	66.53 %	76.78 %
	STD	**1.61 %**	1.56 %	1.70 %	0.55 %	1.74 %	6.78 %
	Precision	97.04 %	89.20 %	91.32 %	**98.13 %**	48.56 %	57.81 %
	Recall	**97.17 %**	82.59 %	84.36 %	94.30 %	48.58 %	53.71 %
	F-measure	**97.11 %**	85.77 %	87.70 %	96.18 %	48.57 %	55.68 %
Euclidean	Accuracy	**99.92 %**	93.39 %	96.03 %	99.75 %	69.42 %	78.93 %
	STD	**0.26 %**	2.08 %	1.73 %	0.40 %	3.14 %	1.31 %
	Precision	**99.95 %**	89.83 %	96.15 %	99.70 %	56.21 %	50.79 %
	Recall	**99.80 %**	90.06 %	91.58 %	99.55 %	57.06 %	50.04 %
	F-measure	**99.87 %**	89.95 %	93.81 %	99.62 %	56.63 %	50.41 %

TABLE 5.6: Accuracy and its std, precision, recall and f-measure for each classifier in the multidimensional CDTW (case 1) - Hausdorff's sub-dataset.

		Supervised				Unsupervised	
	Perf.	**k-NN**	**CART**	**RF**	**SVM**	**k-Means**	**GMM**
Sq. Euclidean	Accuracy	**96.33 %**	85.99 %	91.41 %	96.25 %	70.62 %	71.56 %
	STD	**2.49 %**	4.20 %	3.69 %	0.81 %	3.95 %	14.80 %
	Precision	**96.18 %**	85.80 %	91.28 %	95.74 %	70.38 %	71.46 %
	Recall	**96.57 %**	86.05 %	91.55 %	96.14 %	70.10 %	70.84 %
	F-measure	**96.37 %**	85.92 %	91.41 %	95.94 %	70.24 %	71.15 %
Euclidean	Accuracy	98.59 %	92.81 %	94.84 %	**99.84 %**	73.75 %	76.88 %
	STD	1.02 %	3.44 %	2.06 %	**0.49 %**	3.57 %	7.72 %
	Precision	98.49 %	92.70 %	94.74 %	**99.83 %**	78.42 %	83.11 %
	Recall	98.71 %	93.01 %	94.90 %	**99.86 %**	75.53 %	78.86 %
	F-measure	98.60 %	92.86 %	94.82 %	**99.84 %**	76.95 %	80.93 %

TABLE 5.7: Accuracy and its std, precision, recall and f-measure for each classifier in the multidimensional CDTW (case 1) - Frenkel-Toledo's sub-dataset.

To analyse the confusion among the classified subjects in the three cases (section 5.3), global confusion matrices (tables 5.8, 5.11 and 5.15) obtained using k-NN and SVM classifiers with both unidimensional and multidimensional CDTW-based features under 10-fold cross-validation, are used. The choice of using only k-NN and SVM in the confusion matrices comparison, is due to the fact that those algorithms have achieved best classification rates performances (tables 5.5–5.7, section 5.3).

In all matrices (table 5.8), the classifiers recognize subjects with PD better than healthy subjects, particularly in the Hausdorff's sub-dataset, regardless of the type of distance. The recognition rate improvement using the multidimensional CDTW-based features may reach up to 7 % in healthy subjects, and 3 % in PD subjects with respect to the classification using unidimensional CDTW-based features.

Table 5.8: Global confusion matrix obtained using k-NN and SVM classifiers obtained in the case 1.

				Obtained Classes							
				k-NN (Multi)		**k-NN (Uni)**		**SVM(Multi)**		**SVM(Uni)**	
				0	**1**	**0**	**1**	**0**	**1**	**0**	**1**
Yogev et al.	Sq. Enc	**True Classes**	**0**	**99.06 %**	0.94 %	92.50 %	7.50 %	**97.81 %**	2.19 %	90.31 %	9.69 %
			1	4.07 %	**95.93 %**	6.85 %	93.15 %	2.22 %	**97.78 %**	4.45 %	95.55 %
	Enc	**True Classes**	**0**	**99.69 %**	0.31 %	95.94 %	4.06 %	**100 %**	0 %	96.88 %	3.12 %
			1	0.19 %	**99.81 %**	1.85 %	98.15 %	0.18%	**99.82 %**	0.37 %	99.63 %
Hausdorff et al.	Sq. Enc	**True Classes**	**0**	**95.60 %**	4.40 %	93.60 %	6.40 %	88.80 %	11.20 %	88.80 %	11.20 %
			1	1.25 %	**98.75 %**	1.46 %	98.54 %	0.21 %	**99.79 %**	3.30 %	96.70 %
	Enc	**True Classes**	**0**	99.60 %	0.40 %	99.60 %	0.40 %	**99.20 %**	0.80 %	98.80 %	1.20 %
			1	0 %	**100 %**	0.73 %	99.27 %	0.10%	**99.90 %**	0.83 %	99.17 %
Frenkel-Toledo et al.	Sq. Enc	**True Classes**	**0**	**100 %**	0 %	93.80 %	6.20 %	**100 %**	0 %	88.30 %	11.70 %
			1	6.86 %	**93.14 %**	20.30 %	79.70 %	7.71 %	**92.29 %**	13.40 %	86.60 %
	Enc	**True Classes**	**0**	**100 %**	0 %	99.31 %	0.69 %	**100 %**	0 %	99.31 %	0.69 %
			1	2.57 %	**97.43 %**	2.86 %	97.14 %	0.29%	99.71 %	0.29 %	99.71 %

Tables 5.9 and 5.10 summarize the classifier performances in terms of accuracy and its standard deviation, precision, recall and f-measure in the second case (3 classes according to H & Y scale see section 5.3). A comparison of the classifiers performances, shows that k-NN outperforms both supervised and unsupervised classifiers by achieving an accuracy rate ranging from 87.11 % to 91.93 % regardless of the type of distance used in the computation of the CDTW distances. The same observation can be made when considering the other metrics (precision, recall, and F-measure).

		Supervised				**Unsupervised**	
	Perf.	**k-NN**	**CART**	**RF**	**SVM**	**k-Means**	**GMM**
Sq. Euclidean	Accuracy	**87.34 %**	75.47 %	84.54 %	85.35 %	66.28 %	64.07 %
	STD	**2.09 %**	3.03 %	2.01 %	0.60 %	3.68 %	8.46 %
	Precision	**82.43 %**	64.88 %	77.79 %	80.00 %	55.52 %	66.74 %
	Recall	71.72 %	64.53 %	**71.96 %**	70.16 %	53.01 %	53.68 %
	F-measure	**76.70 %**	64.71 %	74.76 %	74.76 %	54.24 %	59.50 %
Euclidean	Accuracy	**90.43 %**	78.02 %	87.57 %	88.14 %	69.53 %	72.91 %
	STD	**2.11 %**	2.28 %	2.74 %	0.49 %	1.81 %	6.46 %
	Precision	**88.34 %**	68.29 %	80.18 %	85.61 %	69.04 %	64.87 %
	Recall	**77.73 %**	67.34 %	73.71 %	73.76 %	71.08 %	66.40 %
	F-measure	**82.69 %**	67.81 %	76.81 %	79.24 %	70.04 %	65.63 %

TABLE 5.9: Accuracy and its std, precision, recall and f-measure for each classifier in the multidimensional CDTW (case 2) - Yogev's sub-dataset.

		Supervised				Unsupervised	
	Perf.	**k-NN**	**CART**	**RF**	**SVM**	**k-Means**	**GMM**
Sq. Euclidean	Accuracy	**87.11 %**	74.92 %	82.68 %	83.98 %	61.57 %	63.64 %
	STD	**2.61 %**	3.05 %	2.12 %	1.64 %	1.31 %	2.89 %
	Precision	**77.17 %**	54.49 %	62.83 %	62.55 %	68.25 %	54.79 %
	Recall	**65.75 %**	53.66 %	56.91 %	58.45 %	72.22 %	39.41 %
	F-measure	**71.00 %**	54.07 %	59.72 %	60.43 %	70.18 %	45.85 %
Euclidean	Accuracy	**91.93 %**	76.93 %	86.07 %	86.61 %	63.39 %	66.61 %
	STD	**1.61 %**	3.44 %	2.81 %	1.22 %	7.84 %	9.69 %
	Precision	**84.13 %**	59.33 %	76.47 %	67.34 %	64.88 %	35.37 %
	Recall	**75.16 %**	57.00 %	67.05 %	66.65 %	73.01 %	33.82 %
	F-measure	**79.30 %**	58.14 %	71.45 %	66.99 %	68.26 %	34.58 %

TABLE 5.10: Accuracy and its std, precision, recall and f-measure for each classifier in the multidimensional CDTW (case 2) - Hausdorff's sub-dataset.

Table 5.11 represents the global confusion matrices obtained according to the second case. These results show that the use of multidimensional CDTW-based features increases the classification accuracy rate that can reach up to 16 % with respect to the unidimensional CDTW-based features. The high rate of misclassified subjects belonging to class 3 (H & Y=3), is due to the fact that the number of subjects in class 3 is smaller than the one in class 2 (H & Y= 2 and 2.5) (see table 3.3, chapter 3). Finally, k-NN shows better performances than SVM in almost all matrices regardless of the distance type.

TABLE 5.11: Global confusion matrix obtained using k-NN and SVM classifiers obtained in the case 2.

			Obtained Classes											
			k-NN (Multi)			k-NN (Uni)			SVM(Multi)			SVM(Uni)		
			1	**2**	**3**	**1**	**2**	**3**	**1**	**2**	**3**	**1**	**2**	**3**
Yogev et al.	Sq. Euc.	**1**	**97.50 %**	2.50 %	0 %	91.56 %	8.12 %	0.32 %	**100 %**	0 %	0 %	87.19 %	12.81 %	0 %
		2	0.93 %	**96.74 %**	2.33 %	10.70 %	86.74 %	2.56 %	6.28 %	91.39 %	2.33 %	2.41 %	**95.66 %**	1.93 %
		3	18.88 %	60.91 %	**20.21 %**	15.45%	71.83 %	12.72 %	18.18 %	62.73 %	**19.09 %**	0 %	90.91 %	9.09 %
	Euc.	**1**	**99.38 %**	0.62 %	0 %	94.69 %	3.44 %	1.87 %	**96.56 %**	3.44 %	0 %	91.25 %	8.75 %	0 %
		2	0.23 %	**97.44 %**	2.33 %	2.33 %	96.97 %	0.70 %	0.23 %	**97.44 %**	2.33 %	0 %	92.33 %	7.67 %
		3	0 %	63.64 %	**36.36 %**	0 %	91.82 %	8.18 %	0 %	72.73 %	**27.27 %**	0 %	87.27 %	12.73 %
Hausdorff et al.	Sq. Euc.	**1**	80.40 %	19.60 %	0 %	**85.20 %**	14.80 %	0 %	**76.80 %**	22 %	1.2 %	61.38 %	38.62 %	0 %
		2	1.05 %	**96.86 %**	2.09 %	6.63 %	93.26 %	0.11 %	2.92 %	**95.56 %**	1.52 %	0 %	92.09 %	7.91 %
		3	10 %	70 %	**20 %**	0 %	**85 %**	15 %	3 %	94 %	**3 %**	0 %	97 %	**3 %**
	Euc.	**1**	**96.80 %**	3.20 %	0 %	88.00 %	11.20 %	0.80 %	**96.40 %**	3.20 %	0.40 %	94.40 %	5.60 %	0%
		2	0 %	**97.67 %**	2.33 %	0.23 %	97.44 %	2.33 %	0.58 %	**92.56 %**	6.86 %	2.44 %	86.98 %	10.58 %
		3	0 %	69 %	**31 %**	6 %	71 %	23 %	2 %	87 %	11 %	0 %	61 %	**39 %**

Tables 5.12, 5.13 and 5.14 show the classifiers performances (accuracy and its standard deviation, precision, recall and f-measure) in the third case in Yogev's, Hausdorff's and Frenkel-Toledo's sub-datasets, respectively (section 5.3). Results in tables 5.12 and 5.13 show that k-NN outperforms both supervised and unsupervised classifiers with an accuracy rate ranging between 70.58 % and 78.31 % regardless of the type of distance. A similar observation can be drawn when considering the other classification metrics. Results in table 5.14 shows that SVM outperforms both supervised and unsupervised classifiers by achieving the highest performances rate.

			Supervised			**Unsupervised**	
	Perf.	**k-NN**	**CART**	**RF**	**SVM**	**k-Means**	**GMM**
Sq. Euclidean	Accuracy	**75.46 %**	60.68 %	66.80 %	72.56 %	59.65 %	58.60 %
	STD	**1.99 %**	4.40 %	3.64 %	1.91 %	3.88 %	9.48 %
	Precision	**70.45 %**	51.16 %	55.55 %	61.38 %	58.78 %	50.43 %
	Recall	**60.17 %**	51.39 %	53.23 %	57.90 %	49.18 %	45.92 %
	F-measure	**64.91 %**	51.28 %	54.37 %	59.59 %	53.55 %	48.07 %
Euclidean	Accuracy	**78.31 %**	62.02 %	69.04 %	73.49 %	61.28 %	65.23 %
	STD	**3.49 %**	4.53 %	4.79 %	1.63 %	1.74 %	1.68 %
	Precision	**77.39 %**	48.43 %	56.90 %	71.52 %	56.97 %	58.11 %
	Recall	**64.60 %**	48.83 %	55.26 %	57.83 %	57.23 %	56.74 %
	F-measure	**70.42 %**	48.63 %	56.07 %	63.95 %	57.10 %	57.42 %

TABLE 5.12: Accuracy and its std, precision, recall and f-measure for each classifier in the multidimensional CDTW (case 3) - Yogev's sub-dataset.

		Supervised				Unsupervised	
	Perf.	**k-NN**	**CART**	**RF**	SVM	**k-Means**	**GMM**
Sq. Euclidean	Accuracy	**70.58 %**	62.89 %	66.78 %	68.84 %	54.71 %	52.64 %
	STD	**3.68 %**	5.05 %	3.55 %	1.30 %	1.02 %	1.62 %
	Precision	**67.68 %**	52.47 %	58.37 %	62.11 %	51.09 %	50.32 %
	Recall	**63.65 %**	51.91 %	54.77 %	59.17 %	47.07 %	47.40 %
	F-measure	**65.60 %**	52.18 %	56.51 %	60.60 %	49.00 %	48.82 %
Euclidean	Accuracy	**74.65 %**	64.55 %	69.17 %	73.22 %	56.94 %	58.10 %
	STD	**2.84 %**	6.43 %	4.71 %	1.92 %	0.26 %	1.83 %
	Precision	**73.83 %**	58.98 %	58.41 %	59.14 %	56.91 %	50.41 %
	Recall	**68.03 %**	58.41 %	58.31 %	61.40 %	56.27 %	51.48 %
	F-measure	**70.84 %**	58.69 %	58.36 %	60.25 %	56.59 %	50.94 %

TABLE 5.13: Accuracy and its std, precision, recall and f-measure for each classifier in the multidimensional CDTW (case 3) - Hausdorff's sub-dataset.

		Supervised				Unsupervised	
	Perf.	**k-NN**	**CART**	**RF**	**SVM**	**k-Means**	**GMM**
Sq. Euclidean	Accuracy	**84.51 %**	75.44 %	80.59 %	84.37 %	65.00 %	64.69 %
	STD	**2.78 %**	4.67 %	2.93 %	1.28 %	7.91 %	9.24 %
	Precision	**73.04 %**	60.46 %	62.24 %	69.65 %	56.34 %	50.62 %
	Recall	63.82 %	60.22 %	62.76 %	**69.52 %**	54.31 %	49.25 %
	F-measure	68.12 %	60.34 %	62.50 %	**69.59 %**	55.30 %	49.93 %
Euclidean	Accuracy	86.88 %	80.62 %	85.31 %	**88.28 %**	70.16 %	72.34 %
	STD	2.09 %	2.87 %	3.35 %	**1.69 %**	0.49 %	3.46 %
	Precision	80.12 %	72.69 %	83.68 %	**81.44 %**	59.56 %	64.32 %
	Recall	70.36 %	73.91 %	70.99 %	**77.50 %**	59.41 %	64.29 %
	F-measure	74.92 %	73.30 %	76.81 %	**79.42 %**	59.48 %	64.30 %

TABLE 5.14: Accuracy and its std, precision, recall and f-measure for each classifier in the multidimensional CDTW (case 3) - Frenkel-Toledo's sub-dataset.

Table 5.15 represents the global confusion matrices obtained according to the third case in the three sub-datasets. One can observe that the use of multidimensional CDTW-based features increases the classification accuracy rate that can reach up to 13 % with respect to the unidimensional CDTW-based features. The same observation can be made when considering the confusion matrices obtained in Frenkel-Toledo's sub-dataset. The highest rate of misclassified subjects in the case of Hausdorff and Yogev belongs to the class 3 (H & Y = 2.5) classified in class 2 (H & Y = 2), can be explained by the fact that it is difficult to discriminate subjects belonging to these two classes. These observation has been also made in [217]. Moreover, subjects in class 3 (H & Y = 3), are better classified using Hausdorff's sub-dataset compared to Yogev's sub-dataset. This can be explained by the fact, that the number of subjects classified in the class 3 (H & Y = 2.5) in the case of Hausdorff's sub-dataset (13 subjects) is greater than the case of Yogev's (8 subjects). k-NN shows better performances than SVM, in almost all matrices regardless of the type of distance. The high ratio of misclassified subjects belonging to the class 4 (H & Y = 3), can be explained by the fact that the number of subjects belonging to this class is relatively low compared to the number of subjects belonging to the remaining classes (H & Y= 0, H & Y=2 and H & Y=2.5) (see table 3.3, chapter 3).

TABLE 5.15: Global confusion matrix obtained using k-NN and SVM classifiers obtained in the case 3.

			Obtained Classes																	
			k-NN (Multi)				k-NN (Uni)				SVM(Multi)				SVM(Uni)					
			1	2	3	4	1	2	3	4	1	2	3	4	1	2	3	4		
Yogev et al.	Sq. Euc. True Classes	1	**100 %**	0 %	0 %	0 %	95.63 %	4.06 %	0.31 %	0 %	**95.31 %**	0 %	2.50 %	2.19 %	82.19 %	13.75 %	1.25 %	2.81 %		
		2	0.34 %	**91.73 %**	7.59 %	0.34 %	12.41 %	71.03 %	16.21 %	0.35 %	0 %	89.66 %	10 %	0.34 %	3.45 %	**91.03 %**	4.14 %	1.38 %		
		3	7.14 %	58.58 %	**27.14 %**	7.14 %	10.71 %	70.71 %	7.86 %	10.72 %	0.72 %	61.43 %	**25.71 %**	12.14 %	0 %	97.86 %	2.14 %	0 %		
		4	18.18 %	53.64 %	6.36 %	**21.82 %**	0.91 %	67.27 %	22.73 %	9.09%	8.18 %	42.73 %	28.18 %	**20.91 %**	0 %	86.37 %	4.54 %	9.09 %		
	Euc. True Classes	1	**100 %**	0 %	0 %	0 %	96.25 %	1.88 %	0.62 %	1.25 %	**96.56 %**	3.44 %	0 %	0 %	93.44 %	6.25 %	0.31 %	0 %		
		2	0 %	**93.45 %**	6.55 %	0 %	3.45 %	78.97 %	8.62 %	8.96 %	0 %	**94.83 %**	4.14 %	1.03 %	0.69 %	77.59 %	13.79 %	7.93 %		
		3	5 %	59.29 %	**28.57 %**	7.14 %	0 %	84.29 %	0.71 %	15 %	0 %	79.29 %	**13.57 %**	7.14 %	0 %	75.71 %	11.43 %	12.86 %		
		4	0 %	63.64 %	0 %	**36.36 %**	0 %	72.73 %	16.36 %	10.91 %	0 %	72.73 %	0.91 %	**26.36 %**	0 %	60.91 %	13.64 %	25.45 %		
Hausdorff et al.	Sq. Euc. True Classes	1	80 %	4.80 %	15.2 %	0 %	**90.80 %**	8.40 %	0.80 %	0 %	**88 %**	4 %	8 %	0 %	82.80 %	7.60 %	9.20 %	0.40 %		
		2	1.43 %	73.43 %	22.57 %	2.57 %	4%	**77.71 %**	18 %	0.29 %	0 %	**70.29 %**	26 %	3.71 %	3.44 %	69.69 %	25.62 %	1.25 %		
		3	2.16 %	21.17 %	**72.16 %**	4.51 %	3.14 %	36.27 %	60.59 %	0 %	0 %	26.66 %	**70.40 %**	2.94 %	1.96 %	25.88 %	70.39 %	1.77 %		
		4	10 %	20 %	41 %	**29 %**	0 %	48 %	52 %	0%	0 %	70 %	22 %	**8 %**	0 %	35 %	61 %	4 %		
	Euc. True Classes	1	**97.60 %**	2.40 %	0 %	0 %	93.20 %	4 %	2.8 %	0 %	96 %	4 %	0 %	0 %	**98 %**	0 %	1.2 %	0.8 %		
		2	0 %	64.29 %	30 %	5.71 %	0 %	**73.71 %**	26 %	0.29 %	0.28 %	**70.57 %**	20.86 %	8.29 %	0 %	69.43 %	28.29 %	2.28 %		
		3	0.4 %	20.39 %	**79.21 %**	0 %	3.92 %	35.88 %	58.24 %	1.96 %	0 %	20.20 %	**78.04 %**	1.76 %	2.55 %	30 %	62.35 %	5.10 %		
		4	0 %	24 %	45 %	**31 %**	0 %	20 %	50 %	30 %	10 %	58 %	31 %	1 %	0 %	12 %	66 %	**22 %**		
Frenkel-Toledo et al.			k-NN (Multi)				k-NN (Uni)				SVM(Multi)				SVM(Uni)					
			1	2	3		1	2	3		1	2	3		1	2	3			
	Sq. Euc. True Classes	1	**98.97 %**	1.03 %	0 %		94.83 %	5.17 %	0 %		**100 %**	0 %	0 %		78.62 %	21.38 %	0 %			
		2	9.64 %	**89.65 %**	0.71 %		19.64 %	78.57 %	1.79 %		0 %	82.86 %	17.14 %		7.86 %	**92.14 %**	0 %			
		3	8.57 %	88.57 %	**2.86 %**		25.71 %	74.29 %	0 %		0 %	74.29 %	**25.71 %**		4.29 %	95.71 %	0 %			
	Euc. True Classes	1	**100 %**	0 %	0 %		94.14 %	5.86 %	0 %		**100 %**	0 %	0 %		99.66 %	0.34 %	0 %			
		2	7.5 %	89.64 %	2.86 %		6.79 %	**91.43 %**	1.78 %		6.78 %	**86.79 %**	6.43 %		1.79 %	84.64 %	13.57 %			
		3	10 %	68.57 %	**21.43 %**		15.71 %	84.29 %	0 %		0 %	54.29 %	**45.71 %**		1.43 %	70 %	28.57 %			

Figures 5.3, 5.4, and 5.5 show the performances obtained in the case 1, in terms of accuracy rates of the different classifiers using multidimensional CDTW-based feature, unidimensional CDTW-based features and standard features. We can observe that the supervised classifiers achieved the best classification rates with an improvement in the case of multidimensional CDTW-based features ranging from 7 % to 19 % with respect to the case of standard features. On the other hand, the improvement rates in the case of the unsupervised classifiers ranges from 12 % to 16 % regardless of the distance type.

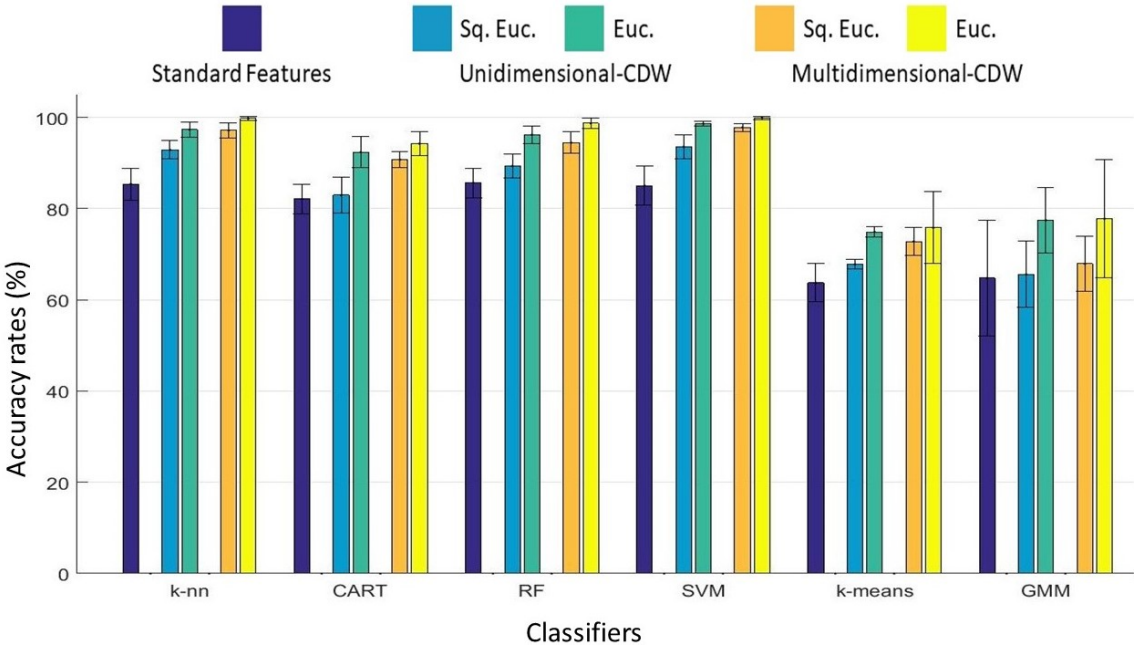

FIGURE 5.3: Accuracy rates and their STD obtained in the unidimensional CDTW-based features, multidimensional CDTW-based features and standard features, according to the case 1 - Yogev's sub-dataset

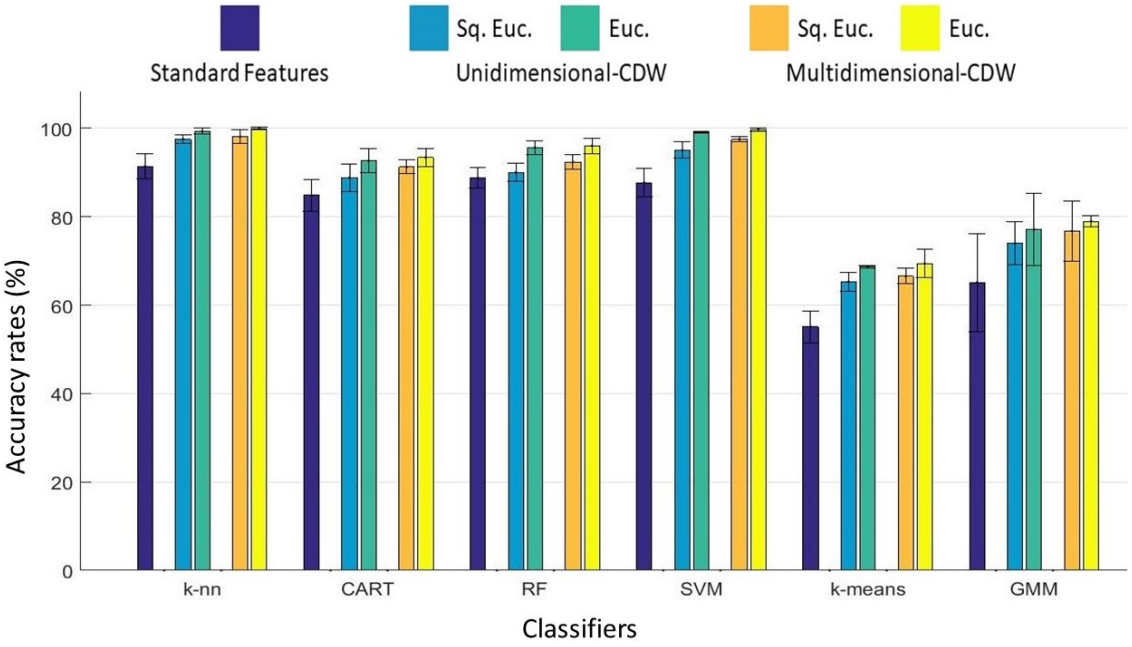

FIGURE 5.4: Accuracy rates and their STD obtained in the unidimensional CDTW-based features, multidimensional CDTW-based features and standard features, according to the case 1 - Hausdorff's sub-dataset

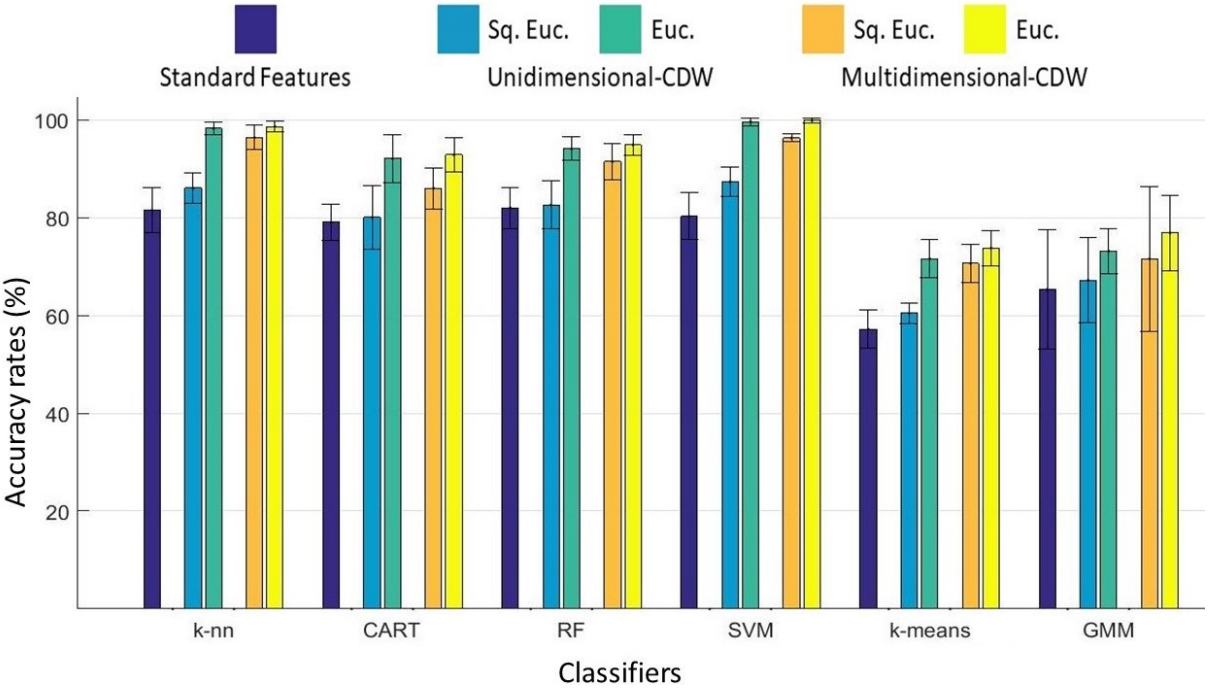

FIGURE 5.5: Accuracy rates and their STD obtained in the unidimensional CDTW-based features, multidimensional CDTW-based features and standard features, according to the case 1 - Frenkel-Toledo's sub-dataset

Figures 5.6 and 5.7 show the performances obtained in the case 2 in terms of accuracy rate. One can note that among the supervised classifiers, k-NN achieves the best improvement ranging from 11 % to 15 % in the case of multidimensional CDTW based-features with respect to the case of standard features. On the other hand, among the unsupervised classifiers, GMM achieves the highest improvement ranging from 15 % to 19 %. In addition, the use of multidimensional CDTW-based features improves the classification rate ranging from 3 % to 10 % with respect to the case of unidimensional-based features.

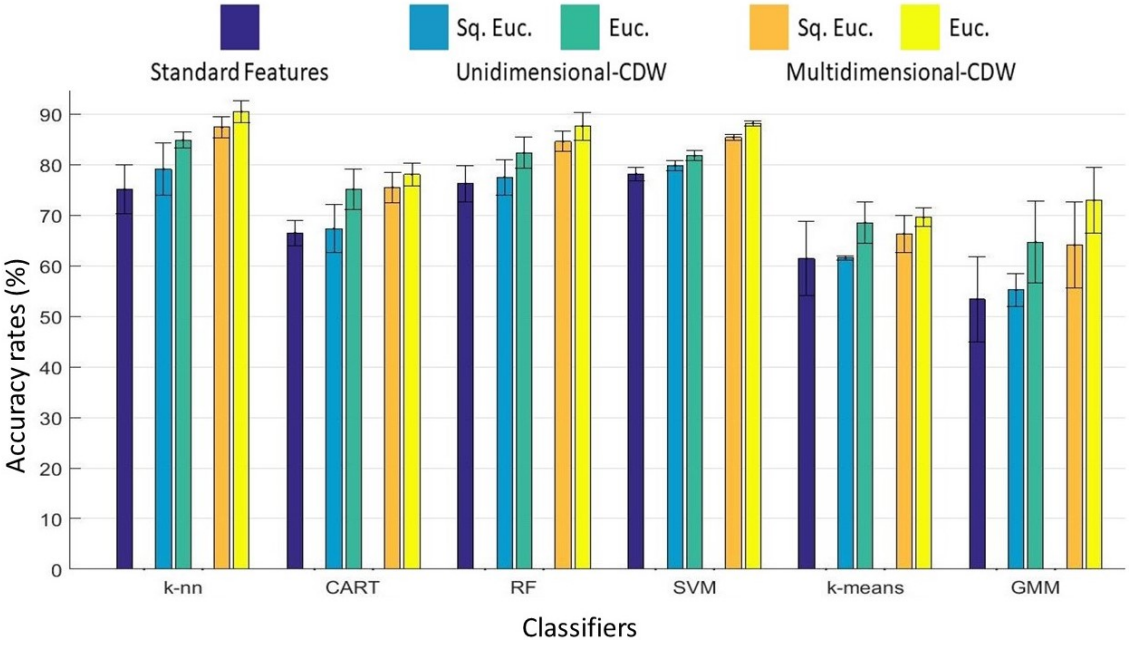

FIGURE 5.6: Accuracy rates and their STD obtained in the unidimensional CDTW-based features, multidimensional CDTW-based features and standard features, according to the case 2 - Yogev's sub-dataset

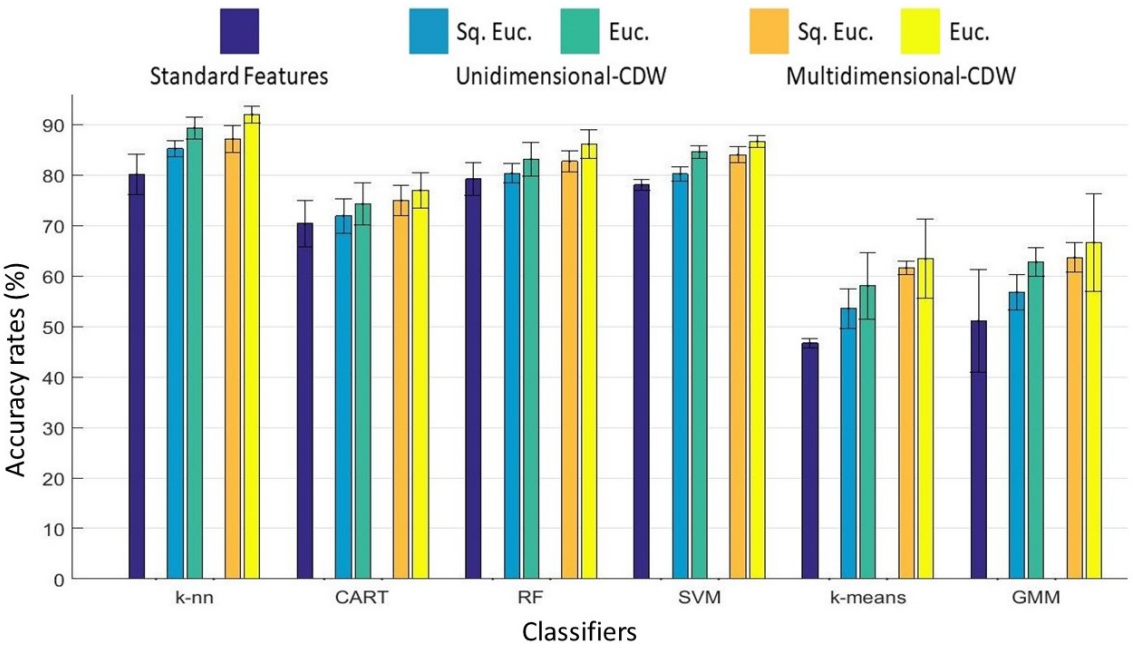

FIGURE 5.7: Accuracy rates and their STD obtained in the unidimensional CDTW-based features, multidimensional CDTW-based features and standard features, according to the case 2 - Hausdorff's sub-dataset

In the case 3, we can observe from Fig. 5.8, 5.9, and 5.10 that in terms of accuracy rate, k-NN achieves the best improvement among the supervised classifiers. This improvement ranges from 11 % to 15 % in the case of multidimensional CDTW based-features compared to the case of standard features. On the other hand, among the unsupervised classifiers, GMM achieves the highest improvement ranging from 15 % to 19 %. In addition, with respect to the case of unidimensional-based features, the use of multidimensional CDTW-based features allows an improvement of classification rate that can reach up to 15 % using the supervised classifiers and 11 % using the unsupervised ones.

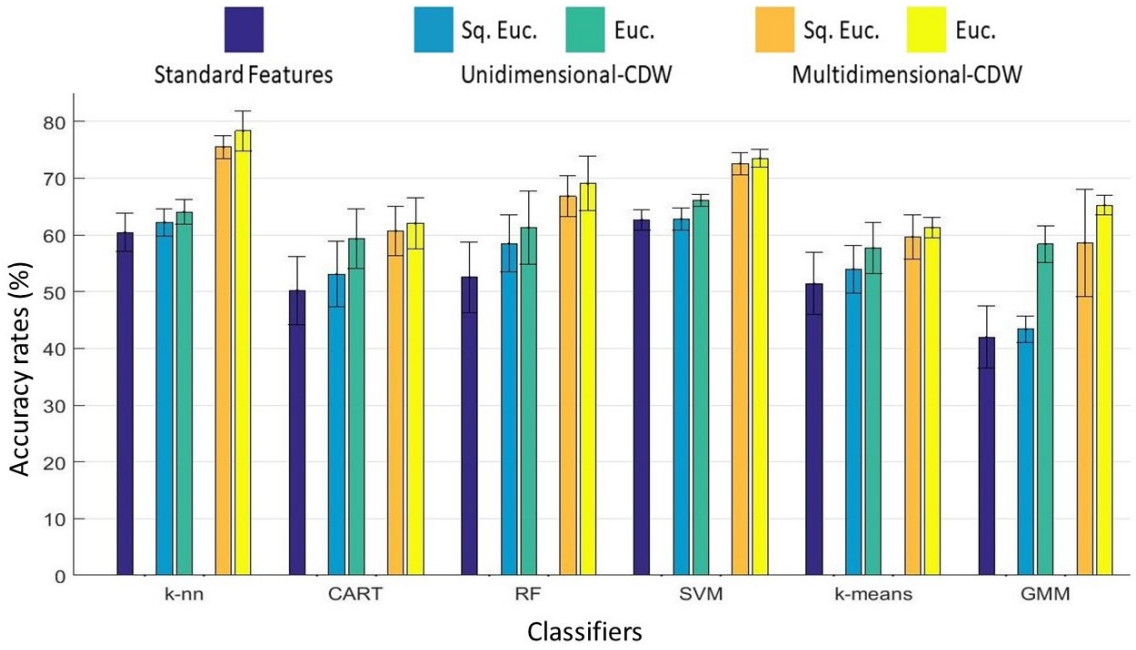

FIGURE 5.8: Accuracy rates and their STD obtained in the unidimensional CDTW-based features, multidimensional CDTW-based features and standard features, according to the case 3 - Yogev's sub-dataset

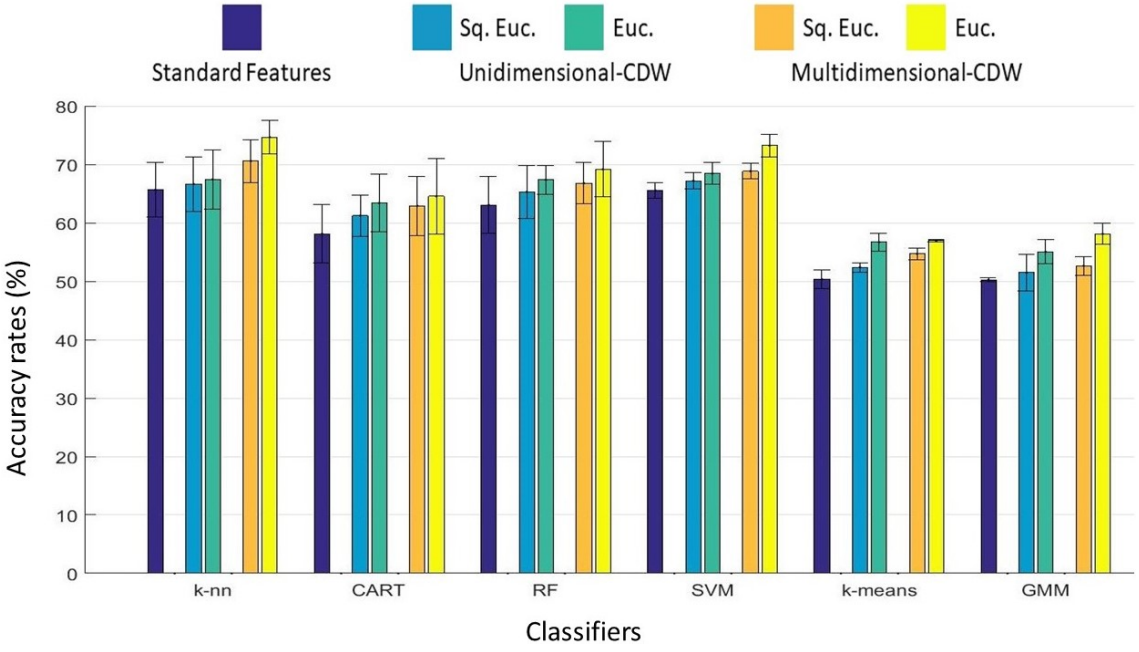

FIGURE 5.9: Accuracy rates and their STD obtained in the unidimensional CDTW-based features, multidimensional CDTW-based features and standard features, according to the case 3 - Hausdorff's sub-dataset

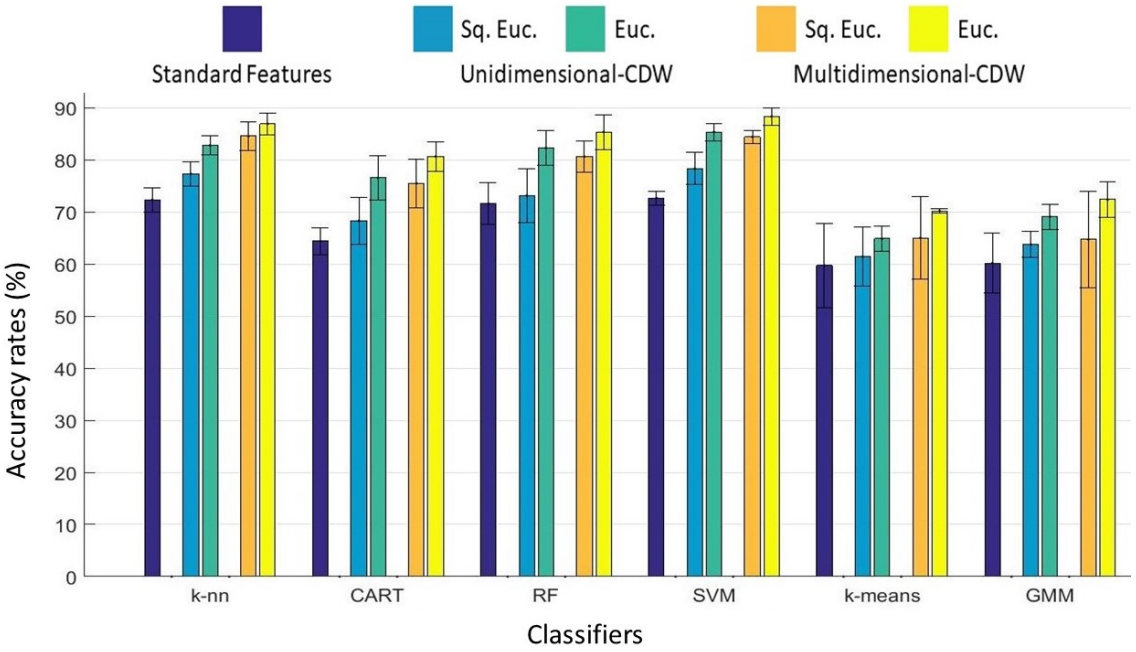

FIGURE 5.10: Accuracy rates and their STD obtained in the unidimensional CDTW-based features, multidimensional CDTW-based features and standard features, according to the case 3 - Frenkel-Toledo's sub-dataset

5.4 Conclusion

In this chapter, we proposed an extension of the CDTW for feature computation by analyzing the similarity between time-series during the stance phases in the multidimensional domain. Different cases were considered with respect to the number of classes of healthy and PD subjects in the three used sub-datasets according to H & Y scale. Several supervised and unsupervised classification methods have been implemented and evaluated. The obtained results showed clearly significant improvements when using multidimensional CDTW based features with respect to the case when using unidimensional ones. As it can be noticed from the obtained results, a more accurate measure of similarity between stance phases times-series, allows a better discrimination between healthy subjects and PD subjects, as well as among the subjects having different disease PD severities.

Chapter 6

Conclusion and Perspectives

6.1 Conclusion

This thesis deals with the diagnosis of PD subjects from gait cycle analysis. Most of the existing studies in the literature are mainly based on the use of time-domain and frequency-domain features extracted from walking patterns to diagnose Parkinson's disease. However, such features could not be easily linked to a clinical diagnosis. The main objective of this thesis was to develop a clinical tool to aid the diagnosis of Parkinson's disease using clinical-based features extracted from vertical Ground Reaction Forces (vGRFs). This tool is mainly devoted to being used in a clinical environment as a support tool to physiotherapists in their PD diagnosis process. To achieve an accurate classification, on the one hand, between healthy and PD subjects, and on the other hand, between subjects with different levels of disease severity, clinical-based features are exploited and more specifically the repeatability of gait cycle in PD subjects by measuring the similarity of stance phases. For evaluation purposes, three gait datasets were used from PhysioNet which is a free web access to large collections of recorded physiologic signals. These datasets contain gait data of 93 patients suffering from Parkinson's disease and 72 healthy subjects.

The contributions of this thesis can be summarized as follows:

We firstly presented the general background of the PD recognition process including data pre-processing (features computation, feature extraction and feature selection) as well as the main supervised and unsupervised classification approaches that were used in this study. We implemented and compared several classification methods to recognize PD based on vGRFs collected from gait cycles: five supervised methods (k-NN, CART, RF, NB and SVM) and two unsupervised methods (k-Means and GMM). In this thesis, a total of 19 standard spatio-temporal features were considered from which five features were selected and used as classifier inputs. The classifiers were compared in terms of classification rate (accuracy) and its standard deviation (STD), precision, recall and F-measure. The supervised classification approaches yielded better results, as it can be expected since they use labelled data in the learning phase. k-NN, RF and SVM provide satisfactory results in terms of accuracy and F-measure.

We secondly proposed a new approach to support Parkinson's Disease (PD) diagnosis. This approach exploits the fact that usually the walking of healthy subject

is characterized by the repetition of gait cycles, while the one of PD subjects show significant variations from one gait cycle to another. For this purpose, a similarity measure between these cycles, carried out using the Continuous Dynamic Time Warping (CDTW) technique, is proposed. By using the mean and the STD of each CDTW distance vector, four features are considered: Mean of the CDTW distance of the Left foot, Mean of the CDTW distance of the Right foot, STD of the CDTW distance of the Left foot, STD of the CDTW distance of the Right foot. To study the effects of applying the CDTW based features with respect to the use of standard features, we have applied a feature selection process of the total 23 features including, on one hand, the 4 CDTW based features, and on the other hand, the 19 standard (spatio-temporal) features. The obtained results showed that the use of CDTW-based features improves significantly the classification accuracy rates for discriminating healthy subjects from PD subjects.

Finally, we proposed an extension of the CDTW for feature computation by analysing the similarity between time-series during the stance phases in the multidimensional domain. Different cases were considered with respect to the number of classes of healthy and PD subjects in the three used sub-datasets according to H & Y scale. Several supervised and unsupervised classification methods have been implemented and evaluated. The obtained results showed clearly significant improvements when using multidimensional CDTW based features with respect to the case when using unidimensional ones. As it can be noticed from the obtained results, a more accurate measure of similarity between stance phases times-series, allows a better discrimination between healthy subjects and PD subjects, as well as among the subjects having different PD disease severities.

6.2 Perspectives

The perspectives resulting from this thesis can be summarized as follows:

In this thesis, we have considered exclusively the features extracted from the stance phase of the gait cycle. One possible perspective to have a more finer analysis of the gait cycle similarities, would be to explore more sub-phases of both stance and swing phases such as Initial contact, Loading response, Mid-stance, Terminal stance, Pre-swing, Initial swing, Mid-swing and Terminal swing.

From an algorithmic point of view, different perspectives could be addressed to improve the PD diagnosis accuracy:

- The fusion of different classifiers could be further implemented to exploit the complementarity that may exists among the classifiers.
- In this thesis, the PD subjects classification is based on the similarity measurements of the stance phase time-series. A potential perspective would be to formulate the classification problem as a curve clustering one. In this case, vGRF data are considered as functional data characterizing a pathology pattern of each subject.
- Other alternatives to the linear interpolation model used in the CDTW formulation can be explored for better assessment of the time-series similarity and better data modelling. The computation of the intermediate matching points resulting from the orthogonal projection is a difficult task and is directly related to the choice of the interpolation model.
- Other machine learning models can also be considered such as deep learning models, however, the application of such models requires large amounts of data or the use of methods such as transfer learning or data augmentation.

Finally, an interesting perspective would be to build in collaboration with the Mondor University Hospital a large-scale dataset including walking data from patients suffering from different neurodegenerative diseases such as Parkinsons disease, Huntington's disease (HD) and Amyotrophic lateral sclerosis (ALS). Such diseases are related to movement disorders and their diagnosis could be addressed using the proposed methodology.

Bibliography

[1] Davie C.A. review of Parkinson's disease. British medical bulletin, **2008**, Volume 86, No. 1, pp. 109-127 [CrossRef]

[2] Parkinson's disease Foundation, Available online:(http://parkinson.org/understanding-parkinsons).

[3] Ahlrichs C.; Lawo M. Parkinson's disease motor symptoms in machine learning: a review. Health Informatics-An International Journal (HIIJ), **2013**, Volume 2, No. 4.

[4] Das, R.A. Comparison of multiple classification methods for diagnosis of Parkinson disease. *Expert Syst. Appl.* **2010**, *37*, 1568–1572. [CrossRef]

[5] Hariharan, M.; Polat, K.; Sindhu, R. A new hybrid intelligent system for accurate detection of Parkinson's disease. *Comput. Methods Programs Biomed.* **2014**, *113*, 904–913. [CrossRef]

[6] Pan, S.; Iplikci, S.; Warwick, K.; Aziz, T.Z. Parkinsons Disease tremor classificationA comparison between Support Vector Machines and neural networks. *Expert Syst. Appl.* **2012**, *39*, 10764–10771. [CrossRef]

[7] Dorsey, E.R.; Constantinescu, R.; Thompson, J.P.; Biglan, K.M.; Holloway, R.G.; Kieburtz, K.; Marshall, F.J.; Ravina, B.M.; Schifitto, G.; Siderowf, A.; et al. Projected number of people with Parkinson disease in the most populous nations, 2005 through 2030. *Neurology* **2007**, *68*, 384–386. [CrossRef] [PubMed]

[8] Circulaire SG/DGOS/R4/DGS/MC3/DGCS/3A/CNSA no 2015-281 du 7 Septembre 2015 Relative la Mise en Oeuvre du Plan Maladies Neuro-DGNRatives 2014–2019. Available online: https://solidarites-sante.gouv.fr/fichiers/bo/2015/15-09/ste_20150009_0000_0056.pdf (accessed on 15 October 2015).

[9] FRANCE PARKINSON et CGE DISTRIBUTION: Un Accord de MCNat Pour Faire Connaitre la Maladie dans le Milieu de L'entreprise. Available online: https://www.franceparkinson.fr/wp-content/uploads/2016/10/CP-FRANCE-PARKINSON-et-CGE-DISTRIBUTION.pdf (accessed on 10 January 2019).

[10] Epidemiology of Parkinson's disease, French national data (https://solidarites-sante.gouv.fr/IMG/pdf/2018_8-9.pdf)

[11] Parkinson et Souffrances de vie. Available online: https://neurologies.fr/parkinson-et-souffrances-de-vie/ (accessed on 25 April 2013).

[12] Beyene, T.J.; Hoek, H.;Zhang, Y.; Vos, T. Global, regional, and national age–sex specific all-cause and cause-specific mortality for 240 causes of death, 1990–2013. *Lancet* **2015**, *385*, 117–171.

[13] Vos, T.; Barber, R.M.; Bell, B.; Bertozzi-Villa, A.; Biryukov, S.; Bolliger, I.; Charlson, F.; Davis, A.; Degenhardt, L.; Dicker, D.; et al. Global, regional, and national incidence, prevalence, and years lived with disability for 301 acute and chronic diseases and injuries in 188 countries, 1990–2013: A systematic analysis for the Global Burden of Disease Study 2013. *Lancet* **2015**, *386*, 743–800. [CrossRef]

[14] Mosley, A.D. *The Encyclopedia of Parkinson's Disease*, 2nd ed.; Facts on File: New York, NY, USA, **2010**; p. 89.

[15] Jankovic, J. Parkinson's disease: clinical features and diagnosis, Journal of Neurology, Neurosurgery & Psychiatry **2008**, Volume 79, No. 4, pp. 368–376. [CrossRef]

[16] O'Sullivan, S.B.; Schmitz, T.J. Physical Rehabilitation: 5th ed. F.A. Davis Company, Philadelphia, **2007**, pp. 1098.

[17] Berardelli, A.; Rothwell, J.C.; Thompson, P.D.; Hallett, M. Pathophysiology of bradykinesia in Parkinson's disease. Brain, **2001**, Volume 124, No. 11, pp. 2131-2146. [CrossRef]

[18] Cooper, J.A.; Sagar, H.J.; Tidswell, P.; Jordan, N. Slowed central processing in simple and go/no-go reaction time tasks in Parkinson's disease. Brain, **1994**, Volume 117, No. 3, pp. 517-529.

[19] Giovannoni, G.; Van Schalkwyk, J.; Fritz, V.U.; Lees, A.J. Bradykinesia akinesia incoordination test (BRAIN TEST): an objective computerised assessment of upper limb motor function. Journal of Neurology, Neurosurgery & Psychiatry **1999**, Volume 67, No. 5, pp. 624-629. [CrossRef]

[20] Adkin, A.L.; Frank, J.S.; Jog, M.S. Fear of falling and postural control in Parkinson's disease. Movement Disorders, **2003**, Volume 18, No. 5, pp. 496-502.

[21] Samii, A.; Nutt, J.G.; Ransom B.R. Parkinson's disease, The Lancet, **2004**, Volume 363, No. 9423, pp. 17831793.

[22] Russell, J.A.; Ciucci, M.R.; Connor, N.P.; Schallert, T. Targeted exercise therapy for voice and swallow in persons with Parkinson's disease. Brain research, **2010**, Volume 1341, pp. 3-11. [CrossRef]

[23] Perumal, S.V. Gait and Tremor Monitoring System for Patients with Parkinson's Disease Using Wearable Sensors. University of South Florida, Tampa, FL, USA, **2016**. [CrossRef]

[24] Perumal, S.V.; Sankar, R. Gait and tremor assessment for patients with Parkinson's disease using wearable sensors. ICT Express, **2016**, Volume 2, No. 4, pp. 168–174. [CrossRef]

[25] Fah, S.; Elton, R.I.; Members of the UPDRS Development Committee. In *Recent Development in Parkinson's Disease*; Fahn, S., Marsden, C.D., Calne, D.B., Goldstein, M., Eds.; Macmillan Health Care Information: New York, NY, USA, 1987; Volume 2, pp. 153–164.

[26] Hoehn, M.M.; Yahr, M.D. Parkinsonism onset, progression, and mortality. *Neurology* **1967**, *17*, 427–427. [CrossRef]

[27] Schwab, R.S. Projection technique for evaluating surgery in Parkinson's disease. In *Third Symposium on Parkinson's Disease*; Gillingham, F.J., Donaldson, I.M.L., Eds.; Scientific Research Publishing: Wuhan, China, 1969; pp. 152–157.

[28] Mahoney, F.I.; Barthel, D.W. The Barthel Index. *Md State Med. J.* **1965**, *14*, 61–65.

[29] Folstein, M.F.; Folstein, S.E.; McHugh, P.R. Mini-mental state. A practical method for grading the cognitive state of patients for the clinician. *J. Psychiatr. Res.* **1975**, *12*, 189–198. [CrossRef]

[30] Schmand, B.; Lindeboom, J.; Van Harskamp, F. *Dutch Adult Reading Test*; Swets & Zeitlinger: Lisse, The Netherlands, **1992**.

[31] Lezak, M.D. *Neuropsychological Assessment*; Oxford University Press: Oxford, NY, USA, **2004**.

[32] Peker, M.; Sen, B.; Delen, D. Computer-aided diagnosis of Parkinson's disease using complex-valued neural networks and mRMR feature selection algorithm. *J. Healthc. Eng.* **2015**, *6*, 281–302. [CrossRef]

[33] Kenneth, R.; Gorunescu, F.; Salem, A.M. Feature selection in Parkinson's disease: A rough sets approach. In Proceedings of the International Multiconference on Computer Science and Information Technology (IMCSIT'09), Mrgowo, Poland, 12–14 October 2009; pp. 425–428.

[34] Yadav, G.; Kumar, Y.; Sahoo, G. Predication of Parkinson's disease using data mining methods: A comparative analysis of tree, statistical and support vector machine classifiers. In Proceedings of the National Conference on Computing and Communication Systems (NCCCS), Durgapur, India, 21–22 November 2012; pp. 1–8.

[35] Safi, K.; Diab, A.; Albertsen, I.M.; Hutin, E.; Mohammed, S.; Khalil, M.; Amirat, Y.; Gracies, J.M. Non-linear analysis of human stability during static posture. In Proceedings of the International Conference on Advances in Biomedical Engineering (ICABME), Beirut, Lebanon, 16–18 September 2015; pp. 285–288.

[36] Prieto, T.E.; Myklebust, J.B.; Myklebust, B.M. Characterization and modeling of postural steadiness in the elderly: A review. *IEEE Trans. Rehabil. Eng.* **1993**, *1*, 26–34. [CrossRef]

[37] Yogev, G.; Plotnik, M.; Peretz, C.; Giladi, N.; Hausdorff, J.M. Gait asymmetry in patients with Parkinson's disease and elderly fallers: When does the bilateral coordination of gait require attention? *Exp. Brain Res.* **2007**, *177*, 336–346. [CrossRef]

[38] Hausdorff, J.M.; Lowenthal, J.; Herman, T.; Gruendlinger, L.; Peretz, C.; Giladi, N. Rhythmic auditory stimulation modulates gait variability in Parkinson's disease. *Eur. J. Neurosci.* **2007**, *26*, 2369–2375. [CrossRef] [PubMed]

[39] FrenkelToledo, S.; Giladi, N.; Peretz, C.; Herman, T.; Gruendlinger, L.; Hausdorff, J.M. Effect of gait speed on gait rhythmicity in Parkinson's disease: Variability of stride time and swing time respond differently. *J. Neuroeng. Rehabil.* **2005**, *2*, 23. [CrossRef] [PubMed]

[40] Peran, P.; Cherubini, A.; Assogna, F.; Piras, F.; Quattrocchi, C.; Peppe, A. et al. Magnetic resonance imaging markers of Parkinson's disease nigrostriatal signature. Brain, **2010**, Volume 133, No. 11, pp. 3423-3433. [CrossRef]

[41] Solomon, N. P.; Robin, D. A.; Luschei, E. S. Strength, endurance, and stability of the tongue and hand in Parkinson disease. Journal of Speech, Language, and Hearing Research, **2000**, Volume 43, No. 1, pp. 256-267. [CrossRef]

[42] Schrag, A.; Barone, P.; Brown, R.G.; Leentjens, A.F.; McDonald, W. M.; Starkstein, S.; et al. Depression rating scales in Parkinson's disease: critique and recommendations. Movement disorders, **2007**, Volume 22, No. 8, pp. 1077-1092. [CrossRef]

[43] Ebersbach, G.; Baas, H.; Csoti, I.; Mngersdorf, M.; Deuschl, G. Scales in Parkinson's disease. Journal of neurology, **2006**, Volume 253, No. 4, pp. iv32-iv35. [CrossRef]

[44] Ramaker, C.; Marinus, J.; Stiggelbout, A.M.; Van Hilten, B.J. Systematic evaluation of rating scales for impairment and disability in Parkinson's disease. Movement disorders: official journal of the Movement Disorder Society, **2002**, Volume 17, No. 5, pp. 867-876. [CrossRef]

[45] Goetz, C.G.; Fahn, S.; MartinezMartin, P.; Poewe, W.; Sampaio, C.; Stebbins, G.T.; et al. Movement Disorder Societysponsored revision of the Unified Parkinson's Disease Rating Scale (MDSUPDRS): process, format, and clinimetric testing plan. Movement Disorders, **2007**, Volume 22, No. 1, pp. 41-47. [CrossRef]

[46] Jankovic, J.; Kapadia, A. S. Functional decline in Parkinson disease. Archives of neurology, **2001**, Volume 58, No. 10, pp. 1611-1615. [CrossRef]

[47] Lang, A. E. The progression of Parkinson disease A hypothesis. Neurology, **2007**, Volume 68, No. 12, pp. 948-952. [PubMed]

[48] Post, B.; Merkus, M.P.; De Haan, R.J.; Speelman, J.D.; CARPA Study Group. Prognostic factors for the progression of Parkinson's disease: a systematic review. Movement Disorders, **2007**, Volume 22, No. 13, pp. 1839-1851. [CrossRef]

[49] Goetz, C.G.; Poewe, W.; Rascol, O.; Sampaio, C.; Stebbins, G.T.; Counsell, C.; Giladi, N.; Holloway, R.;Moore C.G.;Wenning G.K.; Yahr, M.D.; Seidl L. Movement Disorder Society Task Force report on the Hoehn and Yahr staging scale: status and recommendations the Movement Disorder Society Task Force on rating scales for Parkinson's disease. Movement disorders, **2004**, Volume 19; No. 9, pp. 1020-1028. [CrossRef]

[50] Safi, K., Hutin, E., Mohammed, S., Albertsen, I.M., Delechelle, E., Amirat, Y., Khalil, M. and Gracies, J.M. Human static postures analysis using empirical mode decomposition. In Engineering in Medicine and Biology Society (EMBC), 2016 IEEE 38th Annual International Conference of the, **2016**, IEEE, pp. 3765-3768. [PubMed]

[51] Tao, W.; Liu, T.; Zheng, R.; Feng, H. Gait analysis using wearable sensors. *Sensors* **2012**, *12*, 2255–2283. [CrossRef] [PubMed]

[52] Zong, C. Système embarqué de capture et analyse du mouvement humain durant la marche. Diss. Universit Pierre et Marie Curie-Paris VI, **2012**. [CrossRef]

[53] Attal, F.; Amirat, Y.; Chibani, A.; Mohammed, S. Automatic Recognition of Gait phases Using a Multiple Regression Hidden Markov Model. IEEE/ASME Transactions on Mechatronics, **2018**.

[54] Gavrila, D.M.; Davis, L.S. 3-D Model-based tracking of humans in action: A multi-view approach. In Proceedings of the IEEE Computer Vision and Pattern Recognition, San Francisco, CA, USA, **1996**, pp. 7380. [CrossRef]

[55] Karaulova, I.A.; Hall, P M.; Marshall, A.D. Tracking people in three dimensions using a hierarchical model of dynamics. Image and Vision Computing, **2002**, Volume 20, No. 9-10, pp. 691-700. [CrossRef]

[56] Furnée, H.A.N.S. Real-time motion capture systems, Wiley: New York, NY, USA, **1997**, pp. 85-108.

[57] Cappozzo, A.; Della Croce, U.; Leardini, A.; Chiari, L. Human movement analysis using stereophotogrammetry: Part 1: theoretical background. Gait & posture, **2005**, Volume 21, No. 2, pp. 186-196. [PubMed]

[58] Chiari, L.; Della Croce, U.; Leardini, A.; Cappozzo, A. Human movement analysis using stereophotogrammetry: Part 2: Instrumental errors. Gait & posture, **2005**, Volume 21, No. 2, pp. 197-211. [PubMed]

[59] Kim, C.M.; Eng, J.J. Magnitude and pattern of 3D kinematic and kinetic gait profiles in persons with stroke: relationship to walking speed. Gait & posture, **2004**, Volume 20, No. 2, pp. 140-146. [PubMed]

[60] Casadio, M.; Morasso, P.G.; Sanguineti, V. Direct measurement of ankle stiffness during quiet standing: implications for control modelling and clinical application. Gait & posture, **2005**, Volume 21, No. 4, pp. 410-424. [CrossRef]

[61] PERRY, J. Observational gait analysis handbook. Pathokinesiology Serv. Phys, **1989**, pp. 36.

[62] Murray, M. P.; Drought, A. B.; Kory, R. C. Walking patterns of normal men. Journal of Bone and Joint Surgery-American Volume, **1964**, Volume 46, No. 2, pp. 335-360. [PubMed]

[63] Bzner, H.; Oster, M.; Daffertshofer, M.; Hennerici, M. Assessment of gait in subcortical vascular encephalopathy by computerized analysis: A cross-sectional and longitudinal study. *J. Neurol.* **2000**, *247*, 841–849. [CrossRef]

[64] Hausdorff, J.M.; Cudkowicz, M.E.; Firtion, R.; Wei, J.Y.; Goldberger, A.L. Gait variability and basal ganglia disorders: Stridetostride variations of gait cycle timing in parkinson's disease and Huntington's disease. *Mov. Disord.* **1998**, *13*, 428–437. [CrossRef] [PubMed]

[65] Andriacchi, T.P.; Ogle, J.A.; Galante, J.O. Walking speed as a basis for normal and abnormal gait measurements. Journal of biomechanics, **1977**, Volume 10, No. 4, pp. 261-268. [PubMed]

[66] Otis, J.C.; Burstein, A.H. Evaluation of the VA-Rancho gait analyzer, Mark 1. Bulletin of prosthetics research, **1981**, Volume 18, No. 1, pp. 21-25. [PubMed]

[67] Kerrigan, D.C.; Schaufele, M.; Wen, M.N. Gait analysis, Annals of biomedical engineering, Philadelphia: Lippincott-Raven, **1995**, Volume 23.

[68] Inman, V.T.; Ralston, H.J.; Todd, F. Human walking. Williams & Wilkins, European Journal of Neurology, **1981**, Volume 12, No. 1.

[69] Nordin M.; Frankel, V.H. Basic biomechanics of the musculoskeletal system: 3rd ed., Lippincott Williams and Wilkins, **2001**.

[70] Perry, J. Pathological gait. Instructional Course Lectures 39, **1990**, pp. 325-331. [PubMed]

[71] Williamson, R.; Andrews, B. J. Gait event detection for FES using accelerometers and supervised machine learning. IEEE Transactions on Rehabilitation Engineering, **2000**, Volume 8, No. 3, pp. 312-319. [PubMed]

[72] Pappas, I.P.I.; Popovic, M.R.; Keller, T.; Dietz, V.; Morari, M. A Reliable Gait Phase Detection System. Neural Systems and Rehabilitation Engineering, IEEE Transactions on, **2001**, Volume 9, No. 2, pp. 113-125. [CrossRef]

[73] Wu, Y.; Krishnan, S. Statistical analysis of gait rhythm in patients with Parkinson's disease. *IEEE Trans. Neural Syst. Rehabil. Eng.* **2010**, *18*, 150–158.

[74] Joshi, D.; Khajuria, A.; Joshi, P. An automatic non-invasive method for Parkinson's disease classification. *Comput. Methods Programs Biomed.* **2017**, *145*, 135–145. [CrossRef] [PubMed]

[75] McGraw-Hill Concise Dictionary of Modern Medicine. **2002**. Accessed online on **2016**, from (http://medicaldictionary.thefreedictionary.com/shuffling+gait)

[76] Festinating gait. Accessed online from: (https://medical-dictionary.thefreedictionary.com/festinating+gait)

[77] Hausdorff, J.M. Gait dynamics in Parkinsons disease: common and distinct behavior among stride length, gait variability, and fractal-like scaling. Chaos: An Interdisciplinary Journal of Nonlinear Science, **2009**, Volume 19, No. 2, pp. 026113. [CrossRef]

[78] Hausdorff, J.M. Gait dynamics, fractals and falls: Finding meaning in the stride-to-stride fluctuations of human walking. *Hum. Mov. Sci.* **2007**, *26*, 555–589. [CrossRef] [PubMed]

[79] Yogev, G.; Giladi, N.; Peretz, C.; Springer, S.; Simon, E.S.; Hausdorff, J.M. Dual tasking, gait rhythmicity, and Parkinson's disease: Which aspects of gait are attention demanding? *Eur. J. Neurosci.* **2005**, *22*, 1248–1256. [CrossRef] [PubMed]

[80] MacLeod, C.M. Half a century of research on the Stroop effect: An integrative review. *Psychol. Bull.* **1991**, *109*, 163. [CrossRef]

[81] Langenecker, S.A.; Nielson, K.A.; Rao, S.M. fMRI of healthy older adults during Stroop interference. *Neuroimage* **2004**, *21*, 192–200. [CrossRef]

[82] Dwolatzky, T.; Whitehead, V.; Doniger, G.M.; Simon, E.S.; Schweiger, A.; Jaffe, D.; Chertkow, H. Validity of a novel computerized cognitive battery for mild cognitive impairment. *BMC Geriatr.* **2003**, *3*, 4. [CrossRef]

[83] Muro-De-La-Herran, A.; Garcia-Zapirain, B.; Mendez-Zorrilla, A. Gait analysis methods: An overview of wearable and non-wearable systems, highlighting clinical applications. Sensors, **2014**, Volume 14, No. 2, pp. 3362-3394. [CrossRef]

[84] Cutter, G.R.; Baier, M.L.; Rudick, R.A.; Cookfair, D.L.; Fischer, J.S.; Petkau, J.; Syndulko, K.; Weinshenker, B.G.; Antel, J.P.; Confavreux, C.; et al. Development of a multiple sclerosis functional composite as a clinical trial outcome measure. Brain **1999**, Volume 122, pp. 871-882. [CrossRef]

[85] Hobart, J.C.; Riazi, A.; Lamping, D.L.; Fitzpatrick, R.; Thompson, A.J. Measuring the impact of MS on walking ability: The 12-Item MS Walking Scale (MSWS-12). Neurology **2003**, Volume 60, pp. 31-36. [PubMed]

[86] Tinetti, M.E. Performance-oriented assessment of mobility problems in elderly patients. Journal of the American Geriatrics Society, **1986**, Volume 34, pp. 119-126. [PubMed]

[87] Mathias, S.; Nayak, U.S.; Isaacs, B. Balance in elderly patients: "The-get-up and go" test. Archives of physical medicine and rehabilitation, **1986**, Volume 67, pp. 387-389. [PubMed]

[88] Wolfson, L.; Whipple, R.; Amerman, P.; Tobin, J.N. Gait assessment in the elderly: A gait abnormality rating scale and its relation to falls. Journal of Gerontology. **1990**, Volume 45, pp. M12-19. [PubMed]

[89] Fried, A.V.; Cwikel, J.; Ring, H.; Galinsky, D. ELGAM-extra-laboratory gait assessment method: Identification of risk factors for falls among the elderly at home. International disability studies, **1990**, Volume 12, pp. 161164. [CrossRef]

[90] Palleja, T.; Teixido, M.; Tresanchez, M.; Palacn, J. Measuring gait using a ground laser range sensor. Sensors, **2009**, Volume 9, No. 11, pp. 9133-9146. [CrossRef

[91] Papageorgiou, X.S.; Chalvatzaki, G.; Tzafestas, C.S.; Maragos, P. Hidden markov modeling of human normal gait using laser range finder for a mobility assistance robot. In IEEE International Conference on Robotics and Automation (ICRA), **2014** , pp. 482-487. [CrossRef

[92] De Rossi, S.; Crea, S.; Donati, M.; Rebersek, P.; Novak, D.; Vitiello, N.; Lenzi, T.; Podobnik, J.; Munih, M.; Carrozza, M. Gait segmentation using bipedal foot pressure patterns, in Proceedings of the 4th IEEE RAS & EMBS International Conference on Biomedical Robotics and Biomechatronics (BioRob), **2012**, pp. 361366. [CrossRef

[93] Kong, k.; Tomizuka, M. Smooth and continuous human gait phase detection based on foot pressure patterns, in Proceedings of the IEEE International Conference on Robotics and Automation, **2008**, pp. 3678-3683. [CrossRef

[94] Pappas, I.P.; Keller, T.; Mangold, S.; Popovic, M.R.; Dietz, V.; Morari, M. A reliable gyroscope-based gait-phase detection sensor embedded in a shoe insole, IEEE Sensors Journal, **2004**, Volume 4, No. 2, pp. 268-274.

[95] Agostini, V.; Balestra, G.; Knaflitz, M. Segmentation and classification of gait cycles, IEEE Transactions on Neural Systems and Rehabilitation Engineering, **2014**, Volume 22, No. 5, pp. 946-952. [CrossRef

[96] Nickel, C.; Busch, C.; Rangarajan, S.; Mobius, M. Using hidden markov models for accelerometer-based biometric gait recognition, in Proceedings of the 7th IEEE International Colloquium on Signal Processing its Applications (CSPA), **2011**, pp. 5863. [CrossRef

[97] Rampp, A.; Barth, J; Schulein, S.; Gasmann, K.G.; Klucken, J.; Eskofier, B.M. Inertial sensor-based stride parameter calculation from gait sequences in geriatric patients, IEEE Transactions on Biomedical Engineering, **2015**, Volume 62, No. 4, pp. 1089-1097. [CrossRef

[98] Mannini, A.; Sabatini, A.M. A hidden markov model-based technique for gait segmentation using a foot-mounted gyroscope, in Proceedings of the IEEE Annual International Conference on Engineering in Medicine and Biology Society, **2011**, pp. 43694373. [PubMed]

[99] Georgiou, T. Rhythmic Haptic Cueing for Gait Rehabilitation of Hemiparetic Stroke and Brain Injury Survivors, Doctoral Dissertation, The Open University, **2018**. [CrossRef

[100] Jeon, H.S.; Han, J.; Yi, W.J.; Jeon, B.; Park, K.S. Classification of Parkinson gait and normal gait using spatial-temporal image of plantar pressure. In Proceedings of the 30th Annual International Conference of the IEEE Engineering in Medicine and Biology Society, Vancouver, BC, Canada, 20–24 August 2008; pp. 4672–4675.

[101] Andrews, C.J.; Neilson, P.D.; Lance, J.W. Comparison of stretch reflexes and shortening reactions in activated normal subjects with those in Parkinson's disease. *J. Neurol. Neurosurg. Psychiatry* **1973**, *36*, 329–333. [CrossRef] [PubMed]

[102] Latash, M.L.; Aruin, A.S.; Neyman, I.; Nicholas, J.J. Anticipatory postural adjustments during self inflicted and predictable perturbations in Parkinson's disease. *J. Neurol. Neurosurg. Psychiatry* **1995**, *58*, 326–334. [CrossRef]

[103] Nieuwboer, A.; Dom, R.; De Weerdt, W.; Desloovere, K.; Janssens, L.; Stijn, V. Electromyographic profiles of gait prior to onset of freezing episodes in patients with Parkinsons disease. *Brain* **2004**, *127*, 1650–1660. [CrossRef] [PubMed]

[104] Hong, M.; Perlmutter, J.S.; Earhart, G.M. A kinematic and electromyographic analysis of turning in people with Parkinson disease. *Neurorehabil. Neural Repair* **2009**, *23*, 166–176. [CrossRef] [PubMed]

[105] Halliday, S.E.; Winter, D.A.; Frank, J.S.; Patla, A.E.; Prince, F. The initiation of gait in young, elderly, and Parkinson's disease subjects. *Gait Posture* **1998**, *8*, 8–14. [CrossRef]

[106] Ashhar, K.; Soh, C.B.; Kong, K.H. A wearable ultrasonic sensor network for analysis of bilateral gait symmetry. In Proceedings of the 2017 39th Annual International Conference of the IEEE Engineering in Medicine and Biology Society (EMBC), Jeju Island, Korea, 11–15 July 2017; pp. 4455–4458.

[107] Saito, N.; Yamamoto, T.; Sugiura, Y.; Shimizu, S.; Shimizu, M. Lifecorder: A new device for the long-term monitoring of motor activities for Parkinsons disease. *Intern. Med.* **2004**, *43*, 685–692. [CrossRef]

[108] Hoff, J.I.; Van Den Plas, A.A.; Wagemans, E.A.H.; Van Hilten, J.J. Accelerometric assessment of levodopainduced dyskinesias in Parkinson's disease. *Mov. Disord. Off. J. Mov. Disord. Soc.* **2001**, *16*, 58–61. [CrossRef]

[109] Hundza, S.R.; Hook, W.R.; Harris, C.R.; Mahajan, S.V.; Leslie, P.A.; Spani, C.A. et al. Accurate and reliable gait cycle detection in Parkinson's disease. IEEE Transactions on Neural Systems and Rehabilitation Engineering, **2013**, Volume 22, No. 1, pp. 127-137. [CrossRef]

[110] Mariani, B.; Jimnez, M.C.; Vingerhoets, F.J.; Aminian, K. On-shoe wearable sensors for gait and turning assessment of patients with Parkinson's disease. *IEEE Trans. Biomed. Eng.* **2013**, *60*, 155–158. [CrossRef] [PubMed]

[111] Salarian, A.; Russmann, H.; Vingerhoets, F.J.; Dehollain, C.; Blanc, Y.; Burkhard, P.R.; Aminian, K. Gait assessment in Parkinson's disease: Toward an ambulatory system for long-term monitoring. *IEEE Trans. Biomed. Eng.* **2004**, *51*, 1434–1443. [CrossRef] [PubMed]

[112] Salarian, A.; Horak, F.B.; Zampieri, C.; Carlson-Kuhta, P.; Nutt, J.G.; Aminian, K. iTUG, a sensitive and reliable measure of mobility. *IEEE Trans. Neural Syst. Rehabil. Eng.* **2010**, *18*, 303–310. [CrossRef] [PubMed]

[113] Cho, C.W.; Chao, W.H.; Lin, S.H.; Chen, Y.Y. A vision-based analysis system for gait recognition in patients with Parkinsons disease. *Expert Syst. Appl.* **2009**, *36*, 7033–7039. [CrossRef]

[114] Galna, B.; Barry, G.; Jackson, D.; Mhiripiri, D.; Olivier, P.; Rochester, L. Accuracy of the Microsoft Kinect sensor for measuring movement in people with Parkinson's disease. *Gait Posture* **2014**, *39*, 1062–1068. [CrossRef] [PubMed]

[115] Pachoulakis, I.; Kourmoulis, K. Building a gait analysis framework for Parkinson's disease patients: Motion capture and skeleton 3D representation. In Proceedings of the International Conference on IEEE Telecommunications and Multimedia (TEMU), Heraklion, Greece, 28–30 July 2014; pp. 220–225.

[116] Dror, B.; Yanai, E.; Frid, A.; Peleg, N.; Goldenthal, N.; Schlesinger, I.; Hel-Or, H.; Raz, S. Automatic assessment of Parkinson's Disease from natural hands movements using 3D depth sensor. In Proceedings of the 2014 IEEE 28th Convention of Electrical & Electronics Engineers in Israel (IEEEI), Eilat, Israel, 3–5 December 2014; pp. 1–5.

[117] Dyshel, M.; Arkadir, D.; Bergman, H.; Weinshall, D. Quantifying Levodopa-Induced Dyskinesia Using Depth Camera. In Proceedings of the IEEE International Conference on Computer Vision Workshops, Santiago, Chile, 7–13 December 2015; pp. 119–126.

[118] Antonio-Rubio, I.; Madrid-Navarro, C.J.; Salazar-Lpez, E.; Prez-Navarro, M.J.; Sez-Zea, C.; Gmez-Miln, E.; Mnguez-Castellanos, A; Escamilla-Sevilla, F. Abnormal thermography in Parkinson's disease. *Parkinsonism Relat. Disord.* **2015**, *21*, 852–857. [CrossRef] [PubMed]

[119] Song, J.; Sigward, S.; Fisher, B.; Salem, G.J. Altered dynamic postural control during step turning in persons with early-stage Parkinsons disease. *Parkinson's Dis.* **2012**, *2012*, 386962.

[120] Foreman, K.B.; Wisted, C.; Addison, O.; Marcus, R.L.; LaStayo, P.C.; Dibble, L.E. Improved dynamic postural task performance without improvements in postural responses: The blessing and the curse of dopamine replacement. *Parkinson's Dis.* **2012**, *2012*, 692150. [CrossRef]

[121] Muniz, A.M.S.; Liu, H.; Lyons, K.E.; Pahwa, R.; Liu, W.; Nobre, F.F.; Nadal, J. Comparison among probabilistic neural network, support vector machine and logistic regression for evaluating the effect of subthalamic stimulation in Parkinson disease on ground reaction force during gait. *J. Biomech.* **2010**, *43*, 720–726. [CrossRef]

[122] Vaugoyeau, M.; Viallet, F.; Mesure, S.; Massion, J. Coordination of axial rotation and step execution: Deficits in Parkinson's disease. *Gait Posture* **2003**, *18*, 150–157. [CrossRef]

[123] Kolb, A.; Barth, E.; Koch, R.; Larsen, R. Time-of-Flight Sensors in Computer Graphics. In Computer Graphics Forum, Oxford, UK: Blackwell Publishing Ltd, March 2010, Volume 29, No. 1, pp. 141-159. [CrossRef]

[124] Attal, F.; Mohammed, S.; Dedabrishvili, M.; Chamroukhi, F.; Oukhellou, L.; Amirat, Y. Physical human activity recognition using wearable sensors. *Sensors* **2015**, *15*, 31314–31338. [CrossRef] [PubMed]

[125] Qi, Y.; Soh, C.B.; Gunawan, E.; Low, K.S.; Thomas, R. Assessment of foot trajectory for human gait phase detection using wireless ultrasonic sensor network. IEEE Transactions on Neural Systems and Rehabilitation Engineering, **2016**, Volume 24, No. 1, 88-97. [PubMed]

[126] Torrealba, R.R.; Cappelletto, J.; Gonzalez, A.; Fermn-Len, L. Detecting human gait cycle sub-phases from lower limb acceleration signals using k-means algorithm. In Proc. 1st Int. Conf. Appl. Bionics Biomech, **2010**, pp. 3897-3904. [CrossRef]

[127] Taborri, J.; Scalona, E.; Palermo, E.; Rossi, S.; Cappa, P. Validation of inter-subject training for hidden Markov models applied to gait phase detection in children with cerebral palsy. Sensors, **2015**, Volume 15, No. 9, pp. 24514-24529. [CrossRef]

[128] Su, B.L.; Song, R.; Guo, L.Y.; Yen, C.W. Characterizing gait asymmetry via frequency sub-band components of the ground reaction force. *Biomed. Signal Process. Control* **2015**, *18*, 56–60. [CrossRef]

[129] Zeng, W.; Liu, F.; Wang, Q.; Wang, Y.; Ma, L.; Zhang, Y. Parkinson's disease classification using gait analysis via deterministic learning. *Neurosci. Lett.* **2016**, *633*, 268–278. [CrossRef] [PubMed]

[130] Daliri, M.R. Automatic diagnosis of neuro-degenerative diseases using gait dynamics. *Measurement* **2012**, *45*, 1729–1734. [CrossRef]

[131] F-Scan In-Shoe Analysis System (https://www.tekscan.com/advance-your-practice-f-scan)

[132] Multon, F.; Olivier, A.H. Biomechanics of walking in real world: naturalness we wish to reach in virtual reality. In Human Walking in Virtual Environments, Springer, New York, NY, **2013**, pp. 55-77. [CrossRef]

[133] Khoury, N.; Attal, F.; Amirat, Y.; Oukhellou, L.; Mohammed, S. Data-Driven Based Approach to Aid Parkinson's Disease Diagnosis. Sensors, **2019**, Volume 19, No. 2, pp. 242. [CrossRef]

[134] Preece, S. J.; Goulermas, J. Y.; Kenney, L. P.; Howard, D.; Meijer, K.; Crompton, R. Activity identification using body-mounted sensorsa review of classification techniques. Physiological measurement, **2009**, Volume 30, No.4, pp. R1. [CrossRef]

[135] Figo, D.; Diniz, P.C.; Ferreira, D.R.; Cardoso, J.M. Preprocessing techniques for context recognition from accelerometer data. Personal and Ubiquitous Computing, **2010**, Volume 14, No. 7, pp. 645-662. [CrossRef]

[136] Guyon, I.; Elisseeff, A. An introduction to variable and feature selection. Journal of machine learning research, **2003**, Volume 3, pp. 1157-1182. [CrossRef]

[137] Liu, H.; Yu, L. Toward integrating feature selection algorithms for classification and clustering. *IEEE Trans. Knowl. Data Eng.* **2005**, *17*, 491–502.

[138] Kohavi, R.; John, G.H. Wrappers for feature subset selection. *Artif. Intel.* **1997**, *97*, 273–324. [CrossRef]

[139] Das, S. Filters, wrappers and a boosting-based hybrid for feature selection. In Proceedings of the Eighteenth International Conference on Machine Learning (ICML 2001), Williamstown, MA, USA, 28 June–1 July 2001; pp. 74–81.

[140] Chau, T. A review of analytical techniques for gait data. Part 1: fuzzy, statistical and fractal methods. Gait & posture **2001**, Volume 13, No. 1, pp. 49-66. [CrossRef] [PubMed]

[141] Martnez, A.M.; Kak, A.C. Pca versus lda. IEEE transactions on pattern analysis and machine intelligence, **2001**, Volume 23, No. 2, pp. 228233. [CrossRef]

[142] Duda, R.O.; Hart, P.E.; Stork, D.G. Pattern Classification, 2nd ed., a Wiley-Interscience Publication, John Wiley & Sons: Malden, MA, USA, **2012**. [CrossRef]

[143] Webb, A.R. Statistical Pattern Recognition, 2nd ed., a Wiley-Interscience Publication, John Wiley & Sons: Malden, MA, USA, **2003**.

[144] Theodoridis, S.; Pikrakis, A.; Koutroumbas, K.; Cavouras, D. Introduction to Pattern Recognition: A Matlab Approach; Academic Press: Waltham, NA, USA, **2010**.

[145] Vapnik, V.N. *The Nature of Statistical Learning Theory*; Springer Science & Business Media: Berlin/Heidelberg, Germany, 2013.

[146] Trabelsi, D.; Mohammed, S.; Chamroukhi, F.; Oukhellou, L.; Amirat, Y. An unsupervised approach for automatic activity recognition based on hidden Markov model regression. IEEE Transactions on automation science and engineering, **2013**, Volume 10, No. 3, pp. 829-835. [CrossRef]

[147] Breiman, L.; Friedman, J.; Stone, C.J.; Olshen, R.A. *Classification and Regression Trees*; CRC Press: Boca Raton, FL, USA, 1984.

[148] Quinlan, J.R. Induction of decision trees. *Mach. Learn.* **1986**, *1*, 81–106. [CrossRef]

[149] Quinlan, J.R. *C4.5: Programs for Machine Learning*; Morgan Kaufmann Publishers Inc.: San Francisco, CA, USA, 2014.

[150] Neapolitan, R.E. *Learning Bayesian Networks*; Pearson Prentice Hall: Upper Saddle River, NJ, USA, 2004; Volume 38.

[151] Nielsen, T.D.; Jensen, F.V. *Bayesian Networks and Decision Graphs*; Springer: Berlin, Germany, 2009.

[152] Vapnik, V. The Nature of Statistical Learning Theory, 2nd ed., Springer science & business media.: Berlin, Germany, **2013**.

[153] Scholkopf, B.; Smola, A.J. Learning with Kernels: Support Vector Machines, Regularization, Optimization, and Beyond; MIT Press: Cambridge, MA, USA, **2002**.

[154] Cover, T. M. Geometrical and statistical properties of systems of linear inequalities with applications in pattern recognition. IEEE transactions on electronic computers, **1965**, Volume 3, pp. 326-334.

[155] Dempster, A.P.; Laird, N.M.; Rubin, D.B. Maximum likelihood from incomplete data via the EM algorithm. *J. R. Stat. Soc. Ser. B (Methodol.)* **1977**, *39*, 1–38. [CrossRef]

[156] Attal, F. Classification de Situations de Conduite et Dtection des vnements Critiques d'un Deux Roues Motoris. Doctoral dissertation, Universit Paris-Est, Champs-sur-Marne, France, 2015. [CrossRef]

[157] Lennar, L. System identification: theory for the user. PTR Prentice Hall, Upper Saddle River, NJ, **1999**, pp. 1–14.

[158] Stone, M. Cross validation choice and assessment of statistical predictions, Journal of the Royal Statistical Society, **1974**, Volume 36, No. 2, pp. 1116147.

[159] Kohavi, R. A study of cross-validation and bootstrap for accuracy estimation and model selection, the International Joint Conference on Artificial Intelligence (IJCAI), **1995**, Volume 14, No. 2, pp. 11371145. [CrossRef]

[160] Efron, B.; Tibshirani, R.J. An introduction to the Bootstrap, ser. Monographs on Statistics and Applied Probability. Chapman and Hall, **1998**, Volume 57.

[161] Efron, B. Estimating the error rate of a prediction rule; improvement on cross-validation, Journal of the American Statistical Association, **1983**, Volume 78, pp. 316331. [CrossRef]

[162] Russell, S.; Norvig, P. *Artificial Intelligence: A Modern Approach*; Prentice-Hall: Egnlewood Cliffs, NJ, USA, 1995; Volume 25, p. 27.

[163] Lee, S.H.; Lim, J.S. Parkinsons disease classification using gait characteristics and wavelet-based feature extraction. *Expert Syst. Appl.* **2012**, *39*, 7338–7344. [CrossRef]

[164] Daliri, M.R. Chi-square distance kernel of the gaits for the diagnosis of Parkinson's disease. *Biomed. Signal Process. Control* **2013**, *8*, 66–70. [CrossRef]

[165] Khorasani, A.; Daliri M.R. HMM for classification of Parkinsons disease based on the raw gait data. *J. Med. Syst.* **2014**, *38*, 147–152. [CrossRef] [PubMed]

[166] Sarbaz, Y.; Banaie, M.; Pooyan, M.; Gharibzadeh, S.; Towhidkhah, F.; Jafari, A. Modeling the gait of normal and Parkinsonian persons for improving the diagnosis. *Neurosci. Lett.* **2012**, *509*, 72–75. [CrossRef]

[167] Cuzzolin, F.; Sapienza, M.; Esser, P.; Saha, S.; Franssen, M.M.; Collett, J.; Dawes, H. Metric learning for Parkinsonian identification from IMU gait measurements. *Gait Posture* **2017**, *54*, 127–132. [CrossRef]

[168] Jane, Y.N.; Nehemiah, H.K.; Arputharaj, K. A Q-backpropagated time delay neural network for diagnosing severity of gait disturbances in Parkinson's disease. *J. Biomed. Inform.* **2016**, *60*, 169–176. [CrossRef] [PubMed]

[169] Gait in Parkinson's Disease. Available online: https://physionet.org/pn3/gaitpdb/ (accessed on 10 January 2019).

[170] Erturul, .F.; Kaya, Y.; Tekin, R.; Almal, M.N. Detection of Parkinson's disease by shifted one dimensional local binary patterns from gait. *Expert Syst. Appl.* **2016**, *56*, 156–163. [CrossRef]

[171] Aici, K.; Erda, .B.; Aurolu, T.; Toprak, M.K.; Erdem, H.; Oul, H. A Random Forest Method to Detect Parkinsons Disease via Gait Analysis. In Proceedings of the International Conference on Engineering Applications of Neural Networks, Athens, Greece, 25–27 August 2017; Springer: Cham, Switzerland, 2017; pp. 609–619.

[172] Wu, Y.; Chen, P.; Luo, X.; Wu, M.; Liao, L.; Yang, S.; Rangayyan, R.M. Measuring signal fluctuations in gait rhythm time series of patients with Parkinson's disease using entropy parameters. *Biomed. Signal Process. Control* **2017**, *31*, 265–271. [CrossRef]

[173] Alam, M.N.; Garg, A.; Munia, T.T.K.; Fazel-Rezai, R.; Tavakolian, K. Vertical ground reaction force marker for Parkinson's disease. *PLoS ONE* **2017**, *12*, e0175951. [CrossRef] [PubMed]

[174] Bhoi A.K. Classification and Clustering of Parkinson's and Healthy Control Gait Dynamics Using LDA and K-means. *Int. J. Bioautom.* **2017**, *21*, 19–30

[175] Aharonson, V.; Schlesinger, I.; McDonald, A.M.; Dubowsky, S.; Korczyn, A.D. A Practical Measurement of Parkinson's Patients Gait Using Simple Walker-Based Motion Sensing and Data Analysis. *J. Med. Devices* **2018**, *12*, 011012. [CrossRef]

[176] Haji Ghassemi, N.; Hannink, J.; Martindale, C.F.; Gabner, H.; Muller, M.; Klucken, J.; Eskofier, B.M. Segmentation of Gait Sequences in Sensor-Based Movement Analysis: A Comparison of Methods in Parkinsons Disease. *Sensors* **2018**, *18*, 145. [CrossRef]

[177] FrenkelToledo, S.; Giladi, N.; Peretz, C.; Herman, T.; Gruendlinger, L.; Hausdorff, J.M. Treadmill walking as an external pacemaker to improve gait rhythm and stability in Parkinson's disease. *Mov. Disord.* **2005**, *20*, 1109–1114. [CrossRef]

[178] Hausdorff, J.M.; Lertratanakul, A.; Cudkowicz, M.E.; Peterson, A.L.; Kaliton, D.; Goldberger, A.L. Dynamic markers of altered gait rhythm in amyotrophic lateral sclerosis. *J. Appl. Physiol.* **2000**, *88*, 2045–2053. [CrossRef] [PubMed]

[179] Hausdorff, J.M.; Rios, D.A.; Edelberg, H.K. Gait variability and fall risk in community-living older adults: A 1-year prospective study. *Arch. Phys. Med. Rehabil.* **2001**, *82*, 1050–1056. [CrossRef]

[180] Yi, B.K.; Faloutsos, C. Fast time sequence indexing for arbitrary Lp norms. In Proceedings of the 26th International Conference on Very Large Data Bases, **2000**, Volume 385, No. 394, pp. 385394. [CrossRef]

[181] Serra, J.; Arcos, J.L. An empirical evaluation of similarity measures for time series classification. Knowledge-Based Systems, **2014**, Volume 67, pp. 305-314. [CrossRef]

[182] Gusfield, D. Algorithms on strings, trees, and sequences: computer science and computational biology. Cambridge university press, Cambridge, UK, **1997**. [CrossRef]

[183] Wang, X.; Mueen, A.; Ding, H.; Trajcevski, G.; Scheuermann, P.; Keogh, E. Experimental comparison of representation methods and distance measures for time series data. Data Mining and Knowledge Discovery, **2013**, Volume 26, No. 2, pp. 275-309. [CrossRef]

[184] Han, J.; Pei, J.; Kamber, M. Data mining: concepts and techniques, 3th ed., University of Illinois at urbana-Champain, Elsevier, **2011**. [CrossRef]

[185] Liao, T.W. Clustering of time series data: a survey. Pattern recognition, Elseiver, **2005**, Volume 38, No. 11, pp. 1857-1874. [CrossRef]

[186] Marteau, P.F. Time warp edit distance with stiffness adjustment for time series matching. IEEE Transactions on Pattern Analysis and Machine Intelligence,**2009**, Volume 31, No. 2, pp. 306-318. [CrossRef]

[187] Fu, T.C. A review on time series data mining. Engineering Applications of Artificial Intelligence, Elseiver, **2011**, Volume 24, No. 1, pp. 164-181. [CrossRef]

[188] Oppenheim, A.V.; Schafer, R.W.; Buck, J.R. Discrete-time signal processing, 2nd ed., Prentice-Hall, Upper Saddle River, USA, **1999**.

[189] Agrawal, R.; Faloutsos, C.; Swami, A. Efficient similarity search in sequence databases. In International Conference on Foundations of Data Organization and Algorithms, Springer, Berlin, Heidelberg, **1993**, pp. 69-84. [CrossRef]

[190] Maharaj, E.A. Cluster of time series. Journal of Classification,**2000**, Volume 17, No. 2, pp. 297-314.

[191] Ramoni, M.; Sebastiani, P.; Cohen, P. Bayesian clustering by dynamics. Machine learning, **2002**, Volume 47, No. 1, pp. 91-121. [CrossRef]

[192] Povinelli, R.J.; Johnson, M.T.; Lindgren, A.C.; Ye, J. Time series classification using Gaussian mixture models of reconstructed phase spaces. IEEE Transactions on Knowledge and Data Engineering, **2004**, Volume 16, No. 6, pp. 779-783. [CrossRef]

[193] Serra, J.; Kantz, H.; Serra, X.; Andrzejak, R.G. Predictability of music descriptor time series and its application to cover song detection. IEEE Transactions on Audio, Speech, and Language Processing, **2011**, Volume 20, No. 2, pp. 514-525. [CrossRef]

[194] Levenshtein, V. I. Binary codes capable of correcting deletions, insertions, and reversals. In Soviet physics doklady, **1966**, Volume 10, No. 8, pp. 707-710. [CrossRef]

[195] Chen, L., Ozsu, M.T. and Oria, V. Robust and fast similarity search for moving object trajectories. In Proceedings of the 2005 ACM SIGMOD international conference on Management of data, **2005**, pp. 491-502. [CrossRef]

[196] Sakoe, H.; Chiba, S. Dynamic programming algorithm optimization for spoken word recognition. IEEE transactions on acoustics, speech, and signal processing, **1978**, Volume 26, No. 1, pp. 43-50.

[197] Berndt, D.J.; Clifford, J. Using dynamic time warping to find patterns in time series. in: Proc. of the AAAI Workshop on Knowledge Discovery in Databases, **1994**, Volume 10, No. 16, pp. 359-370.

[198] Rodrguez, J.J.; Alonso, C.J. Interval and dynamic time warping-based decision trees. In Proceedings of the 2004 ACM symposium on Applied computing, ACM, **2004**, pp. 548-552. [CrossRef]

[199] Bartolini, I.; Ciaccia, P.; Patella, M. Warp: Accurate retrieval of shapes using phase of fourier descriptors and time warping distance. IEEE transactions on pattern analysis and machine intelligence, **2005**, Volume 27, No. 1, pp. 142-147. [CrossRef] [CrossRef] [PubMed]

[200] Tormene, P.; Giorgino, T.; Quaglini, S.; Stefanelli, M. Matching incomplete time series with dynamic time warping: an algorithm and an application to post-stroke rehabilitation. Artificial intelligence in medicine, **2009**, Volmume 45, No. 1, pp. 11-34. [PubMed]

[201] Kholmatov, A.; Yanikoglu, B. Identity authentication using improved online signature verification method. Pattern recognition letters, **2005**, Volume 26, No. 15, pp. 2400-2408. [CrossRef]

[202] Keogh, E.J.; Pazzani, M.J. Derivative dynamic time warping. In Proceedings of the 2001 SIAM International Conference on Data Mining, Society for Industrial and Applied Mathematics, **2001**, pp. 1-11. [CrossRef]

[203] Chu, S.; Keogh, E.; Hart, D.; Pazzani, M. Iterative deepening dynamic time warping for time series. In Proceedings of the 2002 SIAM International Conference on Data Mining, Society for Industrial and Applied Mathematics, **2002**, pp. 195-212. [CrossRef]

[204] Tavenard, R.; Amsaleg, L. Improving the efficiency of traditional DTW accelerators. Knowledge and Information Systems, **2015**, Volume 42, No. 1, pp. 215-243. [CrossRef]

[205] Jeong, Y.S.; Jeong, M.K.; Omitaomu, O.A. Weighted dynamic time warping for time series classification. Pattern Recognition, **2011**, Volume 44, No. 9, pp. 2231-2240. [CrossRef]

[206] Khoury, N.; Attal, F.; Amirat, Y.; Chibani, A.; Mohammed, S. CDTW-based classification for Parkinson's Disease diagnosis. In Proceedings of the 26th European Symposium on Artificial Neural Networks, Computational Intelligence and Machine Learning (ESANN 2018), Bruges, Belgium, 25–27 April 2018; pp. 621–626.

[207] Shen, J.; Huang, W.; Zhu, D.; Liang, J. A novel similarity measure model for multivariate time series based on LMNN and DTW. Neural Processing Letters, **2017**, Volume 45, No. 3, pp. 925-937.

[208] Munich, M.E.; Perona, P. Continuous dynamic time warping for translation-invariant curve alignment with applications to signature verification. In Computer Vision, 1999. The Proceedings of the Seventh IEEE International Conference on, IEEE, **1999**, Volume 1, pp. 108-115. [CrossRef]

[209] Helwig, N. E.; Hong, S.; Hsiao-Wecksler, E. T.; Polk, J. D. Methods to temporally align gait cycle data. Journal of biomechanics, **2011**, Volume 44, No. 3, pp. 561-566. [PubMed]

[210] Boulgouris, N. V.; Plataniotis, K. N.; Hatzinakos, D. Gait recognition using dynamic time warping. In IEEE 6th Workshop on Multimedia Signal Processing, IEEE, **2004**, pp. 263-266. IEEE. [CrossRef]

[211] Hu, Y. A Method of DTW Based Gait Recognition and Gait Data from Kinect, International Journal of Computer Techniques, **2018**, Volume 5,No. 1, pp. 14-19. [CrossRef]

[212] Kale A.; Cuntoor N.; Yegnanarayana B.; Rajagopalan A.; Chellappa R. Gait Analysis for Human Identification. In: Kittler J., Nixon M.S. (eds) Audio-and Video-Based Biometric Person Authentication. AVBPA Lecture Notes in Computer Science, Springer, Berlin, Heidelberg, **2003**, Volume 2688. [CrossRef]

[213] Switonski, A.; Josinski, H.; Wojciechowski, K. Dynamic time warping in classification and selection of motion capture data. Multidimensional Systems and Signal Processing, , **2019**, Volume 30, No. 3, pp. 1437-1468. [CrossRef]

[214] Muscillo, R.; Conforto, S.; Schmid, M.; Caselli, P.; D'Alessio, T. Classification of motor activities through derivative dynamic time warping applied on accelerometer data. In 2007 29th Annual International Conference of the IEEE Engineering in Medicine and Biology Society, IEEE, **2007**, pp. 4930-4933. [CrossRef] [PubMed]

[215] Deza, M.M.; Deza, E. Encyclopedia of distances, In Encyclopedia of Distances, Springer, Berlin, Heidelberg, **2009**, pp. 1-583.

[216] Mei, J.; Liu, M.; Wang, Y.F.; Gao, H. Learning a mahalanobis distance-based dynamic time warping measure for multivariate time series classification. IEEE transactions on Cybernetics, **2016**, Volume 46, No. 6, pp. 1363-1374. [CrossRef] [PubMed]

[217] Lescano, C.N.; Rodrigo, S.E.; Christian, D.A. A possible parameter for gait clinimetric evaluation in Parkinson's disease patients. In Journal of Physics: Conference Series, IOP Publishing, **2016**, Volume 705, No. 1, pp. 012019. [CrossRef]